POLITECNICO
MILANO 1863

SCUOLA DI INGEGNERIA INDUSTRIALE
E DELL'INFORMAZIONE

Network-Based Representation and Analysis of Rubble-Pile Asteroids Dynamics

Tesi di Laurea Magistrale in
Space Engineering - Ingegneria Spaziale

Author: **Martin Mihnea Stefan**

Student ID: 10903720
Advisor: Prof. Ferrari Fabio
Co-advisors: Alessi Elisa Maria
Academic Year: 2024-25

Abstract

The structural and dynamical evolution of rubble pile asteroids, which are aggregates of rocks held together primarily by gravity, are central to understanding the solar system formation, asteroid deflection strategies, and in-situ observations. Traditional methods for modelling these systems typically rely on particle-based dynamics or finite element models. This thesis introduces and validates a novel approach that models rubble-pile asteroids using complex network theory, enabling the characterisation of internal structures and dynamical behaviours through topological metrics.

The methodology begins with the creation of asteroid systems using smooth and non-smooth contact models, simulating both spherical and convex polyhedral particles. The simulated aggregates are transformed into graph representations, with nodes corresponding to particles and edges reflecting interparticle relationships derived from physical and spatial properties, such as contact forces, distances and energies.

Network analysis techniques, including centrality metrics (degree, eigenvector, betweenness), clustering coefficients, and percolation thresholds, are applied to capture critical aspects of system behaviour such as stability and fragmentation potential. These metrics are studied over time to monitor structural evolution under varying initial conditions of density, shape, and spin rate. The results demonstrate that percolation and clustering analyses reveal phases of aggregation or disaggregation.

Finally, the study proposes a predictive framework using early-time network configurations to forecast possible break-up formations. This thesis concludes that complex network theory offers a powerful, complementary lens for analysing and interpreting rubble-pile asteroid dynamics, paving the way for future high-fidelity and computationally efficient modelling approaches.

Keywords: Rubble-pile asteroids, network theory, centrality, percolation, asteroid dynamics, clustering analysis.

Abstract in lingua italiana

L'integrità strutturale e la corrispondente evoluzione degli asteroidi di tipo rubble-pile, che sono aggregati di rocce tenuti insieme principalmente dall'azione della gravità, costituiscono meccanismi fondamentali per capire la formazione del sistema solare e concepire strategie di difesa planetaria e missioni di osservazione in-situ. I metodi tradizionali per modellizzare questi sistemi si basano tipicamente sulla dinamica delle particelle o su modelli a elementi finiti. Questa tesi introduce e valida un approccio innovativo per rappresentare un asteroide rubble-pile attraverso la teoria delle reti, permettendo la caratterizzazione delle strutture interne e dei loro comportamenti dinamici attraverso specifiche metriche topologiche.

Il metodo applicato prende avvio dalla creazione di sistemi asteroidali usando modelli di contatto smooth e non-smooth, simulando sia particelle sferiche sia particelle dalla forma poliedrica convessa. Gli aggregati così simulati vengono rappresentati come grafi, dove i nodi corrispondono alle particelle e gli spigoli riflettono le relazioni fisiche e spaziali tra le particelle, come per esempio le forze di contatto, le distanze e le energie.

Le tecniche della teoria delle reti, che includono le metriche di centralità (grado, autovettore, betweenness), i coefficienti di clustering e le soglie di percolazione, sono applicate per cogliere gli aspetti critici del comportamento del sistema, come la stabilità e la potenziale frammentazione. Queste metriche sono applicate in diversi momenti per monitorare l'evoluzione strutturale, assumendo diverse condizioni iniziali in termini di densità, forma e frequenza di rotazione. I risultati dimostrano che le tecniche di percolazione e di clustering sono in grado di rivelare fasi di aggregazione o disgregazione.

Infine, lo studio propone un contesto predittivo basato sulla configurazione iniziale della rete per prevedere possibili eventi di rottura. La conclusione della tesi è che la teoria delle reti rappresenta un potente strumento per analizzare e interpretare la dinamica degli asteroidi rubble-pile, aprendo la strada a nuovi modelli computazionalmente efficienti.

Parole chiave: Asteroidi di tipo "rubble-pile", teoria delle reti, centralitá, percolazione, dinamica degli asteroidi, analisi di clustering.

Contents

1 | Introduction

1.1. Importance of asteroids research

Understanding the origin and dynamics of celestial bodies remains one of the most fundamental questions in modern astrophysics and planetary science. For thousands of years, celestial bodies, such as asteroids, meteoroids, and comets, have been of interest to the scientific community. In the second half of the 20^{th} century, research in this field has increased considerably, along the advent of spacecraft missions and technological evolution, allowing more rigorous analyses and thanks also to an increased awareness of the risk that near-Earth objects (NEOs) can pose. This surge is not surprising, as the research of these bodies could answer several questions and provide a better understanding of the early solar system, and, by extension, the origin of life and planetary evolution [3]. In fact, they are considered unchanged remnant debris from solar system formation, and an important source of information for understanding the events that shaped the solar system. At the same time, asteroids can also pose a clear and present danger. Depending on their size and composition, their impact with Earth could cause regional or global devastation and could have a severe impact on all living things. Therefore, it is important to understand their composition and dynamics in order to be able to prevent or mitigate such disruptive events. For these reasons, many space exploration missions have been deployed, focussing on the chemical, biological, and mechanical structure of the asteroids [3], with the latest DART, Psyche, and Hera, which have been used to test a planetary protection scheme against the threats of near-Earth objects, analyse the largest known asteroid (16-Psyche), and analyse the aftermath of the contact between 65803-Didymos and DART. In order to ensure the success of such missions, in addition to understanding the process occurring in an asteroid, such as formation and disaggregation, or environmental requirements necessary for the formation of different types of asteroids, a large body of research for the mission design is required.

The possible environment that the spacecraft could encounter when reaching the asteroid has to be carefully studied. For missions that included a landing or extraction phase (e.g. Hayabusa and OSIRIS Rex), it is important to understand how the spacecraft may affect

the structural reliability of the asteroid (not to create debris) and the possible landing regions of the lander [22]. A good example in this area is the YORP effect, as presented by Holsapple [10] [25], which could lead to asteroid restructuring or the disruption and distortion they may undergo due to tidal effects [39].

Therefore, it is important to understand how the asteroids are formed and their conditions for equilibrium. Several methods have already been proposed for asteroid modelling.

The scope of this paper is to implement a new method of modelling the rubble-pile asteroids applying the network theory to different topologies of asteroids, in order to measure the stability of the aggregate and verify what information could the network theory provide on the dynamical evolution of asteroids. The choice of using network theory is also based on its capability to define communities, and network fragmentation through percolation theory, which could be considered similar to the process of asteroid disaggregation.

From results obtained from in situ measurements investigations and remote measurements, it has been concluded that the majority of asteroids in the range $\sim$ 200 m - 10 km are the so-called rubble piles, that is, they are collections of smaller fragments bounded together by self-gravity [20, 39].

1.2. The Gravitational Aggregates

Richardson et al. [40] offer a clear representation of the difference between the rubble pile and the monolith. The classification is based on the porosity of the body, the relative tensile strength (RTS), and the mass fraction. In this classification, monolithic bodies are considered to rest unaffected by long-term stress but damaged by tensive waves through their propagation. Meanwhile, rubble piles present moderate porosity due to disorganisation and some kind of RTS, presenting long-term changes but less affected than monolithic bodies by tensive waves, as energy is absorbed by compression as presented by Richardson et al. [39].

The systems representing gravitational aggregates are difficult to model, with their rubble-pile nature requiring them to be treated as granular systems, and as such they are complex systems. Therefore, the problem of collision and contact bodies is often analysed through hydrodynamic codes or by implementing hard/soft sphere collision models [15, 18, 40].

Asteroids and comets are usually difficult to represent through hydrodynamics, as the assumption generally does not hold for small granular bodies, which have been confirmed also by observational results. A model based on Mohr-Coulomb (MC) yield criteria is

presented in a series of articles by Holsapple [23, 24, 26], and presents the limits for equilibrium fields and shapes. Furthermore, a spin limit at which structural failure would occur is defined for granular materials that can withstand a significant amount of shear stress and is calculated to be around 2.2 hours, but it depends on the ellipticity and density of the aggregate, with denser aggregates that exhibit a higher resistance to breakup, which reduces the limit period.

The models mentioned previously focus primarily on the failure analysis of rubble-pile asteroids, often emphasising disruption criteria under increasing spin rates or external perturbations. However, these models generally overlook the intermediate dynamical and morphological evolution, specifically the reshaping process that rubble-pile structures may undergo as they approach critical rotational thresholds or in cases where rotational period is very large.

This reshaping behaviour is addressed by Holsapple in [25], where the YORP effect is identified as a key driver of the changing spin state of the asteroid. Holsapple's work demonstrates that as the asteroid nears its critical spin limit, structural deformation occurs due to internal stress redistribution, not merely as an abrupt failure. The rubble pile adjusts its shape gradually to accommodate the increasing rotational stress, highlighting the importance of internal mechanics and shape-dependent mass movement. Bagatin et al. [5] develop a method to analyse the internal structure of gravitational aggregates based on the porosity and relative mass distribution. By incorporating irregular fragment shapes informed by laboratory experiments, the study reveals that the final properties of the resulting aggregates are largely stochastic. However, discernible patterns emerge, such as a loose linear relationship between macroporosity and the relative mass distribution. Additionally, the study posits that slow rotators may naturally result from gravitational reaccumulation.

In [6] the simulations indicate that a significant fraction of asteroids, particularly those ranging from a few kilometres to about 100 km in diameter, are likely reaccumulated bodies. This insight underscores the importance of considering the characteristics of the rubble pile when assessing the evolution of the asteroid and potential hazard mitigation strategies.

In addition, Holsapple's model captures an important nuance: As the spin rate increases, the system does not simply collapse. Instead, the rising angular momentum is increasingly counteracted by a growing moment of inertia, particularly if the mass is redistributed outward or the shape becomes more oblate. This dynamic balance delays catastrophic disruption and allows for quasi-stable reshaped configurations. This was obtained through

an ordinary differential equation and is reasonable for YORP spin-up scenarios, but less probable for impact scenarios and tidal interactions. This is further developed in [13], where the break-up limits of rubble piles are examined based on a set of defined indicators. The 4 defined indicators consider as input the time evolution of different metrics that define the rubble-pile system such as kinetic energy, E_k, pseudo-Jacobi potential, J, moment of inertia, I_p and inertia elongation λ, two of them being considered also in this work, namely the kinetic energy and the moment of inertia.

Although earlier models, such as those already discussed [25], begin to address the onset of reshaping in spinning rubble-pile asteroids, they do not fully integrate complex granular mechanics, particularly the roles of material interactions such as cohesion, heterogeneous structure, and individual grain interactions. These properties are critical in determining the deformation, failure and evolution in fast rotating scenarios of rubble-piles.

More advanced simulations, such as those by Sánchez and Scheeres [44, 45, 47], explicitly incorporate these granular effects using soft-sphere discrete element method (SSDEM) models. Their work shows that rubble-pile asteroids can undergo a range of failure behaviours, including surface landslides and internal deformation depending on the level of cohesion and internal shear strength. Notably, even small variations in material properties can lead to drastically different evolutionary outcomes, especially near the critical spin limit.

Regarding DEM simulations, Richardson et al. [41] consider a hard-sphere model, while Sánchez and Scheeres [44] focus on the soft-sphere/smooth model. Ferrari et al. [15] consider a non-smooth model.

The influence of internal architecture is further examined by Ferrari and Tanga [14], where they simulate the mechanical response of top-shaped asteroids under varying structural configurations. Their study highlights that the angle of friction, the bulk density, the number of particles, and especially the size of a central core significantly affect the overall stability of the aggregate. Rubble-pile asteroids with larger internal cores are found to be more resistant to internal failure, favouring surface-level deformation (e.g., equatorial bulges or landslides) rather than full-scale collapse. These results offer a plausible explanation for the prevalence of top-shaped asteroids observed by missions such as Hayabusa2 (Ryugu) and OSIRIS-REx (Bennu). A similar approach is taken in by Scheeres and Sánchez [46], by considering different sizes for a central core to analyse the effect on the critical spin rate in relation to the core cohesive strength. The application of SSDEM model shows that the core is subject to the greatest stress, and therefore a severely weakened core would fail easily upon rotation, with the disruption and deformation pattern of

the asteroid being determined from the specific size and relative strength of the core.

Crucially, their work also suggests that even large cores cannot entirely prevent mass shedding, particularly in fast-rotating systems, where angular acceleration drives surface material outward. The amount of mass loss in such cases is dependent on the total mass and total volume of the asteroid, with larger systems being more likely to shed more material due to increased gravitational and inertial gradients.

These findings are complemented by Zhang et al. [58], who employ an SSDEM approach to calibrate mechanical parameters such as cohesive strength, angle of internal friction, and interparticle contact laws. Their simulations test the spin limits of aggregates under different material property regimes, showing that increasing internal friction or cohesion can significantly increase the maximum sustainable spin rate before failure occurs. This aligns with observations of small, fast-spinning asteroids that remain intact despite approaching theoretical disruption thresholds.

Different types of models are available for representing granular media, such as smoothed particle hydrodynamics (SPH), finite element modelling (FEM), and discrete element modelling (DEM). From these, in the case of rubble-pile asteroid, the most suitable is DEM as it considers the interactions between individual particles and their evolution over time. Its benefit lies in the higher accuracy during the simulation, which is accompanied by a lower computational efficiency. SPH simulations are more appropriate for long timescale simulations and high-energy impact studies, while FEM is more often used to analyse the evolution of the stress field due to external influences such as tidal interactions, [18]. Benz and Asphaug also use an SPH model in their analysis of catastrophic collisions. They quantified the specific impact energy threshold required for breakup and disperse asteroids of various sizes and compositions. This work established a two-regime model - one dominated by material strength at small scales and another governed by gravity at larger scales - highlighting the complex, scale-dependent nature of fragmentation processes. Their results significantly shaped our understanding of collisional evolution in the asteroid belt and provided a benchmark for follow-up studies.

Recent work by Brown and Scheeres [1] builds on the importance of energy and angular momentum dissipation in rubble-pile asteroid systems undergoing rotational failure and mass shedding. They focus on the long-term evolution of systems that experience mass ejection due to rotational instability, a process increasingly supported by both observation and simulation.

In their framework, the expelled mass significantly affects the system's total energy and angular momentum budget. When fragments escape, the system is transformed into a

multibody configuration, and the authors employ Jacobi transformations to analyse both local and global dynamical parameters. These transformations allow for the identification of conserved quantities and the evolution of the system in rotating frames, particularly relevant to the post-fission dynamics.

This work defines the upper bounds of the amended potential energy of the system, which depends on both mass distribution and the number of ejected bodies. The established bounds help understanding if fragments will escape or remain bound and are used as stability criteria. The defined limits are dependent on the initial angular momentum and mass ratio distributions.

Moreover, Brown and Scheeres demonstrated that the number of ejected bodies plays a crucial role in shaping the system's final configuration. As the number of fragments increases, statistical regularities emerge in their angular momentum and escape energy distributions. Although hyperbolic angular momentum and escape energy thresholds scale with the number of escaping bodies, the distribution patterns tend to converge for higher multiplicities, suggesting a form of self-similarity or convergence in high fragmentation events.

This work is especially relevant for modelling asteroid fission into binary or multiple systems, where not all components necessarily form bound satellites. Instead, many may escape entirely, influencing observational features such as debris trails, satellite multiplicity, and primary spin-down rates. In [7] is shown how initial rotation changes the outcome of rubble pile collisions, by analysing the properties of the largest remnant, and a similar conclusion has been reached to previous researches: a faster-rotating asteroid leads to a larger mass of dispersed bodies. Moreover, Ballouz et al. show that the position of contact is also important, with pole regions-impacts able to efficiently disperse the equatorial material.

Although a large part of the available research focusses on simulating spherical particle rubble piles, [13, 15, 18, 29] create simulations considering more complex shapes, such as polyhedra. This presents several differences, as two particles could stay in contact along a surface or line, not just at one point, as in the case of spheres. As particles can be chosen to have a slightly elongated form, their position in the aggregate is different from that of spheres, as the orientation of the particle plays a role in the final state of the system, leading to geometrical interlocking, non-central collisions and spin motions of individual fragments. Collisions between two rubble piles of similar size could end in several results, as shown by Korycansky and Asphaug [29], where collisions were analysed at different speeds by using a continuum model and considering the gravitational attraction to be

point masses.

In most of the previously stated analysis, the angle of friction has emerged as one of the most influential parameters governing the mechanical stability of rubble-pile asteroids. This parameter, which quantifies the resistance to shear within granular materials, plays a key role in determining how an aggregate responds to rotational acceleration and external perturbations.

Similarly, Sugiura et al. [51] explore the dependence of fission and failure behaviour on friction angle and find that even small increases in this parameter can drastically increase the critical spin rate, thus extending the range of stable configurations. These findings emphasise that cohesion alone is insufficient for structural stability - friction-induced shear resistance is a primary control mechanism, especially in cohesionless or low-cohesion systems.

Taken together, these studies underscore that accurate modelling of asteroid evolution and failure must account not only for global parameters (mass, shape, spin) but also for local mechanical properties, particularly the internal friction angle. Its effect permeates all stages of the evolution of the rubble pile, from initial reaccumulation to long-term YORP-driven spin-up and potential rotational break-up.

1.3. The Network Theory

For simulations of rubble-pile asteroids, the starting point is generally an already aggregated body to which a set of physical parameters is applied. One point of interest when choosing the initial physical parameters is the identification of important particles/set of particles, known as clusters, that could have an important role in the asteroid's dynamical evolution. However, it can be difficult to identify cluster formations in granular media, due to possible overlapping of clusters or lack of a well-defined separation limit. Furthermore, the physical characteristics of the system on which the cluster algorithm is based must be carefully chosen in order to offer meaningful results. An example is presented by Chen et al. [9] in the study of the clustering behaviour in freely cooling granular systems. Using large-scale three-dimensional molecular dynamics simulations involving approximately one million dissipative particles, the authors investigated the formation and evolution of clusters as the system cools. Their findings reveal that over time, particles tend to form interconnected, tube-like high-density regions. The study also quantifies the energy decay rates in relation to particle density and restitution coefficients, and observes that the probability density function of particle density approaches an exponential distribution in the late stages of clustering. Additionally, both the density fluctuations

and the mean cluster size exhibit power-law scaling with time during the inelastic coalescence process. A similar approach applied to cooling gas is developed by Luding [31], which provides a comprehensive analysis of the mechanisms underlying cluster formation in granular systems. Luding emphasises two fundamental phenomena: excluded volume, captured by the hard-sphere model, which is responsible for crystallisation, and dissipation, which leads to the emergence of clusters in non-equilibrium dynamical states. Through event-driven simulations, the study examines energy decay and cluster evolution over time, highlighting the significance of multiparticle contacts and crystallisation effects, especially at higher densities. Both authors have considered physical systems, the evolution of which was known, by applying the network theory have found changes in the network that can characterise the actual physical evolution of the system, which is of interest in the gravitational aggregates.

Several other clustering methods are available and developed for different systems. One of the most common clustering methods is spectral clustering [55], which is based on network theory or HARP[8], which compresses the input graph into a hierarchy of coarser representations, learning embeddings at each level, and using these as initializations for finer levels.

Newman [37] introduces a greedy agglomerative algorithm that merges communities to maximise modularity, significantly reducing computational time compared to previous methods. This algorithm made community detection in large-scale networks practical and has become a foundational technique in network science, widely adopted in social, biological, and technological network analysis, proven to be applicable to a wide range of different types of networks.

In cases of large systems, where many bodies are present, the clustering algorithms become computationally expensive, which is a considerable problem in the case of gravitational aggregates, as in several simulations created, the number of bodies considered exceeds 1000. In such cases, some clustering algorithms prefer to ignore nodes that are not important to the evolution of the cluster.

As several clustering algorithms are based on networks, system representations composed of vertices and links, a good approach is to transform the physical dynamical system into a network, on which the dynamical evolution is represented through the evolution of the attributes of the graph, with a time-dependent network [19].

Furthermore, an increase in the number of real-world applications of network theory is observed because of its capability to represent different complex systems based on the relationships between the system's components. Several topics have been approached

from the point of view of network theory, such as social networks, protein reactions, or Internet networks [28, 33]. In the approach of Coutinho et al. [11] the network of the large-scale structure of the Universe is created and analysed on the basis of the proximity of the network's elements. The results show that in cosmic networks no hubs are present, compared to other well-analysed networks [36], and that the simplest model taken, in which only a simple assumption of spatial proximity is considered, offers the most accurate description of the cosmic web. A similar approach was taken by Gausmann and Ferrari [19], as spatial networks were created in order to analyse galaxy distributions, spatial structure, and how galaxies cluster, form filaments, and relate to their environments. For this, they have calculated the classic network metrics such as degree, centrality, giant component, and transitivity, and created the respective clusters. They have proven that the largest components of the network can be associated to supercluster regions. They showed that the network topology mirrors the physical clustering in real space. However, a problem usually encountered when representing the system as a network is introducing the dynamic factor, as network dynamics and multi-body dynamics focus on different aspects. The network dynamics focusses on the evolution of the network in time, with changes in network structure (presence of nodes or edges) or changes in the attributes of the graph, and they are driven by the rules about connectivity and probabilistic interactions, which are usually a discrete-time or stochastic model. However, the dynamics of a physical system is continuous in space, and time is governed by physical states (velocity, positions, energy) and driven by physical forces. Wang et al. [56], created a stochastic dynamic network model to forecast how space objects interact and evolve over time in Earth's orbit. This approach is different from others as the links between the nodes in the network are based on the actual interactions between the bodies, collisions, or projected flows of objects. A different approach to the analysis of resident space objects is presented in [43], where the links in the network are based on the limited distance between the Resident Space Objects (RSOs). Afterward, a set of relevance scores is calculated and graph-theory metrics are applied to the newly formed network as in the previous models [56][19].

An interesting applicability of the network theory is the bond or node percolation, in order to calculate the reliability or evolution of a network in time. Such processes are computationally expensive, especially for large networks or complete networks, and have been widely applied to random networks [36].

Aziz et al. [4] proposed a new link prediction framework based on information flow dynamics in complex networks, which extends beyond traditional similarity-based metrics by simulating the way signals or information traverse the network structure. This method captures non-local interactions and multi-hop influence, which is especially relevant for

systems where physical or probabilistic propagation of effects plays a role. In a comprehensive review, Sun [52] categorised link prediction approaches into heuristic-based, probabilistic, and embedding-based techniques, with a particular focus on temporal dynamics. This work provides a valuable overview of challenges in dynamic networks, including the instability of predictions under topological change, which is directly relevant for evolving systems like rubble-pile asteroids or orbital collision networks. Newman [35] introduced Monte Carlo-based modularity optimisation, which laid the foundation for the evaluation of the community structure in large-scale networks. Hu et al. [27] proposed a signaling-based approach for community detection, where nodes communicate via virtual signals to iteratively infer local clustering structures. This biologically inspired method captures structural regularities in dynamic environments, which can be leveraged as predictive features in link prediction or structural collapse modelling in granular bodies.

Therefore, network theory is an important tool in describing and representing complex systems that can present certain clustering attributes and also whose evolution is dependent on the interaction between the elements composing the system.

1.4. Thesis Objectives and Structure

As stated above, rubble piles are considered complex systems that can undergo break-ups or reshaping. Their complex behaviour is defined by the contact dynamics that governs the aggregate along with the gravitational attraction between the bodies. Therefore, it is considered that network theory is a viable method of modelling and analysing such a complex system, and that could present a different approach of analysing the asteroid's stability and evolution. Network theory was chosen for its theoretical framework that effectively represents relationships between components. It is particularly suited for problems that emphasise the connections within a network and the emergence of communities, where the significance of each component is determined by its position and attributes within the system.

The main objective of the present work is to model asteroids as networks and to apply network theory to different cases, leading to new methods of measuring the asteroid stability and to try predicting whether clusters form inside the aggregates, thus proving that network theory is capable of producing accurate models of different states of rubble-pile asteroids. A similar approach has not been found to have been applied to the case of asteroid dynamics or structural stability. This work tries to understand whether there are benefits in applying network theory to a complex environment such as an asteroid. The main steps and contributions of the thesis are as follows:

1. The rubble-pile system is encoded as a graph, with nodes representing the grains, and edges the relationships between them. This abstraction allows for the application of topological and statistical tools from network science.
2. Create (dis)similarity metrics of the bodies that make up the rubble-pile. These are based on the physical properties (energy, contact force, contact pairs, gravitational attraction, distance, angular momentum) and dynamical states of each particle in the system, and they account for the dynamical evolution of the system.
3. Incorporating the similarities matrices in the network-theory-specific metrics, and analysing if they offer a good representation of the dynamical systems.
4. Apply clustering methods. The cluster sizes and distribution are analysed in time and their results are compared to the results obtained from the network metrics.
5. Considering the clusters already observed, a simple prediction algorithm is created to check if it is possible to anticipate the creation of clusters, assuming just the network's initial configuration, which could serve as a foundation for more extensive simulations relating asteroid research.

The specific research questions that this thesis addresses are the following:

- How can rubble-piles be represented as networks of interconnected particles and what are similarities metrics that can be used to create a network?
- What information can specific network metrics offer on the stability of rubble piles?
- How does the evolution of the rubble pile affect the evolution of the network?
- What are the clustering methods that could be of interest in the evolution of the rubble piles?
- Is percolation a suitable method for predicting possible changes in the structure of the rubble pile?

After the present introductory chapter, the thesis is structured as follows:

- Chapter 2 introduces the theoretical background of gravitational aggregates, including contact dynamics, as well as the foundational concepts of graph theory and network theory.
- Chapter 3 details the numerical methods and simulation setup used to model the dynamics of the rubble pile and generate the corresponding network structures.

- Chapter 4 presents the results of the study, including the evolution of the network, the clustering behaviour, and the performance of the prediction algorithm.
- Chapter 5 summarises the conclusions of the thesis and discusses potential future improvements, limitations, and further applications of the proposed methodology.

2 | Theoretical Background

This section is divided into two parts. The first part outlines the key physical and mathematical foundations used in the simulations of rubble-pile asteroids, focussing on the contact dynamics between constituent bodies. The second part focusses on the fundamental mathematical definitions used to describe the network and apply its metrics to the system.

2.1. Theory on dynamical systems representing rubble piles

Each system representing a rubble pile is composed of several bodies that interact between them via short-range forces, such as mechanical contact, or long-range forces, such as gravitational attraction. The dynamic behaviour of each body can be generally defined through the following system of equations:

$$\begin{cases} \dfrac{\partial^2 \boldsymbol{r}_i}{\partial t^2} = \dfrac{1}{m_i} \boldsymbol{F}_i(\boldsymbol{r}_j, \dot{\boldsymbol{r}}_j, \boldsymbol{\varphi}_j, \dot{\boldsymbol{\varphi}}_j) \\ \dfrac{\partial^2 \boldsymbol{\varphi}_i}{\partial t^2} = \dfrac{1}{\hat{J}_i} \boldsymbol{M}_i(\boldsymbol{r}_j, \dot{\boldsymbol{r}}_j, \boldsymbol{\varphi}_j, \dot{\boldsymbol{\varphi}}_j) \end{cases} \tag{2.1}$$

On each particle i, of mass m_i, there is a force F_i and a torque M_i, which is a function of position $\boldsymbol{r}_j$, velocity $\dot{\boldsymbol{r}}_j$, angular orientation $\boldsymbol{\varphi}_j$ and angular velocity $\dot{\boldsymbol{\varphi}}_j$.

In a gravitational aggregate, the classical Newton law is dominant on a large scale, representing the interaction each body undergoes under the gravitational pull of the remaining N-1 bodies.

$$m_i \ddot{\boldsymbol{r}}_{\boldsymbol{i}} = G \sum_{j=1, j \neq i}^{N} \frac{m_i m_j}{|\boldsymbol{r}_{ij}|^3} \boldsymbol{r}_{ij} \tag{2.2}$$

The system is considered to be in a fixed absolute reference frame. Usually, in the case of rubble piles, it is of particular interest to investigate a system that has a predefined

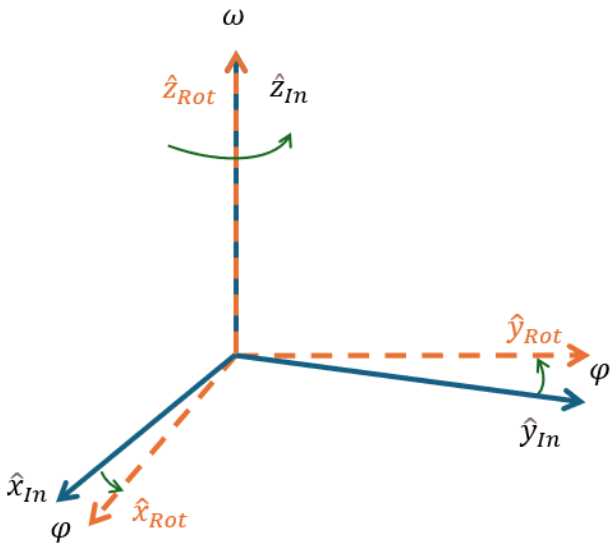

Figure 2.1: Representation of a rotating reference frame (orange) with respect to an inertial reference frame (blue).

orbital angular momentum about origin O. In this case, all bodies rotate about O with a constant angular momentum. Therefore, the system presented in Equation (2.2) can be represented by considering a second rotating reference frame with angular velocity $\dot{\varphi}$, fixed to the centre of the system, whose rotation is calculated with respect to the first fixed reference frame.

$$m_i\ddot{\boldsymbol{r}}_{\boldsymbol{i}} = G\sum_{j=1,j\neq i}^{N}\frac{m_i m_j}{|\boldsymbol{r}_{ij}|^3}\boldsymbol{r}_{ij} - m_i\dot{\boldsymbol{\varphi}}\times(\dot{\boldsymbol{\varphi}}\times\boldsymbol{r}_i) - 2m_i\dot{\boldsymbol{\varphi}}\times\dot{\boldsymbol{r}}_i \tag{2.3}$$

with $\boldsymbol{r}_i$ representing the position vector of the centre of mass of body i with respect to the centre of the system, while m_i represents its mass, $G = 6.674\times10^{-11}$ is the universal gravitational constant and $\mathbf{r}_{ij} = \mathbf{r}_i - \mathbf{r}_j$, the distance vector between body i and body j. Therefore, the dynamic states of the two bodies depend solely on their masses and positions, and for bodies with equal masses, the attraction forces imposed by each body on its pair have the same absolute value. On a smaller scale, when contacts occur, bodies interact in a different manner, undergoing a state change based on their physical properties, in particular material, and its attributes, such as friction coefficient (μ), Young modulus (Y) or Poisson ration (ν).

A contact is said to take place, that is, two particles are in mechanical contact when the mutual compression of bodies i and j is:

$$\xi_{ij} \equiv R_i + R_j - |\boldsymbol{r}_i - \boldsymbol{r}_j| > 0 \tag{2.4}$$

Equation (2.4) says that two bodies are in contact only when the sum of their local radius, R_i and R_j, is greater than the distance between them and for this ξ is the deformation of the two bodies. For each pair of bodies, the associated contact force is zero if the previous expression is not fulfilled; otherwise it is composed of two components, a normal and tangential part, and can be written in the form:

$$\boldsymbol{F_{ij}} = F_{ij}^n \boldsymbol{e}_{ij}^n + F_{ij}^t \boldsymbol{e}_{ij}^t \tag{2.5}$$

where $\boldsymbol{e}_{ij}^n = \frac{\boldsymbol{r}_i - \boldsymbol{r}_j}{|\boldsymbol{r}_i - \boldsymbol{r}_j|}$, is the unit vector in the normal direction and similarly e_{ij}^t is the unit vector perpendicular to the contact direction. The previous force is concentrated at the point of contact and is not spread over an area. Both components of the contact force can be expressed as functions of the properties of the material. The velocity of each particle acting in the contact depends on the coefficient of restitution, which defines if a contact is elastic. The coefficient of restitution, Equation (2.6), is independent of the contact velocity, is a characteristic of the material, and cannot be constant because it violates the theory of viscous bodies, [38]. It is a good representation of the energy dispersed during the contact of each body.

$$\varepsilon_{restituion} = \frac{\dot{r}_{i_{after}}}{\dot{r}_{i_{before}}} = exp\left(-\frac{\pi\gamma^n}{2m^{eff}} \Big/ \sqrt{\frac{Y}{m^{eff}} - \left(\frac{\gamma^n}{2m^{eff}}\right)^2} \right) \tag{2.6}$$

where $\dot{r}_{i_{after}}$ is the velocity of the particle i after the contact and $\dot{r}_{i_{before}}$ is the velocity before the contact. The generalised formula for the damped viscoelastic contact takes the form:

$$F^n = \frac{2Y\sqrt{R^{eff}}}{3(1-\nu^2)}(\xi^{\frac{3}{2}} + A\sqrt{\xi}\frac{d\xi}{dt}) \tag{2.7}$$

In Equation (2.7) A, known as the dissipative constant, it is a function of the viscosity of the material and is related to the rolling friction coefficient. The point of contact is approximate, as there is compression present ξ of the contact spheres, which implies either a contact surface or a contact line. The relative velocities of the spheres at the point of contact are the result of the relative velocities of the two spheres and their rotations:

$$\dot{r}_{rel}^t = (\dot{\boldsymbol{r}}_j - \dot{\boldsymbol{r}}_i) \cdot \boldsymbol{e}_{ij}^t + R_i\dot{\varphi}_i + R_j\dot{\varphi}_j \tag{2.8}$$

A widely used formula for the definition of the shear force is the following:

$$F^t = -sign(\dot{r}_{rel}^t) \cdot min(\gamma^t||\dot{r}_{rel}^t|, \mu|F^n|) \tag{2.9}$$

As it can be observed from Equation (2.9), the shear force is upper limited by Coulomb's friction law:

$$|F^t| \leq \mu |F^n| \tag{2.10}$$

where μ is the friction coefficient. The contact model assumes that the contact area during the collision is small with respect to the size of the colliding bodies.

Other contact models for granular media have been proposed and are presented in [38], such as the case in which the contact particles are made of different materials, which will not be further presented here. In [2, 34] an iterative method is presented to simulate mechanical systems that contain a large number of contacts and joints between rigid bodies, presenting the physical model and its implementation.

In addition to translational damping, rotational damping and rolling resistance are crucial components in accurately simulating the behaviour of granular aggregates. The rolling resistance accounts for the torque that opposes the relative rolling motion of two contact bodies. It is typically modelled as a torque proportional to the rolling angular velocity and depends on the material-specific rolling friction coefficient. This additional damping mechanism contributes to energy dissipation and affects the final stable configurations of the aggregate.

Based on the coefficient of restitution selected during simulations, the problem can become smooth, for elastic collision types, or non-smooth, for fully inelastic collisions. The model chosen further in the simulations will have an impact on the setup and on the results, as a smooth-contact model (SMC) takes into consideration the force penalties but needs a carefully chosen time step to ensure the stability of the simulation. This critical time step ensures that the particles do not unrealistically penetrate each other or induce numerical instabilities. In the case of non-smooth contact system (NSC), the problem becomes a differential variational inequality (DVI) [15], and is solved accordingly by solving the cone complementarity problem (CCP), which is a challenging numerical problem. As opposed to the smooth-contact case, non-smooth methods use implicit time-stepping schemes and solve complementarity problems, allowing for larger time steps but at the cost of increased computational complexity.

Although in the case of spherical bodies, the orientation of each body is not crucial in the final state of the system, in the case of convex hulls, it plays a significant role in the aggregate structure as it affects its porosity.

Finally, starting from Equation (2.3), and accounting for the contacts. The physical system can be defined by a system of equations, taken in an inertial reference frame

centred at the system barycenter of each individual body, as follows:

$$m_i \ddot{\boldsymbol{r}}_i = -G \sum_{j=1, j\neq i}^{N} \frac{m_j}{r_{ij}^3} + \sum_{k \in K} (\boldsymbol{F}_{ik}^n + \boldsymbol{F}_{ik}^t) \tag{2.11}$$

$$\boldsymbol{I}_i \dot{\dot{\boldsymbol{\varphi}}}_i = -\dot{\boldsymbol{\varphi}}_i \times (\boldsymbol{I}_i \dot{\boldsymbol{\varphi}}_i) + \sum_{k \in K} T_{ik} \tag{2.12}$$

where m_i, $\boldsymbol{I}_i$, $\boldsymbol{r}_i$, and $\dot{\boldsymbol{\varphi}}_i$ are the mass, inertia tensor, position, and angular velocity of body i, while $\boldsymbol{T}$ is the torque of the particle due to collisions off-centre and other contact-related torques such as rolling and spinning resistance.

As the system evolves in time, so do its variables, and therefore there is a change in energy and angular momentum of the system. Scheeres [50] considers for the calculations of the minimum energy stable states, the mutual gravitational potential between two bodies $\mathcal{U}_{ij}$, the self-potential $\mathcal{U}_{ii}$ and the moment of inertia of the sphere of mass m_i and radius R_i, I_{H_i}.

$$\begin{cases} \mathcal{U}_{ij} = -\dfrac{G m_i m_j}{r_{ij}} \\ \mathcal{U}_{ii} = -\dfrac{3 G m_i^2}{5 R_i} \\ I_{H_i} = \dfrac{2 m_i R_i^2}{5} \end{cases} \tag{2.13}$$

Other elements that are considered in the stability of a rubble pile are kinetic energy K_i and rotational kinetic energy K_{rot_i}.

$$K_i = \frac{1}{2} m_i v_i^2 \tag{2.14}$$

$$K_{rot_i} = \frac{1}{2} I_i \dot{\varphi}_i^2 \tag{2.15}$$

The angular momentum of the system is important in describing the evolution of the system with time:

$$H = \sum_{i}^{N} r_i \times m_i \dot{r}_i \tag{2.16}$$

In Equation (2.15) I_i is the moment of inertia around the axis of rotation and $\dot{\varphi}_i$ is the

angular velocity of the body i. For each body i, its total energy is the sum of all the energies presented above:

$$E_i = K_i + K_{rot_i} + U_{ij} + U_{ii} \tag{2.17}$$

while the total energy of the system is the sum of the energies of all the bodies included in the system $E = \sum_{i=1}^{N} E_i$, where N is the total number of bodies. An important aspect relating the energies in a system representing a gravitational aggregate is that of escape energy, and subsequently the escape velocity. Considering a stable gravitational aggregate, the bodies are positioned such that only a unique compacted gravitational aggregate exists. The escape energy, defined through the escape velocity Equation (2.18), is the energy needed by a body i to escape the potential attraction of all other $N-1$ bodies, and detach itself from the main gravitational aggregate. In cases when more bodies have large kinetic energies, they can all escape and regroup afterwards, in a secondary aggregate, or similarly the asteroid can get divided into several groups of bodies, until an equilibrium state is reached. This is correlated with the initial angular velocity of the system.

$$\dot{r}_{esc} = \sqrt{\frac{2G\sum_i^N m_i}{r_i}} \tag{2.18}$$

As the initial velocity of each particle depends on the angular velocity of the aggregate and the position with respect to the barycentre, $\dot{r}_i = \dot{\varphi}_i \times r_i$, the velocity to escape from the gravitational pull of the aggregate depends on the position of the particles, as it considered a uniform angular momentum for the entire system of particles. Therefore, it can be concluded that there is a certain limit for the angular momentum above which the velocities of the particles are too large and the aggregate starts to disintegrate. In [42] Leinhardt et al. show that the critical spin period, $P_{crit}(\epsilon, \rho)$, for a rubble pile, depends on its density, ρ, and ellipticity, ϵ, and is defined by Equation (2.19). Another possibility is to consider the critical period based solely on the density [24], and to neglect the ellipticity, as in case of spherical or almost spherical bodies, the critical period becomes very large, $P_{crit} \to \infty$.

$$P_{crit}(\epsilon, \rho) \simeq \frac{1}{1-\epsilon}\sqrt{\frac{3\pi}{G\rho}} \tag{2.19}$$

The critical period is calculated in hours, with those rubble piles that have a spin period smaller than their critical one, (higher angular velocity), disaggregating. When this condition is met, at least some bodies that form the rubble pile have an energy large enough to escape the gravitational attraction force applied by the rest of the N-1 bodies.

Amended potential or the minimum energy function is a parameter implemented in

[1, 45, 50] that describes the interaction between bodies in N-body dynamics systems, incorporating the importance of granularity of the system.

$$\varepsilon = \frac{H^2}{2I_h} + U \leq E \tag{2.20}$$

where H is the angular momentum, Equation (2.16), I_h the moment of inertia along the angular momentum vector, U is the gravitational potential energy, defined in Equation (2.13), and E is the total energy of the system. As energy is lost through contacts, it was shown that an equilibrium state is reached when $\varepsilon = E$. Therefore, the amended potential ε is an important parameter in describing the granularity of the N-body system.

2.2. Network Theory

2.2.1. Background on Graph Theory

A network is based on graph theory, which focusses on analysing the pairwise relationships between the components of the system, in the present case the bodies composing the rubble pile. In real-term applications, a network sometimes is defined as a graph, whose nodes or edges have assigned attributes which define the respective node, such as names.

A *graph* $G = (V, E)$ is a mathematical structure consisting of a set V of vertices (nodes) and a set E of edges (links). A *complete* graph is a graph in which each vertex is connected with every other vertex by exactly one edge. An *unweighted* graph is a graph whose edges are not assigned any value. In this paper, the *directed graphs* will not be used, as the direction of edges between graphs is not taken into consideration. Attention will be paid to the existence of edges between nodes and the weights of the existing edges.

In the context of graph theory, the neighbourhood of a vertex v contains all adjacency vertices, which are the vertices connected through an edge to v. In Figure 2.2 the vertices adjacent to 4 are 5, 1, and 3. For a large finite graph, all the relationships between vertices, meaning the presence of edges and their respective weights are saved in the *adjacency matrix*, *adjacency list*, and the *incidence matrix*. The adjacency matrix is a square matrix $N_v \times N_v$, with N the number of vertices present in the graph. As only undirected graphs are considered, $\mathbf{A}$ is a squared matrix with $A_{ij} = A_{ji}$ that takes the form:

$$A_{ij} = \begin{cases} 1, \text{if } \exists\ e_{ij} \in \text{E} \\ 0, \text{otherwise} \end{cases} \tag{2.21}$$

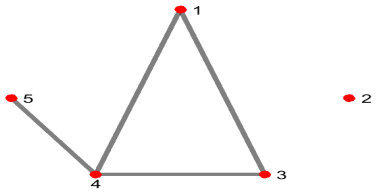

Figure 2.2: Representation of an undirected graph.

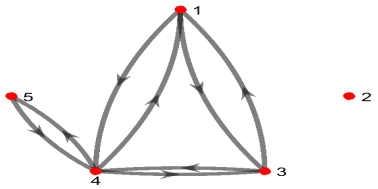

Figure 2.3: Representation of a directed graph, equivalent to that presented in Figure 2.2.

Similarly, *undirected* graphs, can be considered as a directed graph, with a pair of exactly 2 edges between any vertex, with opposite directions and equal weights, as shown in Figure 2.3. An example of an adjacency list is given for G in Table 2.1.

Vertex	Neighbors
1	3,4
2	
3	4,1
4	5,1,3
5	4

Table 2.1: Adjacency list example.

Different types of graph exist according to the structure and the edge configuration. A graph without self-edges, *loops*, $A_{ii} = 0 \; \forall \; i \in V$, is called simple. A *multigraph* is a graph that allows multiple edges between any $v_i, v_j \in \mathbf{V}$, called parallel edges. A *pseudograph* is a multigraph that allows the presence of loops.

For an unweighted graph, the *degree* of a vertex is the number of edges that are incident to it, with the vector d_v containing the degrees of each vertex. The degree can be calculated by summing by column or by row, due to symmetry, all the elements of the matrix $\mathbf{A}$:

$$d_i = \sum_j A_{ij} \tag{2.22}$$

The degree of a graph is then given by the maximum value in d_v. In the case of weighted graphs, the degree takes the name of strength, and it will be calculated using Equation (2.22), even if some authors may use different methods to calculate the degree of a vertix in a weighted graph.

The matrix defined through

$$\mathbf{L} = \mathbf{D} - \mathbf{A} \tag{2.23}$$

is called the *Laplacian* of graph G, where $\mathbf{D} = diag[(d_i) - i \in V]$ is the diagonal matrix that contains the degrees of the graph. The Laplacian is an important attribute of the graph as it offers information on the structure and how connected a graph is, or better, how easy it is to disconnect the graph in different disconnected subgraphs. *Subgraphs* are subsets of the main graph. They are marked as $G' = (V', E')$ with $V' \in V$ and $E' \in E$ and each incident vertex of an edge in E' is part of V'. Thus, a set of all subgraphs of the graph can be considered $\mathcal{P}(G')$ as done by T. Schank [49].

A *path* in a network is any sequence of vertices such that every consecutive pair of vertices in the sequence is connected by an edge in the network [33]. If for any two vertices of the graph, there is no path connecting them, the graph is said to be *disconnected*, otherwise it is called *connected*. The disconnected subgroups of the graph are called *components*. For example, in the previous example, Table 2.1, the vertex 2 has no incident edge, and thus the graph is disconnected with the two components being formed $G'_1 = (V'_1, E'_1)$ and $G'_2 = (V'_2, E'_2)$, with $V'_1 = \{1, 3, 4, 5\}$ and $V'_2 = \{2\}$.

2.2.2. Centrality

Another important aspect of graphs that should be considered is that of *centrality*. The centrality factor sorts the vertices based on their importance or how central are they in the graph. However, there are different definitions on which this factor is based, as the importance can be defined in different ways. The most used definitions are presented hereafter, and are applied to the graph G presented above:

- *Degree centrality*: this method is based on the degree of each vertex, as the vertex importance in the graph is given based on its degree, calculated using Equation (2.22).
- *Eigenvector centrality*: this method is build up on the degree centrality, but besides considering only the importance of the vertex itself, it also takes into account the importance of its neighbours in the network.

  $$\mathbf{A}\mathbf{x} = k_1\mathbf{x} \tag{2.24}$$

  where $\mathbf{A}$ is the adjacency matrix, $\mathbf{x}$ is the right leading eigenvector of $\mathbf{A}$ and the optimal value of k_1 is considered to be the largest eigenvalue [28, 33].
- *PageRank centrality*: this method limits the influence of a vertex with high centrality

may have on the centrality of neighbouring vertices, by dividing the degree of the vertex with the out-degree.

$$x_i = \alpha \sum_j A_{ij} \frac{x_i}{k_j^{out}} + \beta \tag{2.25}$$

In the case of having $k_i^{out} = 0$, this is artificially set to 1, to avoid the indeterminate solution as it does not change the solution. Equation (2.25) can be written in matrix form as:

$$\mathbf{x} = \beta(\mathbf{I} - \alpha\mathbf{A}\mathbf{D}^{-\mathbf{1}})^{-1} \cdot \mathbf{I}_{N\times 1} \tag{2.26}$$

where $\mathbf{D}$ is a diagonal matrix with elements $D_{ii} = max(k_i^{out}, 1)$, α and β being positive constants, $\mathbf{I}$ is the identity matrix and $\mathbf{I}_{N\times 1}$, is the vector $(1, 1, 1, 1, ..)$. If it is considered that $\beta = 1$, Equation (2.26) becomes

$$\mathbf{x} = \mathbf{D}(\mathbf{D} - \alpha\mathbf{A})^{-1}\mathbf{I}_{N\times 1} \tag{2.27}$$

- *Closeness Centrality*: this method measures the mean distance from a vertex to other vertices. However, as this method assigns the higher importance to the lower value of centrality, as opposed to the other methods, another definition has been set in practice in which the lower the centrality, the lower the importance of the vertex. This inverse is called the closeness centrality C_i:

$$C_i = \frac{1}{l_i} = \frac{n}{\sum_j d_{ij}} \tag{2.28}$$

where d_{ij} is the length of the shortest path between vertices i and j, and in an undirected graph $d_{ij} = d_{ji}$. However, it must be mentioned that while some authors consider that $i \neq j$ [28, 43], M.E.J. Newman [33] explains the difference between the two cases and their influence on the results. The graph must be connected for this method to be viable as otherwise, the distance between disconnected vertices is consider to be ∞ and all the vertices will have $C_i = 0$. In the case of disconnected graph, the Closeness Centrality can be nevertheless used, but instead of applying it to the entire system, it is applied to each separate component.

- *Betweenness Centrality*: this concept measures the extent to which a vertex lies on the path between any other vertices. The most common formulation of betweenness centrality is:

$$C_i = \sum_{s\neq t\neq v\in V} \frac{\sigma(s, t|v)}{\sigma(s, t)} \tag{2.29}$$

where $\sigma(s,t|v)$ is the total number of shortest paths between s and t that pass through v, and $\sigma(s,t)$ is the total number of paths that exist in the network between s and t. Similar to the previous method, a condition must be imposed when the graph is disconnected. The convention adopted sets the fraction inside the sum $\frac{\sigma(s,t|v)}{\sigma(s,t)} = 0$ if both $\sigma(s,t|v)$ and $\sigma(s,t)$ are zero.

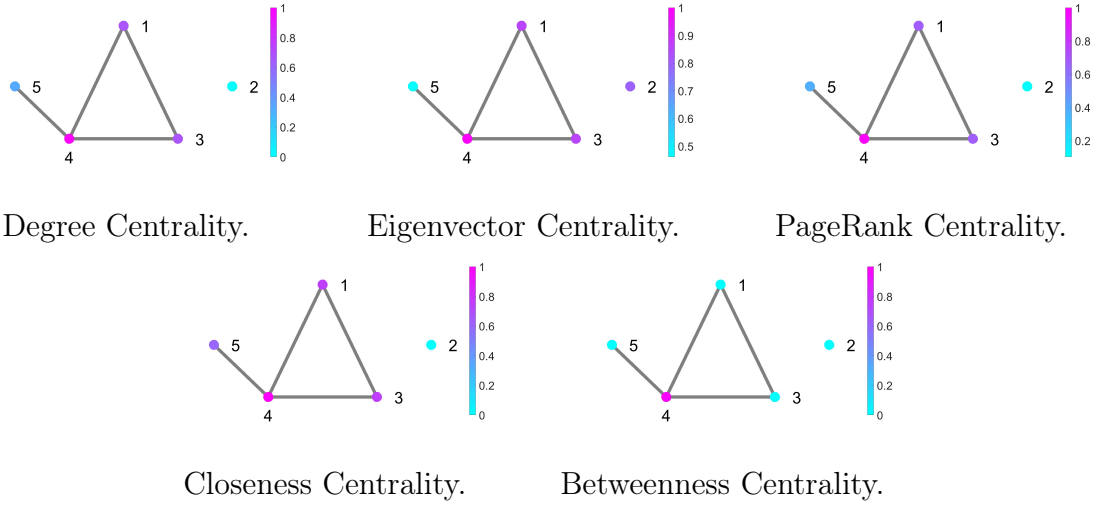

Figure 2.4: Visual representation of centralities methods applied to the graph G presented in Figure 2.2, showing the differences in assigning the importance between methods. The color of the node represents the importance assigned to it through that specific Centrality measure.

2.2.3. Clustering Coefficient

The *clustering coefficient* measures the average probability that two neighbours of a vertex are themselves neighbours and it provides a measure of the density of connections between neighbouring vertices.

$$c = \frac{(\text{number of triangles}) \times 3}{(\text{number of connected triples})} \tag{2.30}$$

Now also the local clustering can be defined as:

$$c_i = \frac{(\text{number of pairs of neighbours of i that are connected})}{\text{number of pairs of neighbours of i}} \tag{2.31}$$

Structural holes (Figure 2.5) [33] are missing links in a triangle, meaning that the two neighbours of vertex i are not connected between them. Therefore, in a triangle of the form ijk, with edges ij and ik and a structural hole between the nodes j and k, the connection between the latter two nodes will be made through node i. The local clustering coefficient

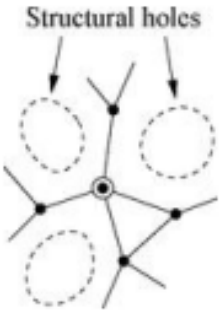

Figure 2.5: Structural Holes. [33]

measures the influence of the node i in the network, as it can regulate the flow that passes through it. For example, considering the case shown in Figure 2.2, v_1 and v_3 will have the largest clustering coefficient, as they are part of the same triangle and are connected to v_4. The local clustering coefficient c_i can be calculated as a function of the redundancy R_i of a node i, which is the mean number of edges between two neighbours of i:

$$c_i = \frac{\frac{1}{2}D_i R_i}{\frac{1}{2}D_i(D_i - 1)} \tag{2.32}$$

This expression can be further written in terms of the elements of $\mathbf{A}$ as follows:

$$c_i = \frac{2}{D_i(D_i - 1)} \sum_{j \neq k}^{n} \sum_{k}^{n} a_{ij} a_{ik} a_{jk} \tag{2.33}$$

where the double sum corresponds to the number of triangles connected to node i. In this case, the triangle was considered, which is the cycle that contains the minimum number of edges; however, cycles with a larger number of edges can be considered for the calculation of c_i.

2.2.4. Graph Partitioning

An important aspect of networks lies in the cohesion properties of the respective network. As there is no unique definition for a cohesive network, it usually focusses on the presence of different aspects of the graph, such as *triads*, *giant components*, *cliques* or *communities*. Partitioning is the method through which a graph undergoes a segmentation process into 'natural' subsets, being a method determining the network's cohesiveness. Such subsets are usually well connected between them and are relatively distinguished from the remaining vertices.

Let $G = (V, E)$ be an undirected graph and let $\mathcal{C} = \{C_1, C_2, \ldots, C_K\}$ be a partition of the vertex set V, such that each $C_k \subseteq V, C_k \cap C_{k'} = \emptyset$ for $k \neq k'$, and $\cup_{k=1}^{K} C_k = V$. The goal of the partition is to ensure that, for each subset $C_k \in \mathcal{C}$, the number of intra-cluster edges (edges with both ends in C_k) is greater than or equal to the number of inter-cluster edges connecting C_k to any other subset C_j with $j \neq k$. Formally:

$$|E(C_k, C_k)| \geq |E(C_k, C_j)| \quad \forall j, k \quad s.t. \quad j \neq k, \tag{2.34}$$

This condition encourages dense connectivity within clusters and sparse connectivity between clusters, which aligns with the notion of community structure of graphs.

In the following part, three methods will be presented, while the others will just be mentioned as there are several documents that assess their performances and applicability [48].

1. *Hierarchical Clustering*: It is a method which takes a greedy approach, to searching the space of all possible partitions $\mathcal{C}$, by iteratively modifying successive candidate partitions. In a multistep process, at each step the current candidate partition is modified in such a way to minimize the considered cost. The measure of cost reflects the most suitable attribute assigned to the network to represent a 'cohesive' subset of vertices. Therefore, in most cases the measure is the (dis)similarity between pairs of vertices v_i, $v_j \in V$. The (dis)similarity can be measured as the Euclidean distance:

$$x_{ij} = \sqrt{\sum_{k \neq i,j} (A_{ik} - A_{jk})^2} \tag{2.35}$$

   Here $\mathbf{A}$ is the adjacency matrix, and x_{ij} measures the standard Euclidean distance between rows i and j. Another way of measuring the (dis)similarity x_{ij} for vertices v_i and v_j is:

$$x_{ij} = \frac{|\mathcal{N}_{v_i} \triangle \mathcal{N}_{v_j}|}{d_{N_v} + d_{(N_v - 1)}} \tag{2.36}$$

   where $\mathcal{N}_v$ is the set of neighbours of vertex v, $\triangle$ indicates the symmetric difference between two sets, and $d_{(i)}$ is the i-th smallest element in the degree sequence.

2. *Spectral Partitioning*: It is a method that exploits the characteristics of graph theory, and creates a graph partitioning based on the eigen-analysis of the network's graph adjacency matrix or Laplacian matrix, defined in Equation (2.23). Thus, this

method is expressed through the equations:

$$\mathbf{A}\mathbf{x}_i = \lambda_i \mathbf{x}_i \tag{2.37}$$

$$\mathbf{L}\mathbf{x}_i = \lambda_i \mathbf{x}_i \tag{2.38}$$

where, $\mathbf{A}$ is the adjacency matrix, $\mathbf{L}$ is the Laplacian matrix, λ_i are the eigenvalues, and $\mathbf{x}_i$ are the corresponding eigenvectors of each matrix. In spectral graph, a K connected component is present if and only if there are k-eigenvalues such that $\lambda_1(\mathbf{L}) = ... = \lambda_k(\mathbf{L}) = 0$ and $\lambda_{k+1}(\mathbf{L}) > 0$. In several cases, the spectral clustering is taken as an iterative process [28, 33], in which each connected component of the graph is bisected. For this cases, λ_2 of each component, carries the largest importance, as it is the second largest eigenvalue, $\lambda_2 \neq 0$. That is $\mathbf{x}_2$, known as the *Fiedler vector* [17], is the partitioning limit of the component, into two sets:

$$S = \{v \in V : \mathbf{x}_2 \geq 0\} \quad \text{and} \quad \bar{S} = \{v \in V : \mathbf{x}_2 < 0\} \tag{2.39}$$

3. *Markov Chain Clustering* [12] : This process starts from the adjacency matrix $\mathbf{A}$. Optionally, the graph is simple, loops are added to the adjacency matrix [54].

$$\mathbf{A}_1 = \mathbf{A}_0 + \alpha\mathbf{I} \tag{2.40}$$

The lower index represent the new form of the matrix after each step. In Equation (2.40) $\mathbf{A}_0$ is the initial adjacency matrix and $\mathbf{A}_1$ is the adjacency matrix including the loops. If $\mathbf{A}_0$ contains largely very small numbers of the order 10^{-3} or smaller, adding the identity matrix would result in a matrix $\mathbf{A}_1$ with the majority of its terms on the main diagonal, which is undesirable. Thus, a term α was considered to account for this effect, and regularize the differences in the orders of magnitude. Moreover, if the graph has disconnected components, representable in the adjacency matrix as $A_i = [0, 0, ...0]$, it is a good practice adding the identity matrix, otherwise this step is optional. Afterwards, the matrix is normalised and expanded by raising it to the e^{th} power.

$$\mathbf{A}_2 = \mathbf{A}_1^e \tag{2.41}$$

Each term of the resulting matrix is inflated with the parameter r, a_{ij}^r:

$$\mathbf{A}_3 = \begin{bmatrix} a_{11}^r & a_{12}^r & \cdots & a_{1n}^r \\ \vdots & \vdots & \ddots & \vdots \\ a_{n1}^r & a_{n2}^r & \cdots & a_{nn}^r \end{bmatrix} \tag{2.42}$$

The expansion and inflation processes are repeated until the matrix reaches convergence. In this case, the values of r and e are chosen based on the desired result.

In the literature, there are cases where after the implementation of one of the previously presented methods, a second clustering analysis is performed on the obtained results to refine them or settle the points of cluster overlapping.

2.2.5. Percolation Theory

Percolation is the process of removing some fractions of the vertices, or the edges connecting those vertices from the network. It is a fundamental model in statistical physics that analyses the possible fragmentation of the network. There are many examples that use percolation, such as internet reliability, disease spread, and the phenomenon of vaccination or immunisation of individuals against the spread of disease. The percolation methods are of two types:

- Site or vertex percolation, which removes vertices from the network.
- Bond or edge percolation, which removes the edges that connect any two vertices in the network. As edges are progressively removed, the structure of the graph changes, eventually leading to fragmentation, where the network loses its global connectivity.

For any undirected graph $G = (V, E)$, edges can be removed:

- Uniformly at random
- Based on probabilistic rules, such as node degree, weighted by traffic, flow or any other dynamic metric associated to the respective edge.

In a general case, the percolation process for a biased probabilistic method is considered based on the degrees and weights. Each edge is subject to removal according to a predefined probability or mechanism. The process can be static (when all selected edges are removed all at once) or dynamic (edges are removed sequentially during a process such as a random walk or flow simulation).

Consider $p \in [0, 1]$, be the retention probability of an edge. In classical percolation, each

edge $e \in E$ is retained independently with probability p and removed with probability $1-p$. As p decreases, the structure of the graph changes, potentially leading to fragmentation into disconnected components.

One of the key concepts in percolation theory is the percolation threshold, denoted p_c, and is the critical edge density at which a giant connected component (GCC) of the graph disappears or appears; below p_c the network breaks down into small disconnected subgraphs. The percolation threshold depends largely on the type of network and its characteristics. In a random tree-like network without degree-degree correlation, the threshold is $p_c = \frac{1}{g_1'(1)}$, where $g_1(z)$ is the generating function corresponding to the excess degree distribution. Therefore, for random Erdos-Renyi networks of average degree $\langle k \rangle$ (also known as the first moment of the network), the percolation threshold becomes $p_c = \frac{1}{\langle k \rangle}$. Similarly, in networks with a low clustering coefficient $0 < C \ll 1$, the threshold becomes $p_c = \frac{1}{1-C}\frac{1}{g_1'(1)}$. Near the percolation threshold, various observables exhibit critical behaviour characterised by scaling laws.

As stated earlier, edges can be eliminated on the basis of a random-walk model. For a graph, considering a walker located at node $v_t \in V$ moves to a neighbouring node $v_{t+1} \in \mathcal{N}(v_t)$, where $\mathcal{N}(v_t)$ is the set of neighbours of v_t. In the simple (uniform) random walk, the walker selects the next node uniformly at random:

$$\mathbb{P}(v_{t+1} = u \quad | \quad v_t = v) = \frac{1}{deg(v)} \quad if(v,u) \in E \tag{2.43}$$

However, in many applications, the transitions are not uniform, as in the case of weighted graphs, and the probability of moving from node i to node j is:

$$\mathbb{P}(v_{t+1} = j \quad | \quad v_t = i) = \frac{w_{ij}}{\sum_{k \in \mathcal{N}(i)} w_{ik}} \tag{2.44}$$

Equation (2.44) reflects a biased (weighted) random walk that presents certain preferences, capacities, or connection strengths between nodes, and thus in the random walk process certain edges are preferred, having a higher probability of being chosen and therefore having a greater influence on the final result [30].

2.3. Monte Carlo method

Monte Carlo processes are based on random number generators, producing an infinite stream $U_1, U_2, U_3, ...Dist$ of a random variables that are independent and identically distributed according to some probability distribution $Dist$. It is a numerical simulation

method that is used to derive the statistical properties of a system's output. A Monte Carlo process estimates the properties of a highly complex probability distribution $p(x)$, by solving Equation (2.45).

$$E[f(x)] = \int h(x)p(x)dx \tag{2.45}$$

where h is supposed to be a useful function for the estimation. However, h cannot be achieved analytically, and the problem is solved by using an approximation of indirectly generated random samples N from the distribution p. Therefore, Equation (2.45) is approximated by using point masses and it becomes:

$$E[f(x)] \approx E_N[f(x)] = \frac{1}{N}\sum_{i=1}^{N}\overline{h}(x_i) \tag{2.46}$$

For the present work, the Monte Carlo process with respect to its applicability to Markov Chains will be presented: "A Markov chain is a stochastic process $X_t, t \in \mathcal{T}$" with a countable index set $\mathcal{T} \subset \mathbb{R}$ which satisfies the Markov property [30]:

$$(X_{t+s}|X_u, u \leq t) \sim (X_{t+s}|X_t) \tag{2.47}$$

The Markov Chain process can be represented through the transition probabilities matrix $P = (p_{ij})$, where

$$p_{ij} = \mathbb{P}(X_{t+1} = j|X_t = i), \quad i, j \in E \tag{2.48}$$

where E is the discrete state space, X_t and X_{t+1} are random variables representing the state of the system at time t and $t+1$, respectively [30]. There are several applications in which the Monte Carlo and Markov Chains processes have been applied to graphs and networks, analysing the network reliability, and have been presented in [30, 36].

3 | Methodology

This chapter presents a step-by-step implementation of the theoretical framework described previously. It begins with the generation of rubble pile aggregates, followed by their transformation into asteroid shapes and rescaling. The initial conditions and physical parameters for the simulations are described below. The generated data are then analysed as networks modelled in a well-defined way, and finally the clustering methods are used to get insights on the dynamical behaviours.

3.1. Rubble Pile Aggregation

The main steps for creating the rubble pile and generating the data are:

- An initial gravitational aggregate of large stable rubble pile is created.
- From the initial aggregate, asteroids were modelled in the shapes of interest by cutting out the outer particles.
- The created desired shaped are analysed through their time evolution based on different initial data.

Similarly to the setup implemented in [13], GRAINS software [16] was used, which is fully integrated in Chrono Project Engine (C:E), a multi-physical simulation tool for granular materials [2, 53]. GRAINS is preferred because it allows the creation of more complex shapes, such as polyhedra, which create a more reliable modelling of particle interactions.

For this, GRAINS is capable of implementing both the non-smooth model (NSC) and the smooth/soft-sphere model (SMC), explained in Chapter 2.1. The process of creating the initial gravitational aggregate and the cut-out shapes is the same as the one implemented by Fodde and Ferrari [18]. The first step of the simulation is to generate a data set. For this, a large aggregate is created, by simulating 10 000 randomly generated particles, which was done for several cases:

1. Spherical particles with equal sizes and the same body properties.

2. Convex hulls with the same sizes and the same body properties.

For the simulation setup, two assumptions were made regarding the properties of the particles modelled. Firstly, it was assumed that a homogeneous density for all the particles and simplified contact models may influence the fine-scale accuracy of the results, although the bulk behaviours remain representative of the asteroid dynamics. Secondly, a constant size was chosen for all the particles in the system. This is useful for network analysis, as no single body will have significantly more energy than the others in the system

The simulations were carried out both in NSC and SMC, however, it was chosen to continue with NSC as no noticeable difference was observed in the final results, and it is not as strict regarding the necessary time step for the simulation as SMC, even though more physically detailed due to force-overlap modelling is offered by the latter. Each body has a density of 2800 kg/m^3 and due to mutual gravitational interactions, the bodies eventually settle over time in a stable aggregate. The particles are first generated as static points, $\dot{r}_i = 0$ and $\dot{\varphi}_i = 0$, and their motion in the subsequent time steps is defined solely by their interactions as described by Equation (2.2).

3.2. Form creation

Once a stable aggregate was formed, that is, the grains show little motion and the angular momentum of the rubble pile converges as shown in [15], the next step is to extract meaningful asteroid-like shapes from this larger structure, which serve as the basis for further dynamic simulations. The obtained rubble pile is used to create smaller aggregates with specific shapes. GRAINS does not have implemented units of measure, and the data retrieved from the simulation must be scaled to assign units to obtain the results and to match the real data of the asteroids, that is, the desired bulk density, which is in international units of measure kg/m^3.

For a desired asteroid shape, the targeted geometry is first aligned and overlapped with the simulated aggregate, and all the particles outside the predefined shape are removed. To estimate the volume of the resulting trimmed aggregate, the alpha shape method is used. This method constructs a polyhedral surface that wraps around the remaining particles, allowing for a more accurate approximation of the aggregate's irregular boundary than a simple convex hull would provide, and calculates the volume inside the polyhedral aggregate.

Once the volume is calculated using the alpha shape, it is compared to the volume presented in Table 3.1. The ratio between the simulated volume and the real volume is

Parameter	Value
Duration	8.0 hrs
Time Step	0.1 s
Integrator	Implicit Euler Linearized
Friction	0.6
Restitution	0.0
Fragment size distribution	Monodisperse
Bulk Volume	1.81e6 m^3

Table 3.1: Simulation Setup.

then used to define a consistent scaling factor. This scaling factor is applied to assign appropriate physical units (e.g. distance, mass) to the simulation, ensuring dimensional consistency with real asteroid properties.

For the purpose of the analysis, it is desired to have different regimes of the dynamical evolution of the rubble pile. Thus, a set of data containing 98 simulations with different combinations of initial conditions was considered, simulated over a period of 8 hours each. The initial conditions used in these simulations are based on two different sets of values, one for the density $\rho = [1200, 1600, 2000, 2400, 2800, 3000]$ kg/m^3, and the other for the initial rotational period $P_0 = [21.82, 5, 3.2, 2.5, 2.1, 1.9]$ hours. The densities are chosen to be in accordance with the observed asteroids properties and to be consistent with the known population of asteroids. The values for the rotational period were chosen so that they have a uniform distribution above and below the classical critical spin period limit, Equation (2.19).

The other simulation data considered for the GRAINS simulations, such as the mechanical material properties of the particles and the simulation setup, are presented in Table 3.1, while the rest of the mechanical properties are those already implemented in GRAINS [2].

From the initial gravitational aggregate, the shapes presented in Figure 3.1 were cut and the aggregates obtained were reintroduced in GRAINS along with the scaled data for each scenario, similar to the process implemented in [15]. When reintroducing the data into GRAINS, attention must be paid to the convex-shaped case, where interlocking of particles is important. Therefore, for this case, the orientation of each particle is also saved from GRAINS during the first simulation, whereas for the case of spherical bodies, the particles do not interlock, and the orientation is ignored. The chosen asteroid shapes were chosen based on their properties and the simulation results obtained by Fodde et al. [18] using similar shapes of asteroids. The aspects that drove the process of choosing

these shapes are the following:

- One shape should present two visible lobes that at large angular velocities would break into two bodies of similar masses (*Kleopatra* case). Moreover, this shape undergoes a reshape when the rotation period is large.
- One shape should be spheroidal, such as *Bennu*, which also presents a bulge around the equator, from which particles would detach in cases of large angular velocity.
- One shape shall be elongated and without two prominent lobes as in the case of *Geographos*, with a more uniform mass distribution than in the case of *Kleopatra*.

Bennu 101955. *Kleopatra* 216. *Geographos* 1620

Figure 3.1: Chosen shapes for formation of gravitational aggregates [47]. The considered shapes are based on the observations of real asteroids.

For all of the different asteroid shapes, a unique volume value was considered in order to compare them based only on their shapes and bulk densities. It is important to keep the positions and particles size almost constant during the simulation, as it is desired to have particles in contact but not to have a large overlap between the particles. For these reasons, during the scaling process, other physical quantities were scaled to adapt the system to the real physical quantities of the asteroid. These quantities are the density, ρ, the gravitational interaction, G, and the rotation period, P.

Regarding the simulation setup, the time step must be carefully chosen, not to lead to instabilities - meaning that if the time step is too large, a contact may not be detected, or it is detected when the overlap between the two bodies is very large, while for a very small time step the simulation becomes computationally expensive. In [15, 16] Ferrari et al. show that the simulation time step implemented in the simulation of gravitational interaction must respect certain limits, as shown in Equation (3.1).

$$\begin{cases} \Delta t < \frac{T_g}{2} = \frac{1}{2\sqrt{G\rho}} \\ \Delta t < \frac{2\sqrt{4R\delta - \delta^2}}{\dot{r}} \end{cases} \tag{3.1}$$

where Δt is the integration time step, T_g is the characteristic time of the problem and depends on the density, ρ, and the universal gravitational constant G, defined by the slow dynamics of the gravitational interactions, and δ is the maximum overlap allowed between two bodies, which can be considered as a tolerance. For the present analysis, δ was considered to be 10^{-3} and was chosen based on the desired tolerance from the simulation.

To properly define the dynamical evolution of the asteroid system during the second phase of the GRAINS simulation (that is, analysing the time evolution of each shape for different combinations of initial conditions), it is essential to initialise the system using well-defined initial conditions. These conditions include the aggregate's shape, its initial density, and its angular velocity, all of which strongly influence the subsequent dynamics.

A crucial step in this initialisation process is the computation of the centre of mass (CoM) of the cut asteroid shape. Because the shapes used are obtained by cutting a preaggregated spheroidal body, the CoM may shift from its original position as a result of the removal of particles.

Therefore, the position of the new CoM must be recalculated with respect to the global inertial frame used in the initial GRAINS simulation. Once the updated CoM is identified, the position of each particle must be adjusted accordingly. This ensures that, upon re-importing the asteroid into GRAINS for the angular momentum simulation, the origin of the simulation domain aligns with the CoM of the aggregate. This alignment guarantees that the rotational dynamics is computed accurately, with the asteroid spinning around its actual centre of mass.

For this, each particle's position is changed as presented in Equation (3.2)

$$\boldsymbol{r}_i' = \boldsymbol{r}_i - \boldsymbol{r}_{CoM} \tag{3.2}$$

where $\boldsymbol{r}_{CoM}$ is the position of CoM and is calculated on the basis of Equation (3.3)

$$\boldsymbol{r}_{CoM} = \frac{\sum_i m_i \boldsymbol{r}_i}{\sum_i m_i} \tag{3.3}$$

Once the simulation is completed, it is possible from GRAINS to save the position, velocity, orientation, and angular velocity of each particle, as well as the forces applied to it (gravitational attraction and contact force) represented in a local frame with the origin in the centre of mass of the body. Furthermore, from GRAINS it is possible to extract for any contact occurring in the system, the bodies in contact, the position of the contact

and the magnitude of the contact.

3.3. Network Implementation

To quantify the structural evolution of the rubble piles, the physical interactions between particles were mapped onto graph structures, enabling the use of network theory tools.

From GRAINS for each case presented in the previous section, a database was saved, including, for each particle in the system, its dynamical state x_i, which includes the position, velocity, orientation, and angular velocity, the gravitational force applied on it by the other $N-1$ bodies, its global contact force $F_{c_i} = \sum_j F_{c_{ij}}$, both considered at the CoM of the body, moment of inertia $\mathbf{I}$, the contact pairs, and for each contact its respective force $F_{c_{ij}}$. This data was saved every $t_{save} = 5$ minutes of simulation time, for the entire duration of the simulation, 8 hrs. From these, only a part of the saved data will be presented hereafter. The saving time step, t_{save}, was considered the same for all simulation cases, and thus it should also be acceptable for the initial phase of the very fast rotating case. Afterwards, from these data the energies K, K_{rot}, U and E were calculated, using Equation (2.14).

Based on these, several adjacency matrices were calculated. In order to represent the entire system of rubble piles, especially in the case when the system is formed from a compact, unique aggregate, the adjacency matrix has the size $[N_B, N_B]$, where N_B is the total number of particles that make up the gravitational aggregate.

3.3.1. Contact Case

In GRAINS, from the contact manager, at each saving time step, the contacts were saved in the form of an adjacency list, similar to the adjacency list presented in Table 2.1. In a similar manner, the contact force of existent contact (pair-wise contact forces, as only two bodies are considered in one contact) can be saved, and the two can be transformed into two adjacency matrices representing the relationships between any two bodies of the system, based on the contacts.

The newly created adjacency matrices follow the structure defined in Equation (2.21). There is a link between two bodies i and j if they are in contact. In the case of a contact-pair adjacency matrix, this is represented as a binary value. For a matrix of contact force adjacency, the entry A_{ij} is set to the magnitude of the contact force, $|F_{c_{ij}}|$. The absolute value is used to ensure that the matrix remains symmetric. Note that if the actual contact force vectors were used directly (e.g. $F_{c_{ij}} = -F_{c_{ji}}$), the resulting matrix

would be asymmetric. However, a directed graph could be considered similar to the one presented in Figure 2.3, in which case the absolute value is no longer necessary because the direction of the link represents the sign of the force. As the two representations are equivalent, from now on only the undirected graph will be considered.

3.3.2. Physical State

More adjacency matrices were created based on physical states of each particle. In all the cases, a distance-based adjacency matrix was created, where:

$$A_{ij} = ||s_i - s_j||_2; \quad \forall i, j \in V \tag{3.4}$$

In Equation (3.4) s_i is the physical characteristic of the body i and can be the kinetic energy E_k, the distance r, the total energy E_t or any other dynamical value of the system that could effectively represent the network.

The properties used in the creation of the different matrices are the distance, the total energy, the kinetic energy, the potential energy, the velocity, forces, angular momentum and angular velocity.

In other researches, similar to [43], the adjacency matrix was created imposing a limit on the distance between two nodes of the network such as:

$$c_{ij}(\epsilon, T) = \Theta(\epsilon - \min_{0 \leq t \leq T} ||\boldsymbol{r}_i(t) - \boldsymbol{r}_j(t)||_2), \tag{3.5}$$

where ϵ is the limit imposed for a link to be considered between bodies i and j, T is a time horizon, $||\cdot||_2$ is the Euclidean norm and Θ is the Heaviside step function. In this case, to create the adjacency matrix, from the near collision matrix $C(\epsilon, T) = (c_{ij})_{i,j}$, the identity matrix $\mathbf{I}$ must be subtracted to avoid self-collision. Although this approach or variations on this concept is widely used in network theory [11], it will not be used here. Firstly, from GRAINS the contacts are already known, and thus imposing an upper limit distance of the neighbour will slightly increase the neighbour of body i, and usually it will add a body, that is, the neighbour of a neighbour of body i, which is not of interest. Secondly, the limit should be imposed based on the physical characteristic chosen. It is not guaranteed that two bodies that are spatially close to each other will also have a similar value of the physical characteristic. For these cases, a complete network will be considered, where each node is connected with all other nodes in the network, all the other bodies in the system. This is another reason why an approach similar to that presented in Equation (3.5) is not suitable, since a complete graph with equal weights

would not offer any kind of useful information, because all edges would have the same importance in the network, as the number of degrees and weights would be the same for each node i. Therefore, a fully weighted graph was used for most simulations related to network analysis. However, it must be admitted that such an approach is computationally expensive, as for large asteroids that contain many particles (e.g. *Bennu*), the matrix is very large, and thus analysing such networks is inefficient.

A different method through which A can be created is using the kernel of the *radius function*:

$$A_{ij} = exp\left(-\frac{||s_i - s_j||^2}{2\sigma^2}\right) \tag{3.6}$$

where σ is a free parameter and in this case it was chosen to be the mean distance. It is a useful approach, being that it considers the similarity in the values between the two nodes, as the kernel decreases with the distance between the two values. However, the difference between this method and the one previously presented is negligible.

Another approach that was used for some cases was to consider a weighted sum of the adjacency matrices described above to interconnect the information they offer. Once each adjacency matrix was created using the Euclidean distance, they were normalised, and a new matrix was formed following the formula:

$$A_{weighted-sum} = \alpha \cdot A_i + \beta \cdot A_j + \gamma \cdot A_k \tag{3.7}$$

where α,β, γ are the weights chosen based on the importance desired for each matrix $\mathbf{A}_i$, and $\mathbf{A}_{i,j,k}$ are the adjacency matrices of the physical states of the system, computed as presented before.

Once the networks are created together with their respective adjacency matrices, for each node the degree, the centrality, and the local clustering coefficient are calculated, while for the entire network the percolation threshold and the global clustering coefficient, along with amended potential, moment of inertia, and angular momentum are calculated. These are calculated using the methods and equations presented in Chapter 2.

3.4. Clustering Method

To observe the possible patterns in the asteroids and communities of particles that have similar characteristics, clustering was applied to the data retrieved from GRAINS and also to the created networks. As stated in Chapter 2, there are several methods that could be used to cluster detection and identification of communities. As the purpose of

this analysis is to detect the clusters in a network, the ones that could detect the clusters and the number of clusters needed were chosen, and those that could be applicable to the network. Thus, hierarchical clustering, spectral clustering, and Markov chain clustering were implemented.

The spectral clustering was implemented using the Equation (2.39). For the spectral clustering, the number of clusters has to be known as well in order to create the communities. Usually, spectral clustering divides the network into two regions, and through a repetitive process, each region is subdivided into two other regions, until no eigenvalue λ of the Laplacian L is equal to zero. Another approach is to consider the number of clusters, k, equal to the number of eigenvalues whose value is zero $\lambda_k = 0$. However, in real networks, it is very rare that the eigenvalues would be zero, while their first k-eigenvalues are very small. Therefore, all eigenvalues less than 10^{-3} are considered equal to 0 and offer information on the number of clusters present. The limit imposed is not fixed, and this could vary based on the observed cases or on the physical property on which the clustering method is based, but during the simulation it was observed that a limit of 10^{-3} yields a good approximation on the number of clusters. Also, if a change is observed in the order of the eigenvalues, from 10^{-5} to 10^{-1}, for example, the imposed limit could be set to 10^{-4}, which would be more strict without affecting the number of clusters.

Regarding the Markov Chain Clustering Method (MCL), the method was implemented using the process presented in Chapter 2.2, for which the exponential power was chosen to be constant along all simulations, $e = 2$, and the inflation parameter r depends on the case. For each different case, the value of r was obtained using a trial and error approach. The value of r must be carefully chosen, as if it is too large, the clusters become tighter and smaller, with fewer intercluster connections able to survive, while if it decreases, the clusters become looser and larger, with more intercluster mixing. For these reasons, it was considered that the inflation parameter should be below 1.5, for contact pairs clustering, as it should not eliminate the edges connecting close nodes, even if they are parts of different communities. In the case where the clustering is based on the distance, the inflation parameter was set to 3 to maximise the number of clusters. Since MCL is an iterative algorithm, a maximum of 100 iterations was established, with a convergence tolerance of 10^{-6}. The algorithm proceeds to the next step when the difference between successive iterations falls below this threshold or when the number of maximum iterations is reached.

Hierarchical clustering was implemented using the built-in MATLAB function. Hierarchical clustering methods were shown to be suitable for networks in Chapter 2.2.4. For this method, the desired number of clusters has to be implemented in the algorithm be-

forehand, and so for the considered cases, the number of clusters was considered to be the same as the one obtained from the MCL method applied to contact pairs. In this way, an approximation of the desired number of clusters is done, which is applied afterwards to the cases in which energy or angular momentum are the physical parameter on which the clustering method is based.

One more clustering method was implemented on the basis of the contacts present in the system and thus on the adjacency matrix. This method is useful in case the asteroid breaks up and more clusters can be visually observed. These clusters take into account only the contacts between the particles and assign a particle to a cluster only if it is in contact with at least one other particle in that cluster. The algorithm for particle assignment to a cluster is as follows:

Algorithm 3.1 Contact-Based Clustering from Adjacency Matrix

Input: Adjacency matrix A of size $N \times N$
Output: List of clusters (each a set of connected bodies)
for each body $i = 1$ to N **do**
  Identify all bodies j such that $A(i, j) = 1$
  Form a temporary group called `contacts` that includes i and all such j
  Initialize a flag `found` as false
  for each existing cluster **do**
    if any member of `contacts` is already in the cluster **then**
      Add all members of `contacts` to this cluster (avoid duplicates)
      Set `found` to true
      Break (merge only with the first matching cluster)
    end if
  end for
  if `found` is false **then**
    Create a new cluster with the members of `contacts`
  end if
end for
Post-processing: Merge any overlapping clusters
for each pair of clusters **do**
  if they share any common member **then**
    Merge them into one cluster
  end if
end for
Remove any empty clusters

In this method, clusters are all the groups of bodies that are in contact with at least one body $\sum_j A_{ij} \geq 1$.

3.5. Percolation

The percolation method considers the evolution in time of the percolation threshold $p_c(t)$ and the clustering coefficient $c(t)$ for each created network. In Chapter 2 the concept of percolation and the equations associated with it were presented.

Moreover, it is interesting to analyse whether through percolation theory the evolution of clusters in time can be predicted and to analyse the evolution of Giant Connected Component (GCC). For this, a method similar to that presented in [33, 36] was implemented. However, the concept of percolation is implemented through the use of random walks and through Monte Carlo simulations.

The process starts from the network at the initial time $t = 0$. The process starts from this time step as in this case the graph is still connected, while in the subsequent time steps the asteroid undergoes rotational breakup. In the case of reshaping, a similar process can be considered to the *link prediction method*, presented in [28], which will not be analysed further.

In the initial graph, the one of the nodes that is closest to the physical CoM of the system is chosen. The closest 3 nodes were selected and from these the node with the highest degree was considered for analysis. From this node, a random walking process is created: at each step, the walker moves from one node, i, to another, j, based on the probabilities of the adjacent edges to node i. These were calculated using Equation (2.44).

It should be noted that the probabilities, P_i, of node i, are a function of time and node, since for each time step, the probability of each node depends on its degree and the strength of the adjacent edges. Each time the walker travels an edge, the edge index is saved, and in cases of weighted graphs, the edge is eliminated. The reason for eliminating the edges in weighted graphs is to prevent the walker from returning on the previously travelled edge several consecutive steps. If the weight of one edge is much larger than those of the others edges, it will return on this edge several times, and thus the algorithm would become very expensive. Meanwhile, in unweighted graphs, similar problems cannot arise, as all edges adjacent to a node will have equal probabilities $P_{ij} = const \ \forall j \in V$.

The free nodes, vertices with $d_i = 0$, are ignored from the walked, as they cannot be reached. If more clusters are present, that are not connected, a process involving random jumps is implemented. When the traveller has walked through all the nodes in the initial community, a random node from another community is selected, and the process continues until each node in the new cluster is reached. This process is repeated until all the nodes in each identified community is reached.

The entire process is repeated through a Monte Carlo process several times, each time saving the index of walked edge. Each time an edge is travelled its index is saved and at the end of the process a ranking of the most walked edges can be created. In the end, the edges that were travelled the most are eliminated from the network.

4 | Results

In this chapter, the results and performance of using a network approach in modelling the gravitational aggregates will be presented. Section 4.1 presents the creation and selection of the asteroid cases used in the analysis and their importance. In Sections 4.2, 4.3 and 4.4, the application of network theory is presented, focussing on the structure of the network and the time evolution of the network. Sec 4.5 offers the solution to the percolation problem in the gravitational aggregate network. The final networks will be used to investigate topological patterns, structural robustness, and community formation.

4.1. Asteroid creation and aggregation

The first objective of this thesis is to model the asteroid as gravitational aggregates that could be converted into networks. For the simulation of an initial aggregate, as presented in the previous chapter, 10 000 spheres with a radius $R = 2$, non-dimensional units, were produced, and placed randomly in a cube with margin length of 250, non-dimensional units. The length of the cube was selected in order to ensure that no overlap between two particles is created during the initial generation process, even if it leads to longer simulation times, due to greater distances and therefore, weaker gravitational interactions during the initial steps. The evolution of the asteroid is presented in Figure 4.1.

As it can be seen, the final aggregate has a spheroidal shape, in which the particles are in a stable configuration, meaning that the aggregate is compacted to the point where no noticeable change in the positions and contacts of the particles is present, nor a change of the aggregate shape, and the results are in accordance to those obtained in [15].

From this spheroidal-shaped aggregate, the shapes presented in Figure 3.1 were cut through the process described in Chapter 3 and the final results are shown in Figs. 4.2, 4.3 and 4.4.

For each shape 36 cases of dynamical evolution were created, applying at the beginning of each simulation different combinations of density and angular velocity as presented in Chapter 3. In the following, only five different evolutions for *Kleopatra* will be presented,

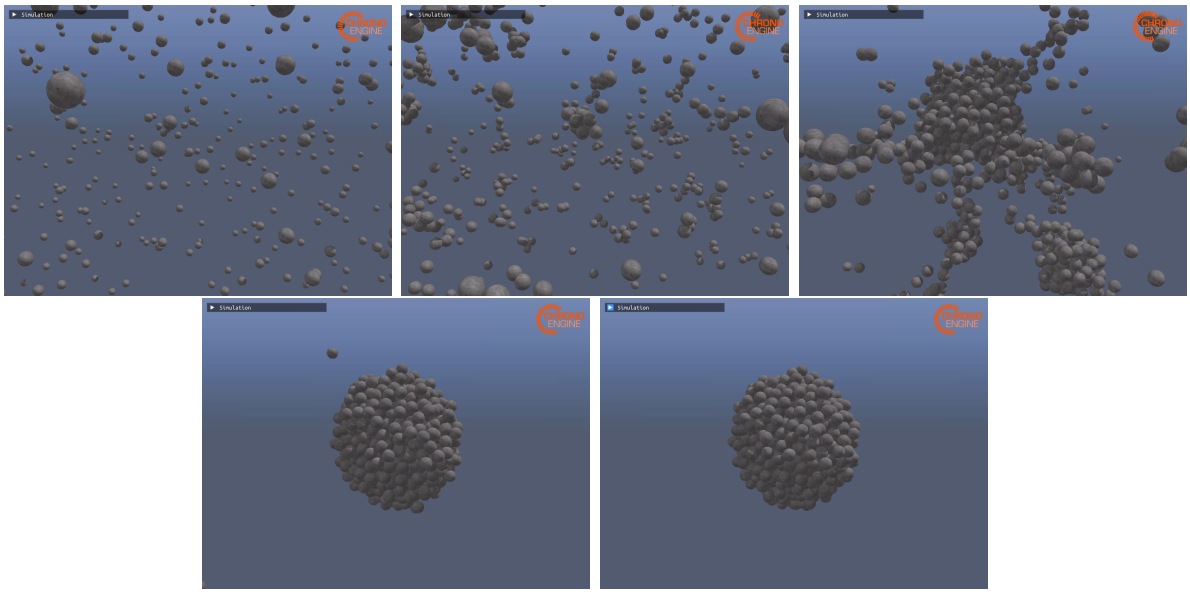

Figure 4.1: Asteroid Evolution during aggregation process in GRAINS.

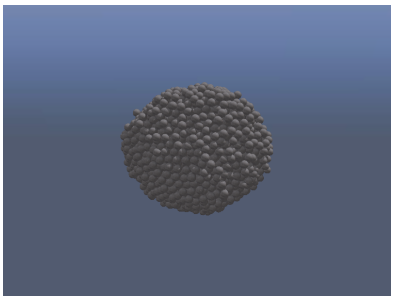

Figure 4.2: *Bennu* 101955.

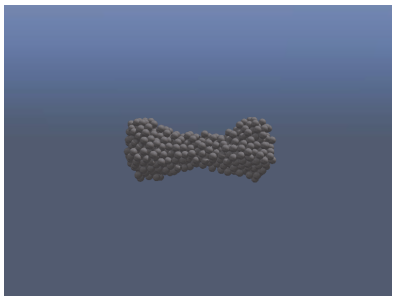

Figure 4.3: *Kleopatra* 216.

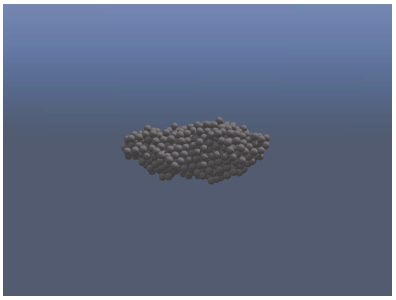

Figure 4.4: *Geographos* 1620.

with others being available in Appendix 1. *Kleopatra* was selected for the presentation of the detailed analysis due to its bilobed shape, which offers a clear structural dichotomy in rotational evolution. The later lobes respond differently to rotational stress, enabling a richer investigation of localised failure, network fragmentation, and community transitions. In Figure 4.5 the 5 cases, labelled from $A - E$, are shown. In case A *Kleopatra* reshapes and tends to form an ellipsoid, as is expected from theory [21]. In case D the asteroid neither changes its shape nor breaks up, meaning that the chosen values for density and angular velocity are close to the real ones, which is in accordance with the observations [32]. Cases B and C undergo breakup but at different rates and with different re-accumulation behaviours. Case B presents the catastrophic disruption in two main components, and 3 remnant bodies, which in the end reattach to the two main components, as observed in Figure 4.5, while in case C, the angular velocity is large enough to prevent the complete reaggregation of the remnant bodies, with some debris remaining behind, Figure 4.5. Case D provides a case in which the asteroid does not suffer from

complete breakup, although, it is reshaped, meaning that it is closed to the breakup limit.

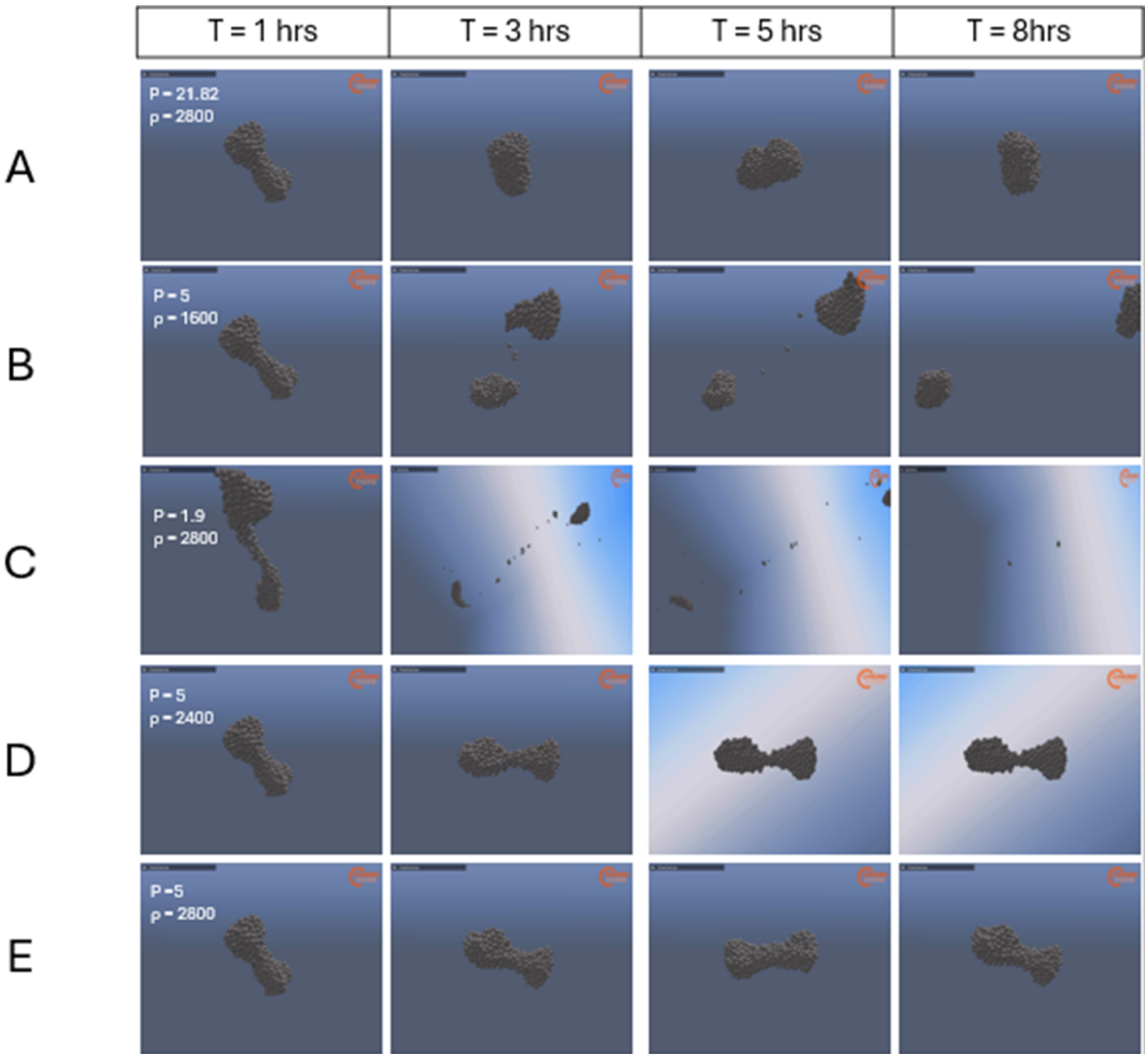

Figure 4.5: Five different example simulations of *Kleopatra* in GRAINS covering different dynamical regimes, reshaping in case A and D, unstable or disaggregation in cases B-C, and stable in case E.

Another reason for choosing to focus on *Kleopatra* lies in the representation of the network. During the cutting process, the spheres that were outside the cutting shape were eliminated from the system. In Table 4.3 the number of bodies composing the final aggregates (representing the shaped asteroids) is presented. It can be observed that the system representing *Kleopatra* contains the smallest number of bodies, and thus a more clear representation of the network simulating the asteroid will be possible.

Similarly to the case of *Kleopatra*, *Bennu* and *Geographos*, Appendix A, present a breakup and reshape behaviour, the limiting cases at which these take place differ due to the shape of the asteroid and density, as provided by Equation (2.19). This is in accordance with

the results obtained through simulations [13, 18]. The changes in the dynamical regime are shown in Table 4.1 for constant density and in Table 4.2 for constant rotation period, where D.R. stands for dynamical regime, R. for reshape, D. for disaggregation, and S. for stable.

During the dynamical evolution of the asteroid, the energy of each particle is calculated using the Equation (2.17). In general for elongated shapes as *Kleopatra*, the particles close to the two extremities of the asteroid, the two lobes, have the highest energy level, because of their large kinetic energy and slightly lower gravitational attraction. The particles have a large kinetic energy with respect to those close to the centre of the asteroid, due to the angular velocity of the asteroid, and thus a large velocity $\dot{r}_i$. Meanwhile, the gravitational attraction of these particles is not very large due to the large distance between the two lobes, and the particles on one lobe are not strongly affected by the attraction of the particles from the second lobe.

$\boldsymbol{\rho}$ **[kg/m^3]**	2000	2000	2000	2000	2000	2000
$\boldsymbol{P}$ **[hrs]**	21.82	5	3.2	2.5	2.1	1.9
D.R.	R.	S.	D.	D.	D.	D.

Table 4.1: Dynamical regime change for *Kleopatra* with constant density $\rho = 2000$ kg/m^3 and different rotation period P. These cases are further analysed through network theory.

$\boldsymbol{\rho}$ **[kg/m^3]**	1200	1600	2000	2400	2800	3000
$\boldsymbol{P}$ **[hrs]**	2.5	2.5	2.5	2.5	2.5	2.5
D.R.	D.	D.	D.	D.	D.	D.

Table 4.2: Dynamical regime change for *Kleopatra* with different densities ρ and constant rotation period $P = 2.5$ hrs. These cases are further analysed through network theory.

The energy balance of each particle is then compared to zero, and those that have a positive total energy will be more likely to detach from the asteroid or be the cause of disaggregation Figure 4.6. Note must be made that, as the asteroid is composed of two lobes, the particles do not necessarily detach from the asteroid, as the asteroid itself breaks into two or more clusters. This also depends on the number of particles with positive energies that can escape the gravitational field of the asteroid. If more particles have energies large enough to escape, they will cluster together and thus lead to a breakup.

Bennu 101955	*Kleopatra* 216	*Geographos* 1620
3331	646	655

Table 4.3: Number of particles present in systems representing each case of asteroid shape.

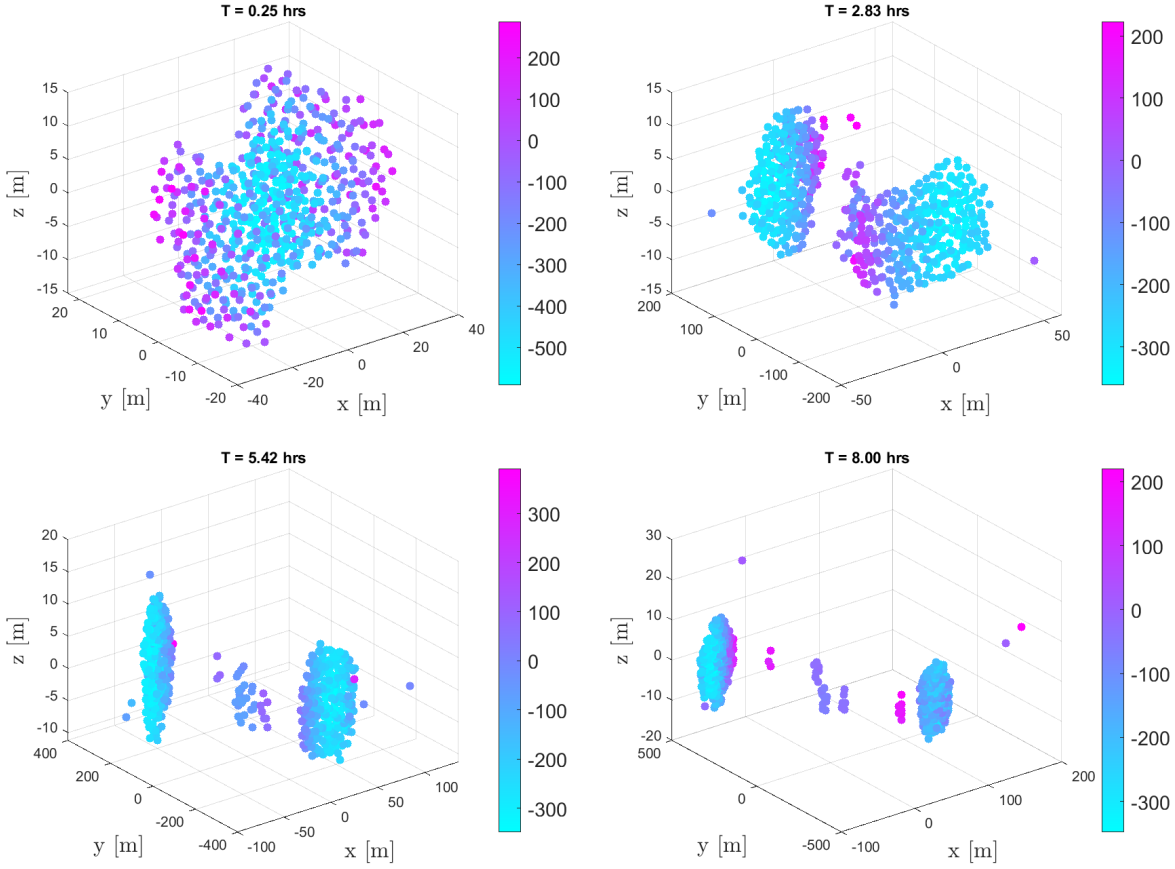

Figure 4.6: The colour bar shows the energy value of each particle, computed as Equation (2.17), in J, for *Kleopatra* at different values of time. In this case $\rho = 2000$ kg/m^3 and $P = 2.5$ hrs.

Another critical factor to consider is the direction of velocity. Each particle is assigned an angular velocity based on its position vector $\mathbf{r}_i$ and velocity vector $\dot{\mathbf{r}}_i$, as described in Equation (2.3). Therefore, both the magnitude and orientation of the velocity vectors play a significant role in the system's dynamics.

This effect is particularly noticeable in small clusters of particles with positive total energy (i.e., unbound in a classical sense) that nonetheless remain temporarily bound together. This occurs when such a cluster is under the influence of a strong gravitational attraction from a nearby massive rubble pile. As a result, the entire cluster accelerates toward the massive body. However, because the particles within the cluster share similar velocity

directions, they stay closely packed, maintaining cohesion, as they move, despite being energetically unbound. The cluster stays intact until it eventually merges or interacts with the larger rubble pile attracting it.

It is obvious that for lower angular velocity values, the particles' velocity distribution is similar, as the velocity depends on the angular velocity of the system and the position of the particle. However, in these cases, as opposed to the previously presented case, no particle has a positive total energy. This means that no particle or group of particles can detach from the asteroid, and thus the gravitational aggregate in this case undergoes a reshape, as shown in Figure 4.5, case A.

Figure 4.6 illustrates the evolution of particle energies over time. The color bars indicate that, overall, the energy levels appear stable, with only minor fluctuations between time steps.

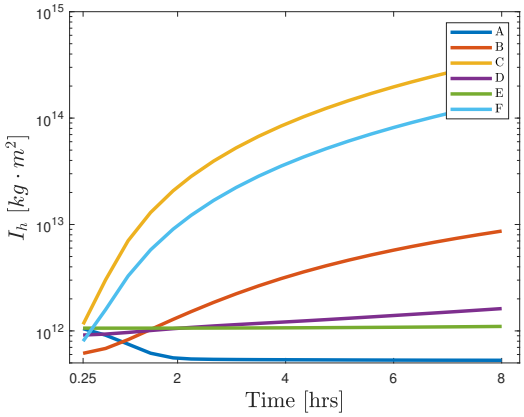

Figure 4.7: Moment of Inertia around **H**.

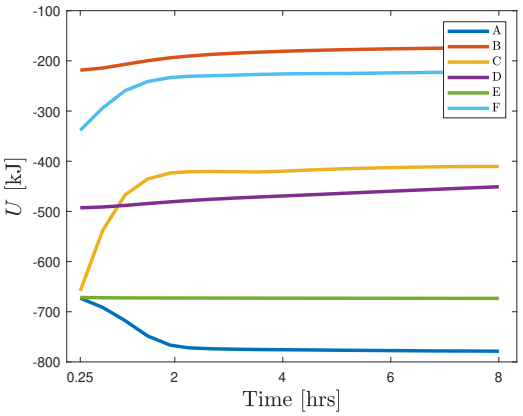

Figure 4.8: Total potential energy.

For the five cases presented above and the case in which $\rho = 2000$ kg/m^3 and $P = 2.5$ hrs, a more quantitative difference is presented in Figure 4.7 and Figure 4.8 where the time evolution of I_h and U of the entire system, Equation (2.13), is plotted. This analysis is crucial because these values define the amended potential, Equation (2.20), which was shown to be a critical parameter in describing the state of the system. It can be seen that for the case involving disaggregation the potential energy, U, increases as the distances between the particles increase and I_h is constantly increasing. The rate of variation of U and I_h also depends on the rate of disaggregation, the asteroid rotating faster and presenting a stepper increase in the moment of inertia. Case A shows a decreasing pattern in both I_h and U which is due to the asteroid's reshape, which becomes more compacted, and the distances between particles decrease. Case E is the case of equilibrium in which the asteroid is not reshaped or disaggregated. This is observed through almost constant

values in both the moment of inertia and the total potential potential energy (the variation is less than 0.2%). A similar behaviour to case E can be observed in case D, but this is due to a reconfiguration of the asteroid, but found at the limit of breakup, and thus the distances are larger than in case A, and the potential energy is much larger.

4.2. Network Formation

The main objective of this thesis is to analyse the gravitational aggregate from the point of view of a network whose nodes are given by the particles composing the system and connected by well-defined relationships between them.

For each asteroid, the number of nodes present in the network is equal to the number of bodies composing the gravitational aggregate, given in Table 4.3. The edges between the nodes, that is, the relationships defining the dynamic connection between grains, are based on the adjacency matrices, which were created using the method presented in Chapter 3.3.2.

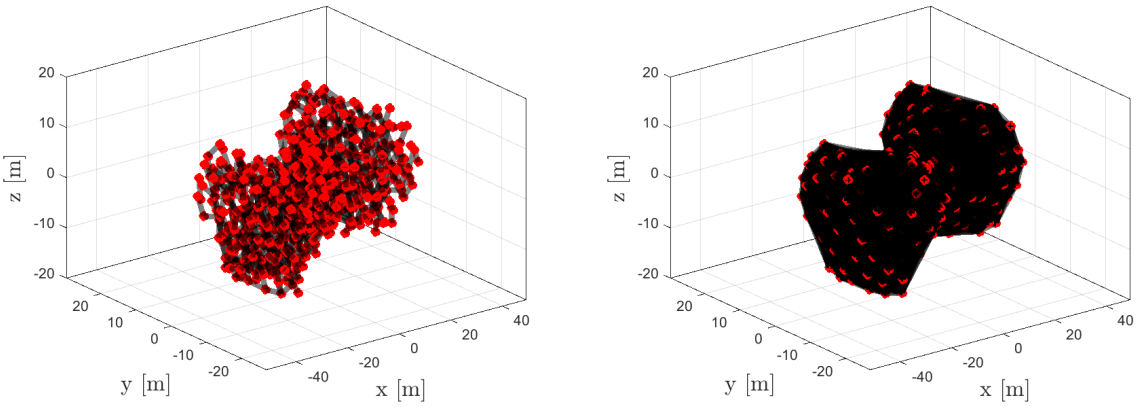

(a) (b)

Figure 4.9: Created network representing a gravitational aggregate based on contact pairs (a), and on gravity (b).

In Figure 4.9 the created networks are shown. In Figure 4.9(a) the shown network is created based on contacts pairs, and in Figure 4.9(b) the network based on gravity is shown. It can be seen that the network defined by the graph composed based on gravity attributes of the nodes $G_{Gravity}$ is more complex, as it is a complete network and presents a larger number of edges, $N(N-1)/2$, with N being the number of bodies in the system. For the complete graph of gravity it was chosen not to show all the edges, as in that case the figure would be incomprehensible, and thus the longest edges were made transparent.

For the case of contact forces, a network similar to the one presented in Figure 4.9(a) was created, in which the same edges exist as in Figure 4.9 (a), but are defined by weights, while for the case of energy and other physical parameters, the networks are very similar to the one attributed to $G_{Gravity}$, with the sole difference being in the weights assigned to each edge.

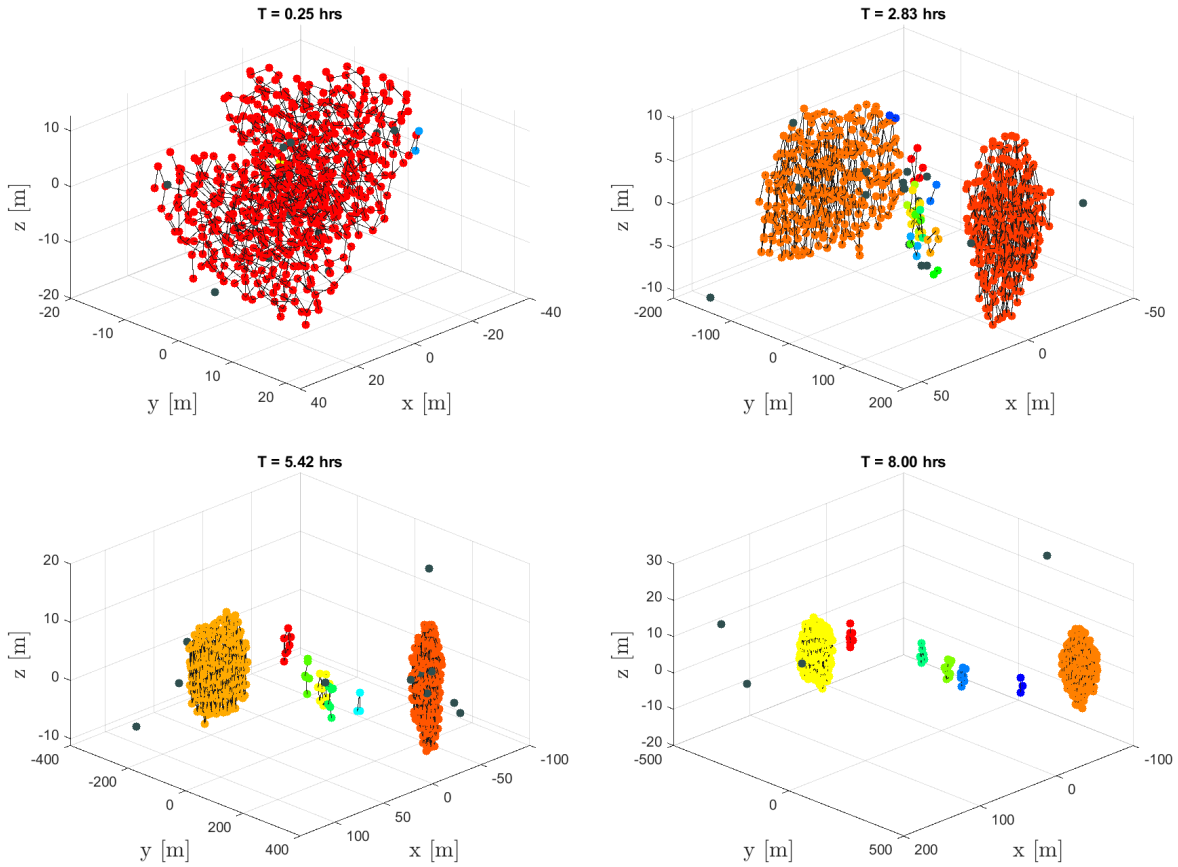

Figure 4.10: Identified clusters using Algorithm 3.1 based on contact pairs for *Kleopatra*, when the density is $\rho = 2000$ kg/m^3 and rotation period is $P = 2.5$ hrs. Each cluster is represented by a different color, while free bodies (bodies that do not belong to any cluster), are shown in black. For a better clustering representation the grains in contact are connected by a black edge, similar to the network representation, Figure 4.9.

.

All networks are considered to be time dependent and thus their form changes in time, but through different topological means. The complete networks are considered to be complete at each time step; therefore, their time dependency relates solely to the links' weight, which actually represents the physical time evolution of the aggregate, through the simulation done in GRAINS. However, in the case of contact pairs and contact forces, the time dependence behaves in the presence of edges between nodes and their weights

(contact force). Moreover, during the time evolution of the network, only the existence of edges is questioned, as the presence of nodes is known not to change.

4.3. Clusters Identification

Before applying specific clustering algorithms, the global clustering coefficient (GC), Equation (2.30), was computed to evaluate the degree of local cohesion within the network over time. The evolution of the GC is illustrated in Figure 4.11 and Figure 4.12, where multiple simulation cases are shown. In the initial phases of the simulation, some cases exhibit a GC of zero, indicating the complete absence of triangles in the network. This implies that, at those times, the network lacks any locally cohesive groupings, that is, there are no interconnected triplets of particles.

As the simulation progresses, the GC gradually increases, reflecting the emergence of a local structure. This growth signifies that particles are forming tightly interconnected clusters or 'triangles', suggesting that aggregation occurs within small localised regions. However, even with this increase, the overall structure remains relatively weak, as the GC does not reach a large value, from a clustering point of view, meaning that the network remains sparse. It is interesting to observe the difference between the cases of reshape and those of breakup. The reshape case $P = 21.8$ hrs and $\rho = 2000$ kg/m^3 has a smaller GC than the breakup cases. This means that the reshaped asteroid has a sparse structure, while the breakup cases have a higher edge-density. A sparse structure means that there are fewer contacts between the particles, which is surprising. This is explained through the rubble piles in which the particles reaggregate after the disaggregation, forming more homogeneous shapes.

The values obtained towards the end of the simulation indicate a moderate level of clustering. These values are comparable to those observed in large complex networks in the real world [57], particularly in spatial or physical systems with hundreds of nodes, such as those representing granular media. The observed convergence suggests that the system transitions from a disordered configuration toward a more structured and locally cohesive one as gravitational and contact forces drive particle interactions.

For each time step, the clustering methods were used to detect communities, and so the number of clusters detected is time dependent. As a first clustering method, the one presented in Algorithm 3.1 was used, which is represented in Figure 4.10. As this method was used by applying the adjacency matrix of the contact pairs, the result offers clusters based on the contacts. From this it is clear that during the breakup there are several communities and free bodies (bodies that compose themselves the entire cluster). Some

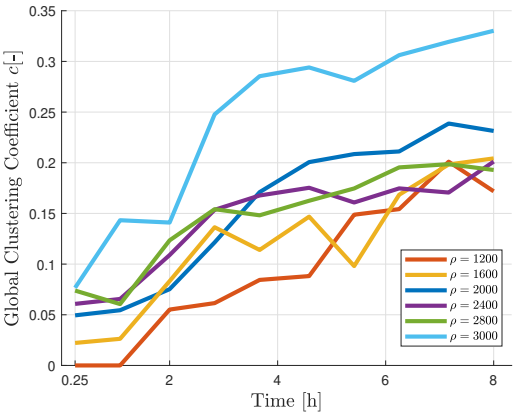

Figure 4.11: Global clustering coefficient time evolution for *Kleopatra* at constant rotation $P = 2.5$ hrs.

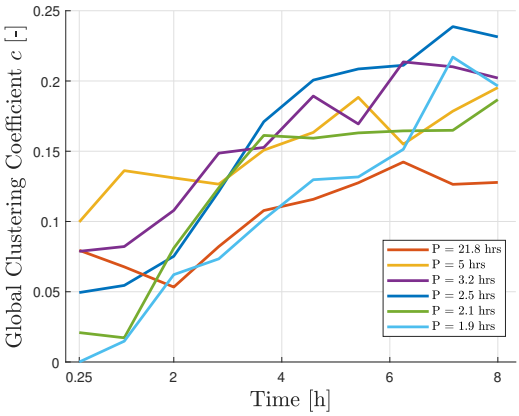

Figure 4.12: Global clustering coefficient time evolution for *Kleopatra* at constant density $\rho = 2000$ kg/m^3.

.

of these clusters will merge into larger ones. There are also cases in which some clusters or particles remain part of a small central cluster without connecting with a larger aggregate. This is understandable, as the two new large rubble piles usually have similar masses, so an equilibrium can be found through the rapport $\frac{m_i m_j}{r_{ij}}$, which keeps the remnant part close to the centre of the system. The direction of the gravitational attraction force and its magnitude must also be considered.

When two clusters reaggregate, the process resembles the formation of the initial large aggregate. The clusters and individual nodes interact over long ranges through weak gravitational forces, with smaller, less connected communities being drawn toward the larger ones. This phenomenon is observed in case B of Figure 4.5, where the 3 remaining central bodies regroup with the two larger communities, in order to create a system of 2 gravitational aggregates orbiting each other.

With respect to the clustering methods, the Markov chain, Figure 4.13, offers results similar to the one presented above, Figure 4.10, with the two being identical. This was expected as both methods are based on the adjacency matrices of the network. However, in this case, the Markov Chain presents several advantages with respect to the method presented in Algorithm 3.1. The first advantage would be its applicability to other types of networks, not only those based on the contact pairs. The Markov Chain method is applicable also to networks based on distances or gravity, offering good results, similar to those presented in Figure 4.10. It is interesting to notice that when clustering based on distance, Figure 4.14, the Markov Chain gives a similar result to that of spectral clustering based on *Fiedler vector*. Even if the two methods have different concepts they

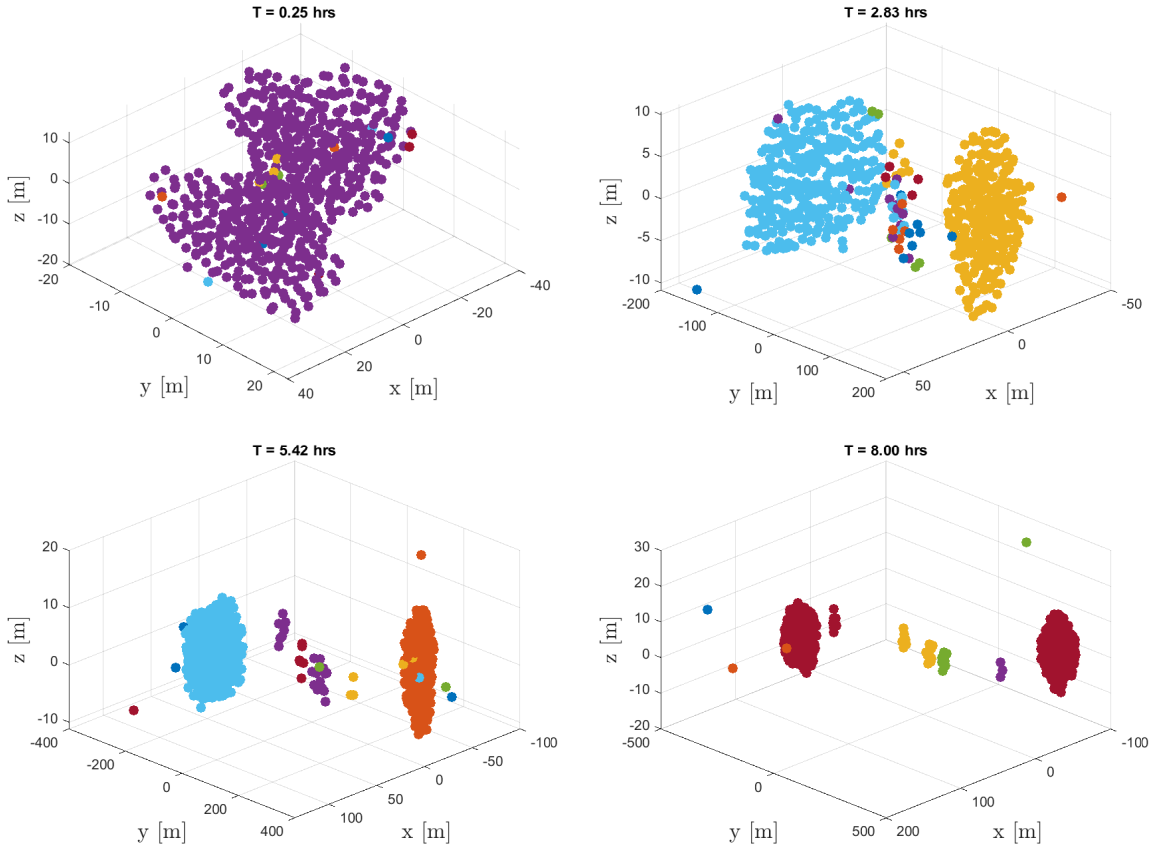

Figure 4.13: Identified clusters using Markov Chain Algorithm (Equations (2.40), (2.41) and (2.42)) based on contact pairs for *Kleopatra*, when the density is $\rho = 2000$ kg/m^3 and rotation period is $P = 2.5$ hrs. Each cluster is represented by a different color.

are useful to make comparisons between the detected communities in the gravitational asteroids network. Spectral clustering is useful because not many assumptions must be made before applying the method. In theory, only the limit for considering $\lambda = 0$ must be taken, as in real networks it is rare to have more than one eigenvalue equal to zero. When applying the Markov Chain Clustering method, one must consider the values of expansion and inflation parameters, which largely influence the results of the analysis. However, one limitation when using the Markov Chain Clustering on positions, is that it is able to detect solely two clusters, regardless of the initial set-up. Therefore, this method could be a simple method to observe the cluster change for particles close to the centre of the system.

In Chapter 3.4 the implementation of the hierarchical clustering method was presented. At first, it was checked if applying the number of clusters obtained from MCL or from Algorithm 3.1 would offer good results. The problem at the initial step is observed, when

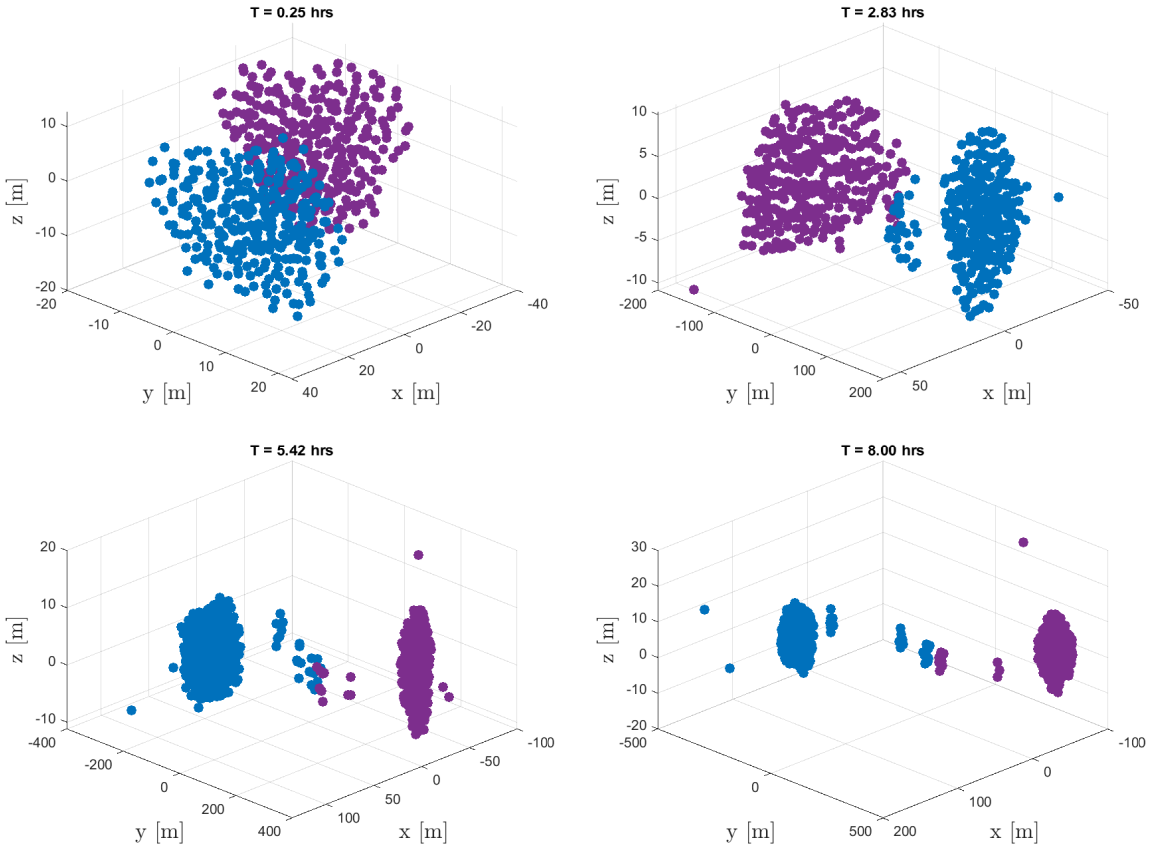

Figure 4.14: Identified clusters using Markov Chain Algorithm (Equations (2.40), (2.41) and (2.42)) based on distances between particles in *Kleopatra*, when the density is $\rho = 2000$ kg/m^3 and rotation period is $P = 2.5$ hrs. Two clusters are identified, represented in different colors.

this method is not able to identify the clusters clearly, especially the free body cases. However, in subsequent time steps, the process starts to improve results, and at larger time instances the results for the distance clustering hierarchical method offer identical results to those already presented by the previous two methods applied to contact pairs. Thus, if the clustering process is based on the vector of positions of each particle, the hierarchical method offers improved results over the MCL.

In Figure 4.15 they are presented the identified clusters and their time evolution, using the hierarchical method and applied to particles' energy level. Hierarchical clustering was implemented following the process presented in Chapter 3.4. Through this method it is possible to identify the particles with larger energy levels, especially those particles that have their total energy larger than that of the two rubble piles. For example, comparing the results presented in Figure 4.6 with those obtained in 4.15, it can be seen that the

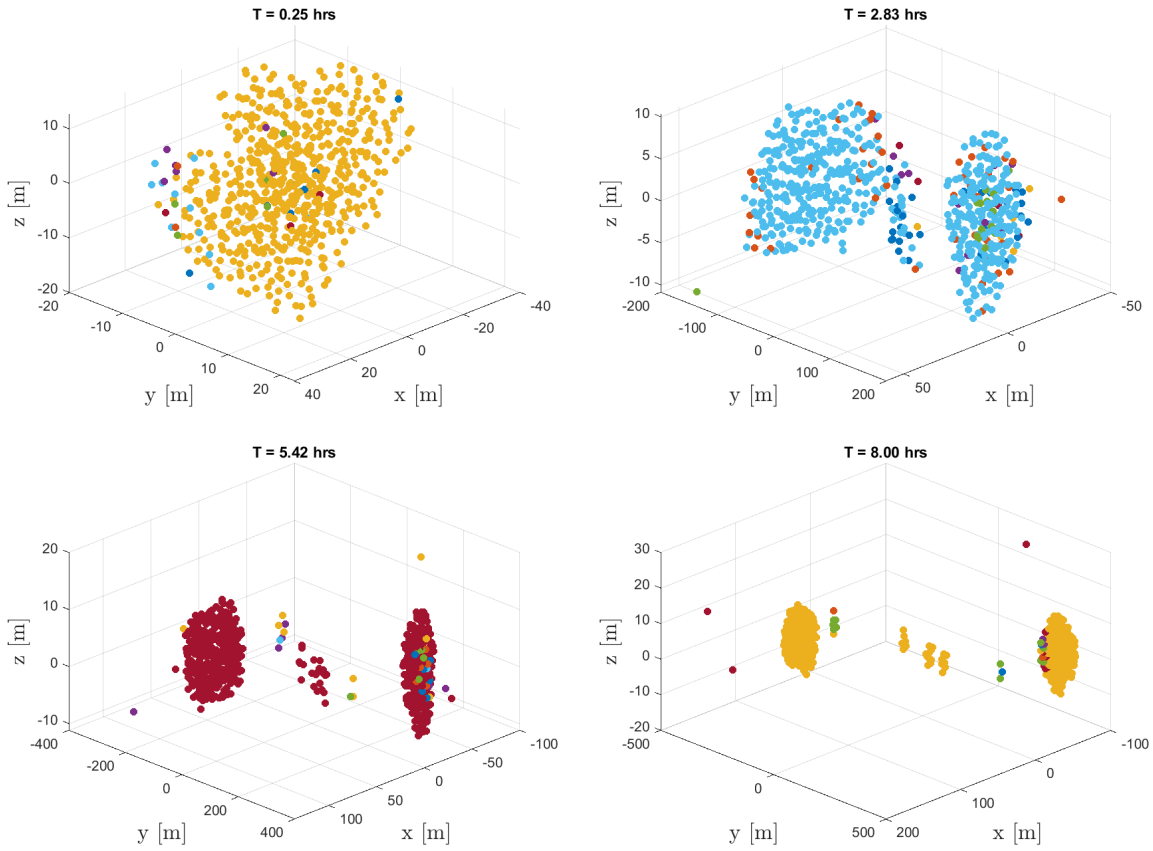

Figure 4.15: Identified clusters using hierarchical method (Equations (2.35) and (2.36), based on energy levels for *Kleopatra*, when the density is $\rho = 2000$ kg/m^3 and rotation period is $P = 2.5$ hrs. Each cluster is represented by a different color.

particles remaining at the centre of the system during the asteroid's evolution have similar energy values with those of the particles composing the two rubble piles. This is due to the gravitational effect the two rubble piles have on the central region particles and on the fact that the two rubble piles have similar masses and are at similar distances from the CoM of the system, thus their gravitational interaction with the remnant bodies will be of the same magnitude. Slightly increasing the number of desired clusters during the simulation offers a clearer image of the possible breakup configurations of the asteroid. For example, in Figure 4.16 is shown a case in which the number of clusters increased slightly and the algorithm identified the central region, the *bridge* between the two lobes, where the particles break up, and thus changing the value for desired clusters can lead to an improved solution, and the method for choosing the number of clusters is presented in Chapter 3.4.

Figure 4.16 suggests that the two lobes will eventually separate, leaving behind fragments in the central region. As shown in Figure 4.6, the energy of each particle subsequently

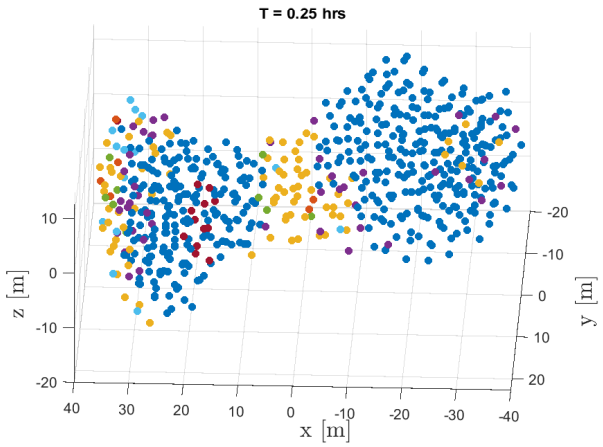

Figure 4.16: Initial time step clusters identified based on particle energy level of particles and increasing the number of clusters desired from 16 to 26, for *Kleopatra*, when the density is $\rho = 2000$ kg/m^3 and rotation period is $P = 2.5$ hrs. Each cluster is represented by a different color.

depends on its spatial location. However, calculating particle energies solely with respect to the global reference frame does not accurately indicate whether particles within the newly formed clusters possess sufficient energy to escape.

Some particles that remain near the original centre of mass, and are not clearly part of either lobe, are gravitationally attracted toward one of the larger rubble piles. This interaction increases their velocity over time, in accordance with Equation (2.3), potentially resulting in a positive total global energy.

This can lead to a misinterpretation: while a particle's global energy may suggest it is unbound ($E > 0$), its local energy—computed relative to the moving cluster—may still be negative, meaning the particle remains dynamically bound, Figure 4.17. As a result, no actual breakup occurs. This emphasizes the need to consider both global and local energy perspectives when analyzing the stability and evolution of gravitational aggregates.

4.4. Network Analysis

For each created network, its characteristics were calculated and analysed as functions of time. In the following cases, the analyses will focus mainly on the case of *Kleopatra*, for a density $\rho = 2000$ kg/m^3 and a rotation period $P = 2.5$ hrs. The other cases were used in the analyses and will be included for certain comparisons, however, this will be the main case, as it presents a breakup case, with a small number of remnant communities, and 2 large gravitational aggregates.

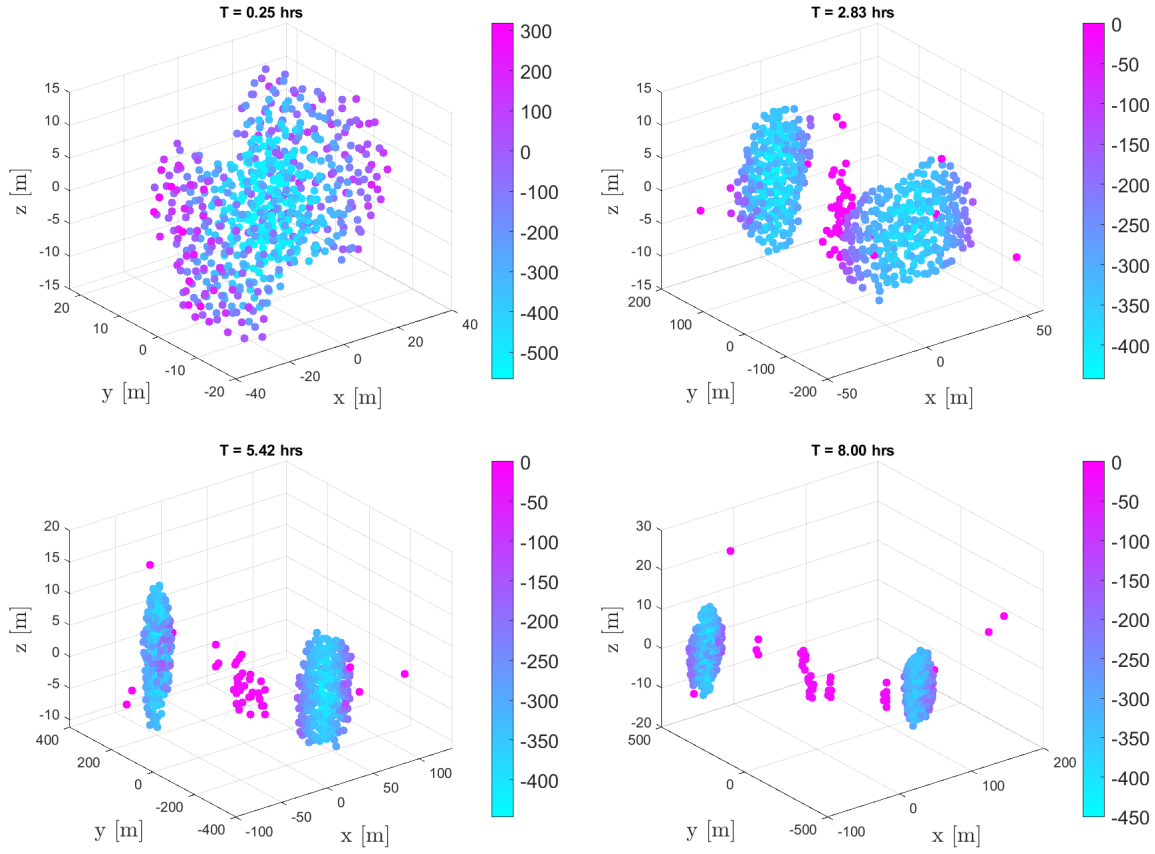

Figure 4.17: The color bar shows the energy value of each particle relative to the dynamical evolution of its respective cluster, computed as in Equation (2.17), in J, for *Kleopatra* at different values of time. In this case, density is $\rho = 2000$ kg/m^3 and rotation period is $P = 2.5$ hrs.

4.4.1. Degree

The degree metric in network analysis offers a simplified yet powerful way to quantify the number of physical or gravitational connections that each particle maintains. In the context of rubble-pile asteroids, this can reveal local density and dynamic clustering, especially during processes such as breakup and re-accumulation.

The degrees were calculated for each network considering the existence of the edge and the strength of the edge. The most interesting case from the degree point of view is the one that presents the contact pairs, as it is the only one not considering any weights, and thus it is more probable to have nodes of the same degree. In Figure 4.18 they are shown the degree of each node in the asteroid, while Figure 4.20 shows the degree distribution of the network. The average degree of the network is considered to be small, being equal to 2.8. This can be explained through the large number of particles found on the surface

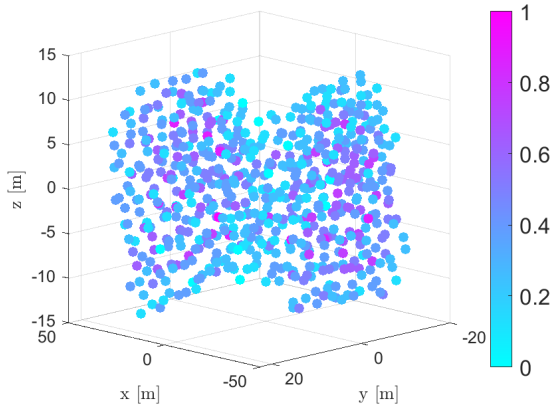

Figure 4.18: Node Degree - Contact Pairs.

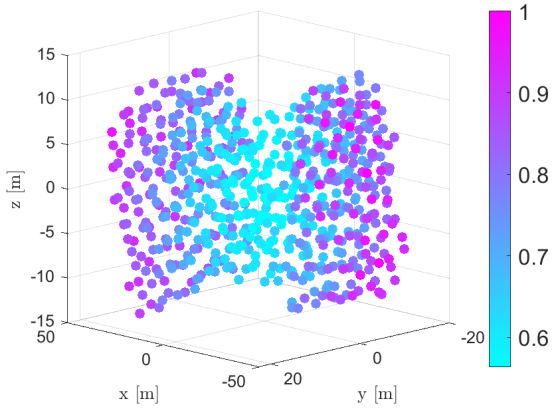

Figure 4.19: Node Degree - Distance.

of the asteroid, where the degree is smaller, which can be observed in Figure 4.18. It is observed that the central region is higher in degree than the outer region of the asteroid. This is expected as the outer bodies, the ones creating the surface of the asteroid are surrounded by fewer bodies, and thus their degree is also smaller. Furthermore, it can be observed that the bodies forming the *bridge* of *Kleopatra* have a lower average degree than those of the two lobes.

A higher node degree typically indicates a particle embedded deeper within a gravitational cluster or a dense region of the body, whereas lower degree values are more typical of surface or loosely connected particles. This interpretation holds for both contact-based networks and distance-based networks, although the latter is smoother and more global.

Each vector of degrees was normalized, such that the values are in the range $[0, 1]$. The difference between the two methods is the following. The degrees based on contact pairs show the distribution of particles inside the asteroid, and it is equivalent to the mass distribution of the asteroid, with the two lobes containing the majority of the mass of the asteroid, and thus the degrees tend to be larger, while in the centre of the asteroid they tend to be smaller, as there are fewer grains present. Meanwhile, in the case of a complete weighted network, the degree is simply representing the actual distance of each particle with respect to CoM. This is valid for all the complete weighted networks considered in the analysis. Through this method the particles are sorted based on the chosen physical characteristic, with those having a larger absolute value, being closer to 1, and those having a smaller value, being closer to 0. This is obvious, as the adjacency matrices, A, and therefore the links' strength, are defined as the Euclidean distance between particle i and all others, with the degree of node i, becoming $d_i = \sum_j ||r_i - r_j||_2$.

The average degree of a graph depends on the dynamical evolution of the rubble pile

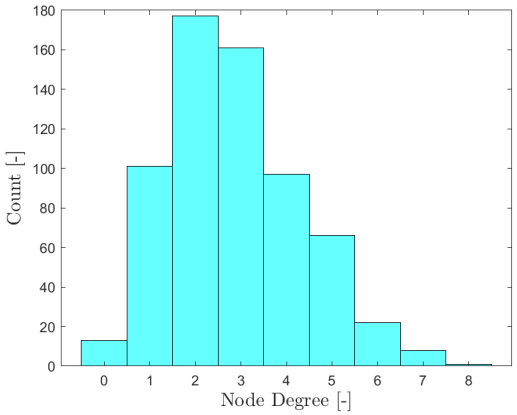

Figure 4.20: Degree Distribution at t = 0 for $\rho = 2000$ kg/m^3 and $P = 2.5$ hrs.

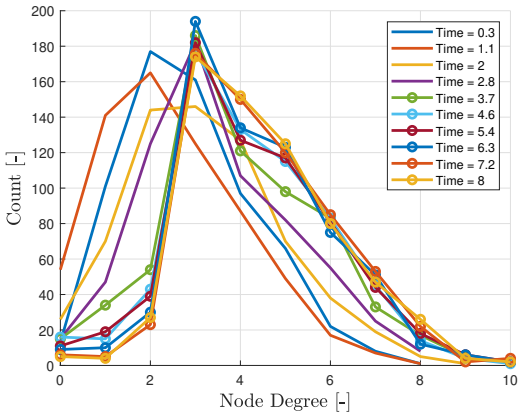

Figure 4.21: Time evolution of degree distribution for $\rho = 2000$ kg/m^3 and $P = 2.5$ hrs.

and is therefore a function of density and angular velocity $\bar{d}(\rho, \omega)$, as these are the two components that describe the evolution of the system.

The evolution of the mean degree and the degree distribution of the system are presented in Figure 4.21 and Figure 4.23. The two cases $P = 5$ hrs and $P = 3.2$ hrs present interesting results. The reshape case, $P = 21.8$ hrs, was expected to have an increase in average degree from the start, while $P = 5$ hrs and $P = 3.2$ hrs had an initial drop, since the asteroid breaks up in both cases. However, this could be explained by the positions of the particles in the rubble piles. In the reshape case, the particles composing the two lobes towards the centre slowly increase the degree in the bridge. The first particles to move towards the centre are the surface particles of the two lobes. Therefore, in this case, each time a surface particle moves towards the centre degree increases, while that in the lobes decreases, and for this reason the average degree has a smaller increase with respect to the other two cases, as shown in Table. 4.4. Meanwhile, in the cases with rotation periods $P = 5$ hrs and $P = 3.2$ hrs, the aggregates break up into two rubble piles with a small amount of bodies of remnants left behind. In each of the two rubble piles the average degree is large as they are compacted. In comparison, the cases that present the fastest rotation have the smallest average degree. This is due to a larger number of remnant bodies that have lower degrees and free bodies that are not able to attach to other particles because of the large angular velocity.

This is expected as the number of particles in contact decreases, and afterwards, under the effect of gravitational interactions, the bodies particles start to re-accumulate into two smaller rubble piles.The re-accumulation is observed through the increase in the

Rotation Period P $[hrs]$	21.8	5	3.2	2.5	2.1	1.9
Initial average degree	3.37	3.70	3.43	2.87	2.22	2.10
Minimum average degree	3.13	3.70	3.37	2.47	1.82	1.64
Maximum average degree	4.29	4.61	4.46	4.48	4.06	4.18

Table 4.4: The minimum, maximum and initial average degree of the network representing *Kleopatra*, for different rotation periods.

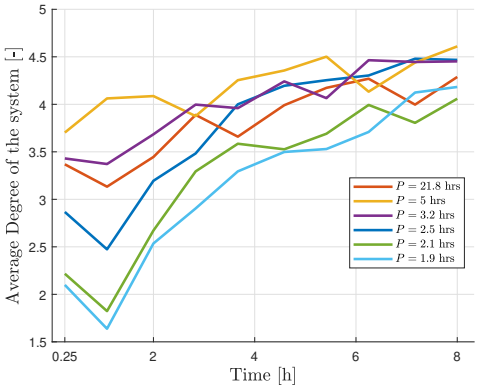

Figure 4.22: Mean degree time evolution for *Kleopatra* at constant density $\rho = 2000$ kg/m^3.

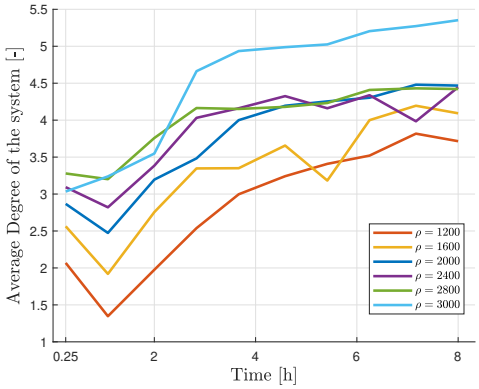

Figure 4.23: Mean degree time evolution for *Kleopatra* at constant rotation period $P = 2.5$ hrs.

average degree, but also through the degree distribution. In Figure 4.21, the degree distribution evolves significantly: the peak value shifts from approximately 2 at the start of the simulation to around 3 at the end. Additionally, the maximum node degree increases from 8 to 11, reflecting the formation of denser central structures in the new aggregates.

This is correlated to the evolution of the shape of the asteroid. The unique initial shape of *Kleopatra* consists in many particles with a small degree as they form the surface of the asteroid, while the final shapes are close to ellipsoidal shapes, and thus the particles present in the centre of each rubble pile will have larger degrees.

At the end of the simulation, it is observed that the average degree converges for each case towards a value that depends on the case. This is understandable as the two newly formed rubble piles begin to stabilise, creating two ellipsoidal forms with little particle movement, and thus the change in the average degree would result only from the change of degree of the free particles that are attracted to one of the two main bodies but did not aggregate yet. The increase in the average degree and the shift in the degree distribution to higher values is due to the creation of ellipsoidal rubble piles. In Appendix 1, a similar analysis is shown for *Bennu*, which starts from a more spheroidal shape and therefore the

change in average degree is not as noticeable as in the case of *Kleopatra*.

The dependency on density is shown in Figure 4.23. In this case the average degree tends to be larger for asteroids with larger densities. The explanation is similar to that presented for the different rotation periods. As the ρ increases, the particles are less scattered, and tend to remain together even if different clusters are formed. Meaning that, for small densities, there are more free bodies present, than for the cases in which the density is large.

The analysis considering the degree distribution is representative only in the case of contact pairs, because in this case the degrees are not unique, and a distribution can be represented. In other cases, the degrees do not repeat, being usually unique, and obtaining a set of N different degrees, which add no meaningful value to the analysis.

By modelling the asteroid as a network, the breakup limit can be considered as a function of the average degree of the system, with systems with higher average degree presenting an improved resistance to breakup. In the case of reshape, the average degree increases from the beginning, without presenting any decreasing behaviour. These findings suggest that the average degree could serve as an early-warning indicator for structural instability. A sharp decrease in average degree corresponds to the presence of a small core, with many surface particles, whereas rising trends signals the strengthening of the core, more particles composing the core. This implies that a critical threshold in $\bar{d}$ may define size of the core of the rubble piles and its strength, which is important in reaching equilibrium, as explained in [14, 46].

4.4.2. Centrality

Centrality measures aim to quantify the importance of nodes within a network. As discussed in Chapter 2, this importance is not uniquely defined, as different centrality metrics evaluate the influence of the nodes using distinct criteria. Consequently, centrality analysis became a powerful tool in network science, particularly for identifying key nodes that influence structural dynamics such as breakups and reshaping events in rubble-pile systems.

The degree centrality considers the degree of each vertex. Therefore, this method will not be of interest in complete networks, and so the focus will be placed on eigenvector, betweenness, and closeness centralities, as they focus on how important are the neighbours of a node and the number of shortest paths on which a node is found.

For this analysis, the same rubble-pile model used in previous sections was employed.

However, the focus here shifts to physical quantities that include angular momentum, total energy, contact forces, and contact pairs.

A more insightful analysis involves the closeness and eigenvector centralities applied to angular momentum and energy distributions across the network. As illustrated in Figure 4.24, closeness centrality clearly outlines the two lobes of the rubble pile, while the connecting bridge between them exhibits lower centrality values. Conversely, eigenvector centrality yields an inverse interpretation where the bridge region is assigned the highest centrality values, whereas the lobes are deemed less central. This inversion suggests that the bridge, although less physically massive, may serve a critical structural or dynamical role within the network's topology.

A similar analysis was conducted using the total energy of the system as the node attribute. Interestingly, when comparing the centrality results with those obtained by hierarchical clustering (Figure 4.15), both methods independently identify the lobes as regions of higher energy concentration. This cross-validation supports the reliability of centrality-based methods in capturing meaningful structural patterns within rubble-pile aggregates.

It was observed that degree, eigenvector, and pagerank centralities yield similar results, assigning similar importances during the asteroid evolution. The maximum relative error between the eigenvector and pagerank is of 13%, which is considered to be small, considering that the two methods measure the importance on different bases. Similarly, the degree centrality is compared to the two methods above; however, the maximum relative error increases slightly. This is because the degree centrality measures the degree of the nodes, and thus in the present context it can take only natural values, as opposed to the other methods which take values in the rational positive set.

In Figure 4.25 the closeness and betweenness centralities are presented as observed for energies. As networks are considered to be complete, for both betweenness and closeness, centrality considers the importance based on the weights between the two bodies. Therefore, the difference between the cases, as seen in Figure 4.25, is based on calculating the importance with respect to the Euclidean distance between the nodes, considering the energy.

An interesting case consists of comparing the case of contact pairs with the case of contact forces. In Figs. 4.26 and 4.27 the centralities' time evolution is shown. In Chapter 2.2 was stated that betweenness and closeness centralities require a connected network. Despite the disaggregation of the asteroid, in the case of energy and angular momentum, the networks are modelled as complete graphs. In the cases of contact pairs and contact forces, the networks are not modelled as complete graphs, and during the disaggregation

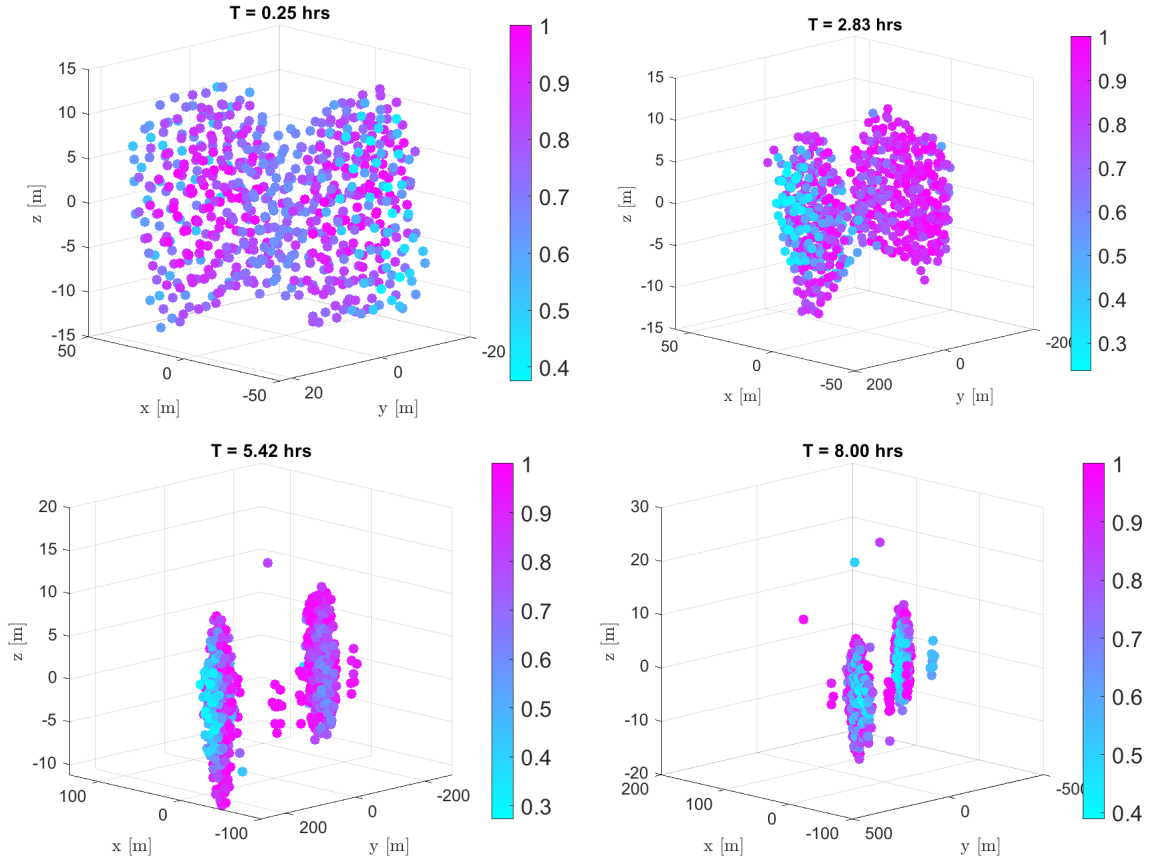

Figure 4.24: Angular Momentum Closeness Centrality time evolution for *Kleopatra* with $\rho = 2000$ kg/m^3 and $P = 2.5$ hrs.

of the asteroid, disconnected components form in the network. The centrality of these disconnected components is set to zero, such that they do not have any influence over the importance of other nodes.

The time evolutions of betweenness, eigenvector, and degree centralities are presented in Figure 4.26 and Figure 4.27. Betweenness assigns a larger importance to nodes found in the bridge between the two lobes. These results are expected, considering the network presented in Figure 4.9 and 4.10, it can be seen that there are no links connecting the two lobes and thus the paths cross the central region, where the nodes will have the largest centrality. Meanwhile, eigenvector clustering is based on the eigenvalues and eigenvectors of the system. It results through this method that in each lobe (right lobe for pairs eigenvector centralities and left lobe for contact forces eigenvector centralities, as seen in Figure 4.26 and Figure 4.27, respectively) there are nodes present that are assigned a larger importance in the network (darker colour in the figures), with respect to the remaining nodes in the graph. It is interesting to note the importance of weights during simulations. The results in Figure 4.27 are based on the contact forces, which have the same edge

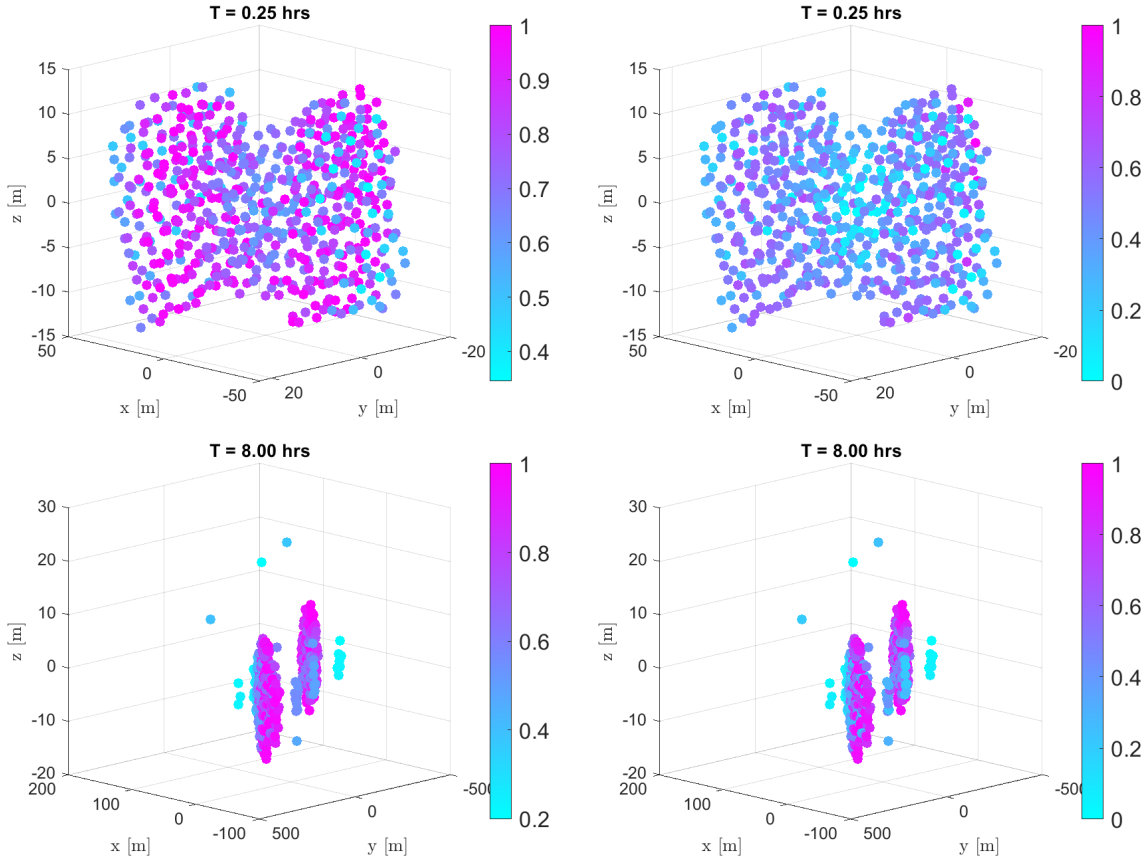

Figure 4.25: Initial and final time steps for energy closeness and betweenness centralities for *Kleopatra* with $\rho = 2000$ kg/m^3 and $P = 2.5$ hrs.

configuration as the contact pairs, but the edges in this case are weighted. This difference can be seen clearly in all three centralities simulations. For the eigenvector simulation the most important nodes from a force perspective are placed in the opposite lobe with respect to the contact pairs case, while the betweenness centrality spreads towards the central regions of the two lobes, and is not limited anymore in the bridge.

Considering from a time perspective, the results hold a similar change in the centrality measures with respect to the initial time step. Furthermore, since the two newly created rubble piles have a similar composition and their shape is created through the aggregation process, the centrality between the two rubble piles is also similar.

These results demonstrate the importance of using multiple centrality metrics when analysing rubble-pile networks. Although the eigenvector and PageRank centralities reveal persistent influence zones within lobes, betweenness centrality is more sensitive to structural connectivity and potential fracture pathways. The consistent difference be-

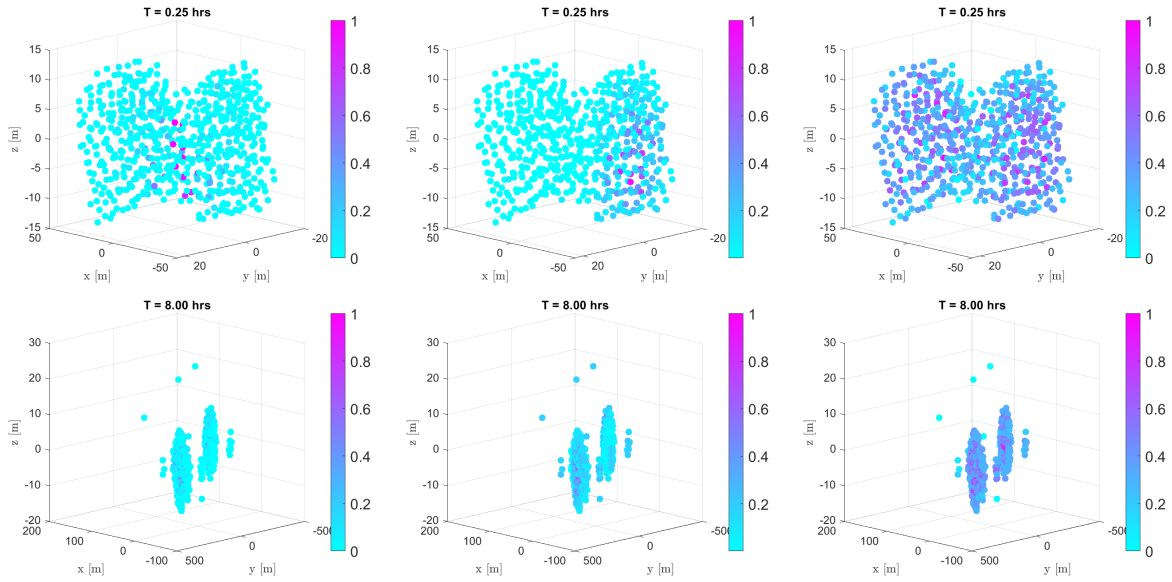

Betweenness Eigenvector Degree

Figure 4.26: Pairs centralities time evolution, for *Kleopatra* with $\rho = 2000$ kg/m^3 and $P = 2.5$ hrs. Only the initial and final time steps are shown.

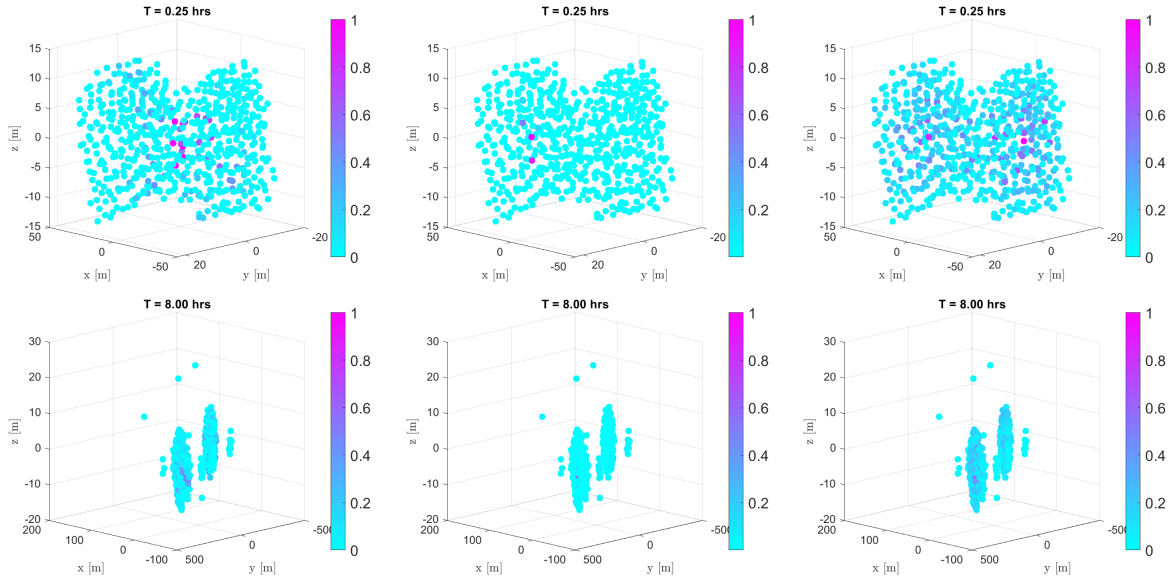

Betweenness Eigenvector Degree

Figure 4.27: Contact forces centralities time evolution, for *Kleopatra* with $\rho = 2000$ kg/m^3 and $P = 2.5$ hrs. Only the initial and final time steps are shown.

tween contact pair and contact force networks further underlines the importance of edge weighting in capturing real structural dynamics.

4.5. Percolation Process

The percolation process was employed to assess whether the groups identified in Chapter 4.2 - specifically those based on contact pairs - can be replicated or predicted through a process of iterative edge elimination and link prediction. The underlying hypothesis was that by simulating edge failures in the network, one could anticipate the fragmentation patterns of the aggregate. However, this approach was ultimately unsuccessful, as it failed to replicate the observed clustering behaviour. This is largely due to the critical role of physical contact forces in the actual dynamics of the evolution of the rubble pile, which cannot be fully captured through topological manipulation alone.

Before implementing the percolation algorithm, the time evolution of the percolation threshold, p_c, was calculated to assess the global connectivity of the rubble-pile system over time. The results are presented in Figure 4.28 and Figure 4.29. In the context of network theory, the percolation threshold indicates the critical fraction of edges that must remain in the system for a *giant component*—a large-scale connected subgraph—to persist. Therefore, the evolution of p_c provides valuable insight into the structural transitions of the system and global resilience.

Figures 4.28 and 4.29 reveal that in scenarios where the asteroid undergoes substantial disruption or fragmentation, the percolation threshold reaches its peak values. This behaviour indicates that only a small fraction of edges, approximately $1 - p_c$, must be removed before the system no longer contains a single giant component, but rather separates into multiple disconnected clusters. This aligns with physical observations of breakup scenarios, in which the rubble pile loses cohesion and fragments into smaller aggregates.

Interestingly, after a certain number of time steps, p_c tends to reach values of around 0.2 across all simulations, regardless of the initial conditions. This convergence occurs even in two very different cases: one where the asteroid remains structurally intact and undergoes only slight reshaping (e.g., $\rho = 2000$ kg/m^3, $P = 5$ hrs), and another where catastrophic disaggregation occurs almost immediately (e.g., $\rho = 2000$ kg/m^3, $P = 1.9$ hrs). This suggests that, despite the differences in angular momentum or bulk density, the network representation of the rubble pile eventually stabilizes into a configuration that exhibits similar large-scale connectivity.

From a structural interpretation standpoint, a low percolation threshold implies that the

network—hence the asteroid—is robust, maintaining connectivity even after many edge removals. This would reflect a system with strong cohesion and redundancy in particle contacts. In contrast, a high p_c implies fragility: the network (and by extension, the rubble pile) is vulnerable to fragmentation, and a large fraction of edges must remain intact to preserve global connectivity.

When particles were considered spherical, the convergence of p_c within the range $[0.2, 0.26]$ may serve as an empirical signature of network-level stability and the transition toward a post-disruption equilibrium. Regarding the information percolation threshold can offer with respect to the structural and dynamical evolution of the rubble pile, the results can be compared to those obtained for the total potential energy (Fig: 4.8) and the moment of inertia (Figure 4.7). When analysing the moment of inertia and the potential energy, it was observed that they increase when the asteroid disaggregates, with the rate of increase directly proportional to the level of disaggregation. Depending on the case, it was observed that the potential energy reaches a point where it starts to converge. A similar behaviour can be observed in the evolution of the percolation threshold. For the cases where the particle undergoes reshape or is found in stable configurations ($\rho = 2000$ kg/m^3 and $P = 21.8$ hrs and $P = 5$ hrs), the variation in the percolation threshold is small. For cases, where the asteroid disaggregate, the percolation threshold present during the evolution a drop in the percolation threshold, with $p_c(t_0) \geq p_c(t_f)$. The line steepness is proportional to the severity of the breakup, similar to potential energy. The most severe cases occur at $P = 1.9$ hrs and $\rho = 2000$ kg/m^3, Figure 4.28, or $P = 2.5$ hrs and $\rho = 1200$ kg/m^3, Figure 4.29. However, while the potential energy would converge to a value close to the maximum value reached (the distances between particles stop growing), the percolation threshold starts to decrease and converges to a small value representing the compactness of the network (greater number of edges present). Therefore, the evolution of potential energy is valuable indicating that dynamical system is in equilibrium, while the percolation threshold is capable of showing that the system reaches equilibrium from a structural point of view. The results are further supported by the time evolution of the percolation threshold for the asteroids *Bennu* and *Geographos*. Although p_c converges to different final values in each case, a common pattern is observed: an initial increase followed by a sharp drop, suggesting the disaggregation. This behaviour indicates the onset of structural instability.

The methodology outlined in Chapter 3.5 was applied across three different types of adjacency matrices: those based on energy thresholds, gravitational attraction, and direct contact pairs. For this analysis, a static framework was assumed, which means that the physical state of each particle, denoted $\mathbf{x}_i$, was kept constant in all iterations. The only

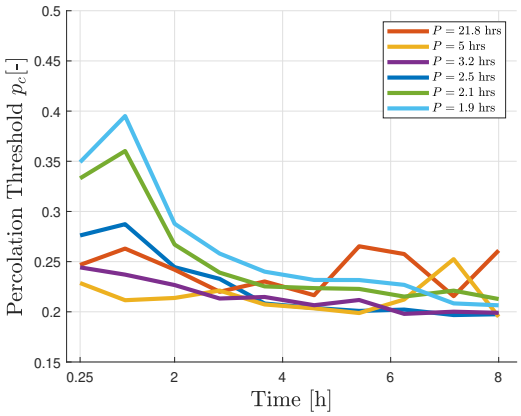

Figure 4.28: Percolation threshold time evolution for *Kleopatra* at constant density $\rho = 2000$ kg/m^3.

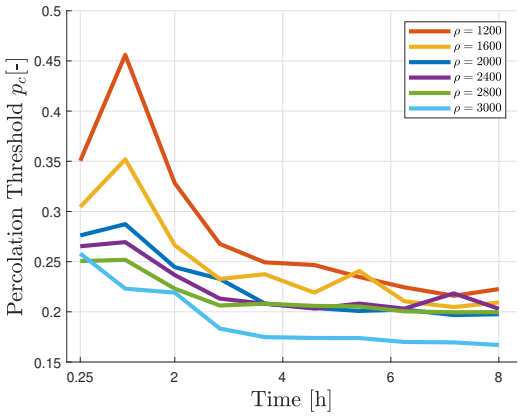

Figure 4.29: Percolation threshold time evolution for *Kleopatra* at constant rotation period $P = 2.5$ hrs.

dynamic component was the presence or absence of edges, which were systematically removed based on specified criteria. The most important disadvantage of this method is the oversimplification it implies: the inclusion of a particle within a certain cluster is dependent on the physical evolution of the system (the dynamical state x_i of each particle), which are governed by parameters such as density (ρ), rotational period (P), and time (t). By neglecting this dynamical evolution, the percolation model fails to capture the temporal development and reconfiguration of the structure. Moreover, in the dynamical system, an important aspect is the creation of new links, contacts between nodes, for which the percolation method fails to account.

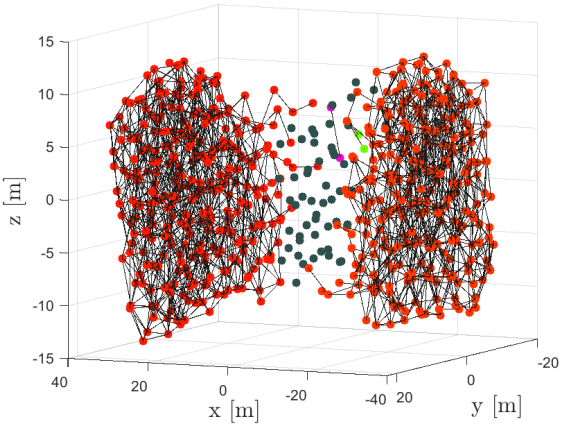

Figure 4.30: Resulting network after edges were eliminated based on energy difference between nodes, representing the initial time step of *Kleopatra* $\rho = 2000$ kg/m^3 and $P = 2.5$ hrs.

To mitigate superficial fragmentation—particularly the removal of peripheral nodes that do not contribute to meaningful structural failure—the algorithm was designed to avoid eliminating leaf nodes (nodes with degree $d_i = 1$). These nodes typically correspond to surface particles on the asteroid. Removing their connections prematurely could artificially strip away outer layers of the body without meaningful insight into the internal structure. Therefore, the algorithm was constrained such that only edges connected to nodes with degree $d_i \geq 2$ were eligible for removal. This ensures that the core structure is prioritized for fragmentation, while still allowing surface nodes with higher connectivity to eventually detach through subsequent iterations.

Despite this refinement, the algorithm was unable to accurately assign nodes to their correct physical clusters. The primary issue stems from the need to manually define the number of degrees (or proportion of edges) to remove in each iteration. This value is non-trivial to estimate, especially in large or complete networks, where the number of existing edges grows quadratically with the number of nodes. Moreover, as the size and density of the network increase, the computational complexity of simulating random walks or cascading failures also increases significantly, leading to longer processing times and greater resource consumption.

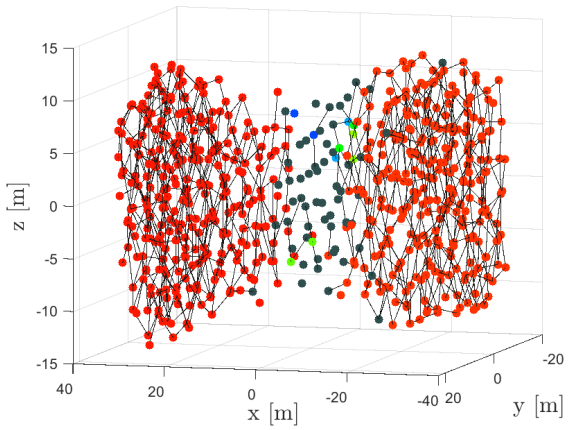

Figure 4.31: Resulting network after edges were eliminated based on gravity attraction between the nodes, representing the initial time step of *Kleopatra* $\rho = 2000$ kg/m^3 and $P = 2.5$ hrs.

Despite these, this process proved valuable in predicting the size of the largest connected component of the network and in identifying the weak region of the asteroid. Figures 4.30 and 4.31 show the results of this algorithm applied to energies and gravity. Firstly, the probability of each edge was calculated based on the adjacency matrix that defines the

network. In this case,the relative energies of the particles and the gravity attraction between two particles were used when implementing the algorithm.

It can be observed that through this process, the two lobes detached from one another, similar to the real behaviour of the asteroid in subsequent steps. Therefore, through this process, the weaker parts of the asteroid can be identified and analyse the prediction of the asteroid.

As stated before, this process is not capable of assigning the correct clusters to the particles, due to the dynamics involved in the process. Between two consecutive time steps, the particles can evolve dynamically and interact with each other through contacts. However, this process considers just the physical characteristic of the system at the considered time, and so important physical events could not be accounted for that are paramount in the evolution of the asteroid.

5 | Conclusions and future developments

The interest in asteroid research increases because of its importance in the scientific community as it could offer answers to several questions. The modelling of such rubble piles and the efficiency of the model present a great interest for possible future developments, discoveries, and space missions.

This thesis has as main objective the modelling of a rubble pile as a network of particles, representing a N-body system, in which grains are represented as nodes. The second objective is to analyse the evolution of these network's characteristics over time and the information they can carry. A third objective of the thesis is to identify the clusters and their importance in the breakup of an asteroid.

Furthermore, it offers a detailed analysis of the factors that influence the network analysis metrics over time, enhancing the understanding of the gravitational aggregates structure and formation. Hereafter, they are presented the key findings derived from the results:

- The similarities between the particles composing the system can be created based on the dynamical state of the particles in the system. From centralities analyses it was observed that considering the edge weights, not just their existence, changes the distribution of nodes importance in the system, resulting in a more uniform distribution, that is based on the contact pairs network. Considering the time evolution of the contact networks, the topological evolution (existence of edges) it was observed to be the most important factor in describing the system's evolution. If a complete graph is considered throughout the simulation, there is no topological variation throughout the simulations, and in these cases the edge weights become the most important factor influencing the results of the analysis.
- The dynamic balance can delay catastrophic disruption, and allows for quasi-stable reshaped configurations, that is predicted through reaching faster a convergence rate for percolation threshold.

- Furthermore, it was observed that for cases of breakup, when the initial aggregate breaks into two newly formed rubble piles, the system presents a decrease in the average degree and when it reshapes or is stable, the average degree remains almost constant (a much smaller variation is observed with respect to the breakup cases). The system approaches stability, when the average degree of the system approaches an average degree of 4.5, for spheres with $R = 2$, for *Kleopatra*, while for *Bennu* two stable case were observed at 4.5 and 5.

- To identify clusters within the asteroid, both the Markov Chain clustering method and the spectral clustering method produce strong results. These methods not only detect clusters based on position and contact pairs but also offer valuable insight into the likely number of clusters in the system—an essential input for clustering techniques that require this parameter in advance. The estimated number of clusters can then be slightly adjusted and applied to other methods, such as hierarchical clustering. This approach enables the detection of multiple communities that later play a significant role in the dynamical evolution of the asteroid. The identified clusters are representative, providing a useful approximation of the regions where the asteroid is likely to break apart. The identified clusters that are based on the energy level of each particle, through spectral and hierarchical clustering show the weak regions of the asteroid, turn out that can be consolidated by the calculation of centrality and by the application of percolation algorithm. The results also hold in the cases of *Geographos* and *Bennu*, where the asteroids do not necessarily break into several different components, but some particles detach from the main body. These particles are identified through both the centralities and the clustering methods. The time evolution of the percolation threshold and clustering coefficient have been analysed, revealing key insights into the system's dynamical behavior. Based on the convergence of the percolation threshold, the structural stability and breakup limits can be defined, similar to [13], offering a way to characterise the dynamical regime of the system, and for the presented case it was observed that it is around 0.22, for *Kleopatra*. The clustering coefficient indicates that gravitational aggregates exhibit similar clustering behavior to other real-world networks, suggesting that established network analysis techniques can be applied to study their structural evolution. By combining the percolation threshold with the evolution of potential energy and moment of inertia, it is possible to assess the stability of a gravitational aggregate from both a dynamical and structural standpoint. Similar to [31], it was observed the importance of contacts in the asteroid evolution, especially at higher densities. Through percolation the severity of a breakup and the dynamical regime of the

system can be identified. It was observed that in both stable and reshape configurations, the percolation threshold exhibits only a small variation between the initial and final time steps of the simulation. In contrast, disaggregation scenarios show a significant decrease in the percolation threshold over time. In cases of severe disaggregation, there was initially a sharp increase in the percolation threshold, followed by a drop proportional to the severity of the disruption. Furthermore, the percolation threshold tended to converge toward the end of the simulation, indicating that a quasi-stable state was reached. These results are further supported by the similar trends observed in the evolution of the percolation threshold and clustering coefficient for *Bennu* and *Geographos*, where stable cases present an almost constant percolation threshold, with reshape cases presenting a small variation between the initial value and final value. The disaggregation cases for these two asteroids show a drop between the initial and final state also when only a few particles detach from the asteroid.

- The percolation method is not suitable for predicting clusters formation based on contact pairs or relative particle distances, as the implemented model does not consistently assign bodies to their correct clusters over time. However, it can still effectively identify weak regions within the network and provide useful predictions about the likely breakup topology in subsequent time steps.

5.1. Future developments

This thesis is meant as a foundation for more detailed analysis and as a continuation of previous works. Despite the large body of research already available in the context of asteroid dynamics, structural compositions, and dynamical evolution of rubble piles, a small amount of research focusses on the benefits of modelling asteroid as networks. Therefore, as this paper is among the firsts to focus on this subject, several potential developments are possible and they are as follow:

- Firstly, the analysis could benefit from accounting for limits when creating the adjacency matrices. Spatial limit or physical characteristic limits would lead to matrices that are more sparse, and thus to a more efficient algorithm. A network with nodes, placed at opposite ends of an asteroid, that are not connected, would still provide reliable results.

  For instance, for the case of *Kleopatra*, two particles, each being part of one of the core of the two lobes, will not interact between them, as they will be bound to stay in their respective lobe (reshape), or will be ejected in opposite direction

(disaggregation). Gravitational interaction that each play on the other shall still be accounted for, but the (dis)similarities between them could be neglected. Through this process, $A_{ij} = 0$ for any physical characteristic considered for the analysis, as they are dynamically decoupled in terms of cluster evolution. This type of spatial or physical filtering leads to a more accurate representation of the system's true interactive structure and reduces the complexity of network analysis.

- Additional adjacency matrices can be generated to account for local structural aggregate of the rubble pile. Local mechanical properties - such as cohesion, tensile/compressive stress, and friction angle can be implemented to generate the similarities between the particles. This would result in a more mechanically-grounded network, where edges reflect the actual structural bonds between particles. For instance, particles connected via high-cohesion links or exhibiting high shear strength would form stronger clusters in the network. This enables a more precise prediction of fragmentation points or stress concentration zones.

  Such a matrix could become a unified representation of the asteroid's internal architecture, where nodes are particles and edge weights reflect bond strength. This would allow network theory to track also structural damage and local failure.

- Modelling the asteroid as a network influenced by external factors such as, tidal forces, YORP-effect and possible impacts with other asteroid. In fact, in the case of two asteroid collision, they could be both represented as distinct networks that interact and bind together as represented in other research papers [6, 40]. This would lead to a more complex system that could be represented through a node percolation process, in which nodes are added and their adjacent edges to the network of one asteroid, and they would represent the evolution of the second asteroid.

- In [14, 46] shows the importance of a core in a gravitational aggregate, and the importance of its characteristics on the asteroid stability, and possibility of reshaping and breakup. Therefore, the system could be created through several polydisperse particles. In this case, the degree distribution of contact pairs of particles would increase, spreading over a large domain of possible number of contacts. Furthermore, the particle masses would be different (as opposed to the present case in which particles were considered of equal masses), and thus the energies and physical measurements characterizing the system would not depend solely on the dynamical state of the particle $\mathbf{x}_i$, but also on the physical state. Introducing a dense internal core, would allow a more complete representation of asteroid structures commonly observed in space missions.

- Lastly, a more complex system could be considered in which more complex shapes would be considered for the particles. This would allow two particles to be in contact in more than one point, as compared to spherical models that allow single contacts between pairs of particles. In this way the network representing the system would become a multigraph, and the network model would not be a simple binary adjacency matrix anymore.

Bibliography

[1] D. S. amd G.M. Brown. Bounds on energy and angular momentum loss in the full n-body problem. *Celestial Mechanics and Dynamical Astronomy*, 135(3):35, 2023. doi: 10.1007/s10569-023-10148-1.

[2] A.Tasora and M.Anitescu. A matrix-free cone complementarity approach for solving large-scale, nonsmooth,rigid body dynamics. *Comput. Methods Appl. Mech. Engrg.*, 200:439–453, 2010. doi: 10.1016/j.cma.2010.06.030.

[3] M. Azadmanesh, J. Roshanian, and M. Hassanalian. On the importance of studying asteroids: A comprehensive review. *Progress in Aerospace Sciences*, 142:100957, 2023. doi: 10.1016/j.paerosci.2023.100957.

[4] F. Aziz, L. T. Slater, L. Bravo-Merodio, A. Acharjee, and G. V. Gkoutos. Link prediction in complex network using information flow. *Scientific Reports*, 2023. doi: 10.1038/s41598-023-41476-9.

[5] A. C. Bagatin, R. A. Alemañ, P. G. Benavidez, and D. C. Richardson. Internal structure of asteroid gravitational aggregates. *Icarus*, 302:343–359, 2018. doi: 10.1016/j.icarus.2017.11.024.

[6] A. C. Bagatin, R. A. Alemañ, P. G. Benavidez, M. Pérez-Molina, and D. C. Richardson. Gravitational re-accumulation as the origin of most contact binaries and other small body shapes. *Icarus*, 339:113603, 2019. doi: 10.1016/j.icarus.2019.113603.

[7] R.-L. Ballouz, D. C. Richardson, P. Michel, and S. R. Schwartz. Rotation-dependent catastrophic disruption of gravitational aggregates. *The Astrophysical Journal*, 789 (2):158, 2014. doi: 10.1088/0004-637X/789/2/158.

[8] H. Chen, Y. Hu, B. Perozzi, and S. Skiena. HARP: Hierarchical learning for networks. *Association for the Advancement of Artificial Intelligence*, 2018. doi: 10.48550/arXiv.1706.07845.

[9] S. Chen, Y. Deng, X. Nie1, and Y. Tu. Clustering kinetics of granular media in

three dimensions. *Physics Letters A*, 269(4):218–223, 2000. doi: doi.org/10.1016/S0375-9601(00)00243-7.

[10] D. Cotto-Figueroa, T. S. Statler, D. C. Richardson, and P. Tanga. Coupled spin and shape evolution of small rubble-pile asteroids: self-limitation of the YORP effect. *The Astrophysical Journal*, 803(1):25, 2015. doi: 10.1088/0004-637X/803/1/25.

[11] B. Coutinho, S. Hong, K. Albrecht, A. Dey, A. Barabási, P. Torrey, M. Vogelberger, and L. Hernquist. The network behind the cosmic web. *arXiv*, 2016. doi: 10.48550/arXiv.1604.03236.

[12] S. V. DONGEN. Graph clustering via a discrete uncoupling process. *Society for Industrial and Applied Mathematics*, 30(1):121–141, 2008. doi: 10.1137/040608635.

[13] F. Ferrari and E. M. Alessi. A new method for identifying dynamical transitions in rubble-pile asteroid scenarios. *Astronomy & Astrophysics*, 672(A35):10, 2023. doi: doi.org/10.1051/0004-6361/202244540.

[14] F. Ferrari and P. Tanga. Interior of top-shaped asteroids with cohesionless surface. *Icarus*, 378:114914, 2022. doi: 10.1016/j.icarus.2022.114914.

[15] F. Ferrari, A. Tasora, P. Masarati, and M. Lavagna. N-body gravitational and contact dynamics for asteroid aggregation. *Multibody System Dynamics*, 39:3–20, 2017. doi: 10.1007/s11044-016-9547-2.

[16] F. Ferrari, M. Lavagna, and E. Blazquez. A parallel-gpu code for asteroid aggregation problems with angular particles. *Royal Astronomical Society*, 492:749–761, 2018. doi: 10.1093/mnras/stz3458.

[17] M. Fiedler. Algebraic connectivity of graphs. *Czechoslovak Mathematical Journal*, 23(2):298–305, 1973.

[18] I. Fodde and F. Ferrari. Dynamical modelling of rubble pile asteroids using data-driven techniques. *Astronomy & Astrophysics*, 695(A30), 2025. doi: doi.org/10.1051/0004-6361/202452432.

[19] E. Gausmann and F. Ferrari. Network theory in galaxy distributions: The coma supercluster neighborhood. *arXiv*, 2024. doi: 10.48550/arXiv.2407.02213.

[20] D. Hestroffer. Small solar system bodies as granular media. *Springer Nature*, 2019.

[21] M. Hirabayashi and D. J. Scheeres. Analysis of asteroid (216) KLEOPATRA using dynamical and structural constraints. *The Astrophysical Journal*, page 160, 2014. doi: 10.1088/0004-637X/780/2/160.

[22] T.-M. Ho, R. Jaumann, J.-P. Bibring, M. Grott, K.-H. Glaßmeier, A. Moussi, C. Krause, U. Auster, V. Baturkin, J. Biele, F. Cordero, B. Cozzoni, C. Dudal, C. Fantinati, C. Grimm, J.-T. Grundmann, M. Hamm, D. Herčik, K. Kayal, J. Knollenberg, O. Küchemann, E. Ksenik, C. Lange, M. Lange, L. Lorda, M. Maibaum, Y. Mimasu, C. Cenac-Morthe, T. Okada, K. Otto, C. Pilorget, J. Reill, T. Saiki, K. Sasaki, M. Schlotterer, N. Schmitz, S. Schröder, N. Termtanasombat, N. Toth, Y. Tsuda, S. Ulamec, F. Wolff, T. Yoshimitsu, and C. Ziach. The MASCOT lander aboard Hayabusa2: The in-situ exploration of NEA (162173) Ryugu. *Planetary and Space Science*, 200:105200, 2021. doi: 10.1016/j.pss.2021.105200.

[23] K. Holsapple. Equilibrium configurations of solid cohesionless bodies. *Icarus*, 154: 432–448, 2001. doi: 10.1006/icar.2001.6683.

[24] K. Holsapple. Equilibrium figures of spinning bodies with self-gravity. *Icarus*, 172: 272–303, 2004. doi: 10.1016/j.icarus.2004.05.023.

[25] K. Holsapple. On YORP-induced spin deformations of asteroids. *Icarus*, pages 430–442, 2009. doi: 10.1016/j.icarus.2009.08.014.

[26] K. A. Holsapple. Spin limits of solar system bodies: From the small fast-rotators to 2003 EL61. *Icarus*, 187:500–509, 2006. doi: 10.1016/j.icarus.2006.08.012.

[27] Y. Hu, M. Li, P. Zhang, Y. Fan, and Z. Di. Community detection by signaling on complex networks. *Phys. Rev. E*, 78:016115, 2008. doi: 10.1103/PhysRevE.78.016115.

[28] E. D. Kolaczyk. *Statistical Analysis of Network Data Methods and Models*. Springer Series in Statistics, 2009.

[29] D. Korycansky and E. Asphaug. Low-speed impacts between rubble piles modeled as collections of polyhedra. *Icarus*, 181:605–617, 2006. doi: 10.1016/j.icarus.2005.10.028.

[30] D. Kroese, T. Taimre, and Z. I. Botev. *Handbook of Monte Carlo Methods*. Wiley, 2011.

[31] S. Luding. Structure and cluster formation in granular media. *Pramana - journal of physics*, 64:893–902, 2005. doi: 10.1007/BF02704151.

[32] F. Marchis, L. Jorda, P. Vernazza, M. Brož, J. Hanuš, M. Ferrais, F. Vachier, N. Rambaux, M. V. M. Marsset, E. Jehin, S. Benseguane, E. Podlewska-Gacaa, B. Carry, A. Drouard, S. Fauvauda, M. Birlan, J. Berthier, P. Bartczak, C. Dumas, G. Dudziński, J. Ďurech, J. Castillo-Rogez, F. Cipriani, F. Colas, R. Fetick, T. Fusco, J. Grice, A. Kryszczynska, P. Lamy, A. Marciniak, T. Michalowski, P. Michel, M. Pajuelo, T. Santana-Ros, P. Tanga, A. Vigan, O. Witasse, , and B. Yang. (216) Kleopatra, a

low density critically rotating M-type asteroid. *Astronomy & Astrophysics*, 653:A57, 2021.

[33] M.E.J.Newman. *Networks An Introduction*. Oxford University Press, 2010.

[34] D. Negrut, R. Serban, and A. Tasora. Posing multibody dynamics with friction and contact as a differential complementarity problem. *J. Comput. Nonlinear Dynamics*, 2017. doi: 10.1115/1.4037415.

[35] M. Newman and R. Ziff. A fast Monte Carlo for site or bond percolation. *Phys. Rev. E*, 64:016706, 2001. doi: 10.1103/PhysRevE.64.016706.

[36] M. Newman, A.L.Barabasi, and D.J.Watts. *The structure and dynamics of networks*. Princeton University Press, 2006.

[37] M. E. J. Newman. Fast algorithm for detecting community structure in networks. *Physical Review E*, 69:066133, 2004. doi: 10.1103/PhysRevE.69.066133.

[38] T. Pöschel and T. Schwager. *Computational Granular Dynamics*. Springer, 2005.

[39] D. Richardson, W. B. Jr., and S. Love. Tidal distortion and disruption of Earth-crossing asteroids. *Icarus*, 134(IS985954):47–76, 1998. doi: 10.1006/icar.1998.5954.

[40] D. Richardson, Z. Leinhardt, H. Melosh, W. B. Jr., and E. Asphaug. Gravitational aggregates: Evidence and evolution. *University of Arizona Press*, 2002.

[41] D. C. Richardson, K. J. Walsh, N. Murdoch, and P. Michel. Numerical simulations of granular dynamics: I. Hard-sphere discrete element method and tests. *Icarus*, 212: 427–437, 2011. doi: 10.1016/j.icarus.2010.11.030.

[42] Z. M. L. D. C. Richardson and T. Quinn. Direct N-body simulations of rubble pile collisions. *Icarus*, pages 133–151, 2000. doi: 10.1006/icar.2000.6370.

[43] M. Romano, T. Carletti, and J. Daquin. The resident space objects network: A complex system approach for shaping space sustainability. *The Journal of the Astronautical Sciences*, 71(31), 2024. doi: doi.org/10.1007/s40295-024-00449-4.

[44] D. P. Sánchez and D. J. Scheeres. Simulating asteroid rubble piles with a self-gravitating soft-sphere distinct element method model. *The Astrophysical Journal*, 727:120–134, 2011. doi: 10.1088/0004-637X/727/2/120.

[45] D. P. Sánchez and D. J. Scheeres. Dem simulation of rotation-induced reshaping and disruption of rubble-pile asteroids. *Icarus*, 218:876–894, 2012. doi: 10.1016/j.icarus.2012.01.014.

[46] D. P. Sánchez and D. J. Scheeres. Rotational evolution of self-gravitating aggregates with cores of variable strength. *Planetary and Space Science*, 157:39–47, 2018. doi: 10.1016/j.pss.2018.04.001.

[47] P. Sánchez. Asteroid evolution: Role of geotechnical properties. In S. R. Chesley, A. Morbidelli, R. Jedicke, and D. Farnocchia, editors, *Asteroids: New Observations, New Models, Proceedings IAU Symposium No. 318*. International Astronomical Union, 2016. doi: 10.1017/S1743921315008583.

[48] A. Saxena, M. Prasad, A. Gupta, N. Bharill, O. P. Patel, A. Tiwari, M. J. Er, W. Ding, and C.-T. Lin. A review of clustering techniques and developments. *Neurocomputing*, 267:664–681, 2017. doi: doi.org/10.1016/j.neucom.2017.06.053.

[49] T. Schank. *Algorithmic Aspects of Triangle-Based Network Analysis*. PhD thesis, Universitat Fridericiana zu Karlsruhe, 2007.

[50] D. Scheeres. An energy-angular momentum phase function for rubble pile asteroids. *Icarus*, 436:116563, 2025. doi: doi.org/10.1016/j.icarus.2025.116563.

[51] K. Sugiura, H. Kobayashi, S. ichiro Watanabe, H. Genda, R. Hyodo, and S. ichiro Inutsuka. SPH simulations for shape deformation of rubble-pile asteroids through spinup: The challenge for making top-shaped asteroids ryugu and bennu. *Icarus*, 365:114505, 2021. doi: 10.1016/j.icarus.2021.114505.

[52] M. Sun and M. Tang. A review of link prediction algorithms in dynamic networks. *Mathematics*, 13(5):807, 2025.

[53] A. Tasora, R. Serban, H. Mazhar, A. Pazouki, D. Melanz, J. Fleischmann, M. Taylor, H. Sugiyama, and D. Negrut. Chrono: An open source multi-physics dynamics engine. *Lecture Notes in Computer Science High Performance Computing in Science and Engineering*, pages 19–49, 2016.

[54] S. van Dongen. A cluster algorithm for graphs. Technical report, Centrum voor Wiskunde en Informatica, 2000.

[55] U. von Luxburg. A tutorial on spectral clustering. *Springer*, 17:395–416, 2007. doi: DOI10.1007/s11222-007-9033-z.

[56] Y. Wang, P. D. Marchi, and M. Vasile. A stochastic dynamical network model of the space environment. *Elsevier*, 2025.

[57] B. Yan and S. Gregory. Finding missing edges in networks based on their community structure. *Physical Review E*, 80(4):056112, 2009. doi: 10.1103/PhysRevE.80.046122.

[58] Y. Zhang, D. C. Richardson, O. S. Barnouin, P. Michel, S. R. Schwartz, and R.-L. Ballouz. Rotational failure of rubble-pile bodies: Influences of shear and cohesive strengths. *The Astrophysical Journal*, 857(1):15, 2018. doi: 10.3847/1538-4357/aab5b2.

A | Appendix A

In this chapter the evolutions of other asteroid shapes, *Geographos* and *Bennu* resulted from GRAINS. The evolutions are presented in a similar way to Figure 4.5, for five different cases that show different behaviours, which are similar to those of *Kleopatra*.

A.1. Geographos

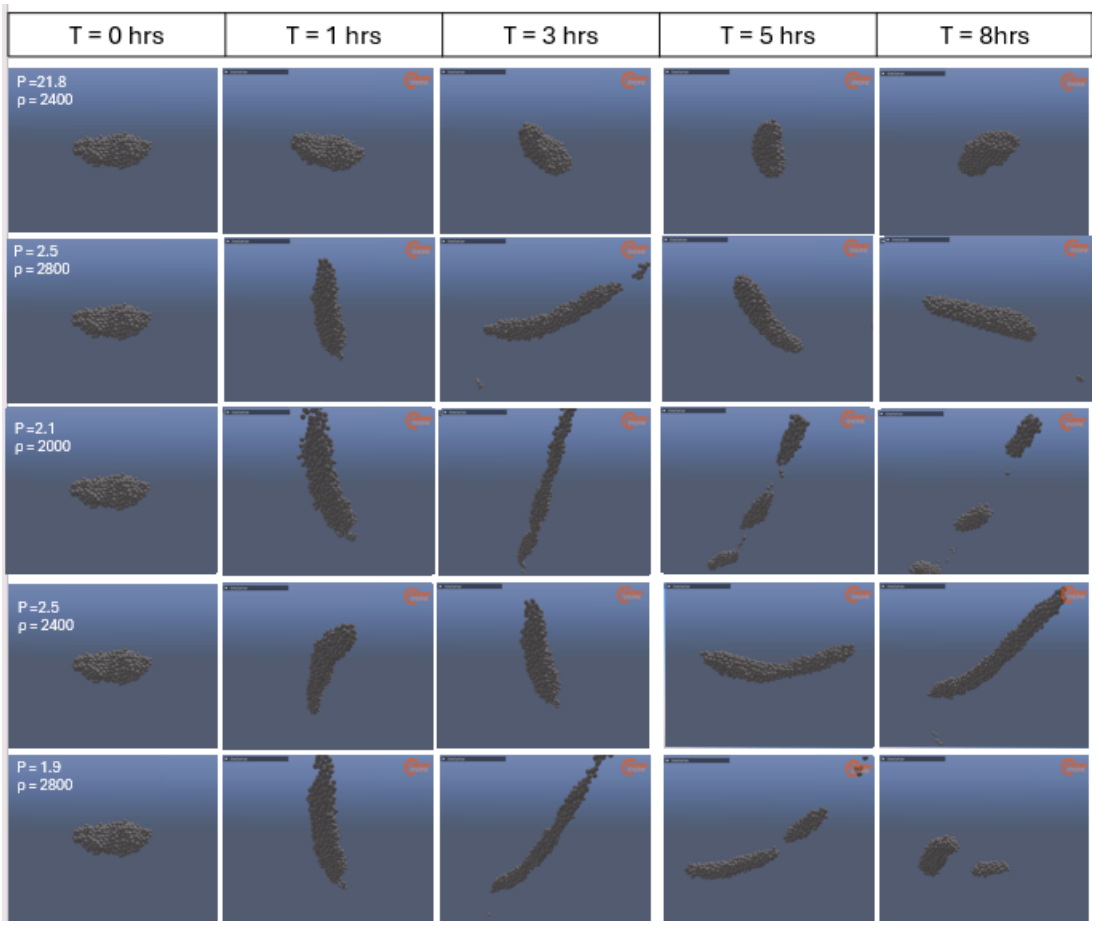

Figure A.1: Five different simulations of *Geographos* in GRAINS covering different dynamical regimes, reshaping in case A, unstable or disaggregation in cases B, C, D and E.

Geographos has a more elongated shape than *Kleopatra*, and it does not present the two lobes. This results in an evolution through which the asteroid stretches before breaking, as opposed to *Kleopatra*, which due to the mass distribution of the particles, would not undergo an elongation process. Otherwise, the two evolutions are similar, with reshape occurring when the rotation period is very small, and break-up in two or several rubble piles when the rotation period is below the critical one.

A.2. Bennu

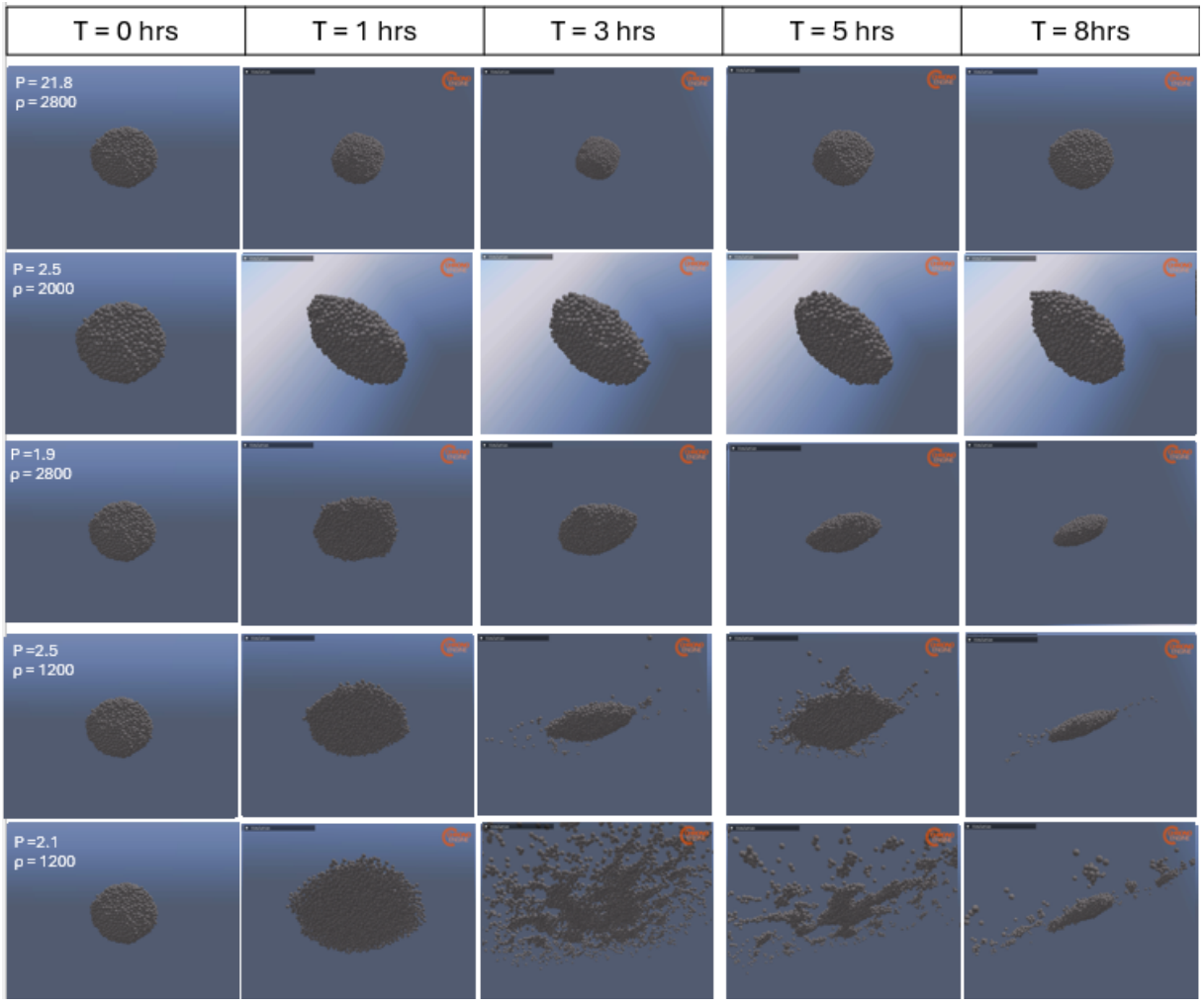

Figure A.2: Five different simulations of *Bennu* in GRAINS covering different dynamical regimes, reshaping in cases B and C, unstable or disaggregation in cases D and E, and stable in case A.

Bennu is the only asteroid chosen that presents a spheroidal shape. It was shown in Table 4.3 that *Bennu* is created from more particles than the other two asteroids, and its

elongation ϵ is completely different from those of *Kleopatra* and *Geographos*. Therefore, the critical period for *Bennu* is the largest for the chosen asteroids. This is seen in case C where, despite the large angular velocity, the asteroid does not break.

B | Appendix B

In this part will be presented the network characteristics for *Geographos* and *Bennu*. For comparison with the results from *Kleopatra*, the initial conditions chosen for these analyses are $\rho = 2000$ kg/m^3 and $P = 2.5$ hrs.

B.1. Geographos

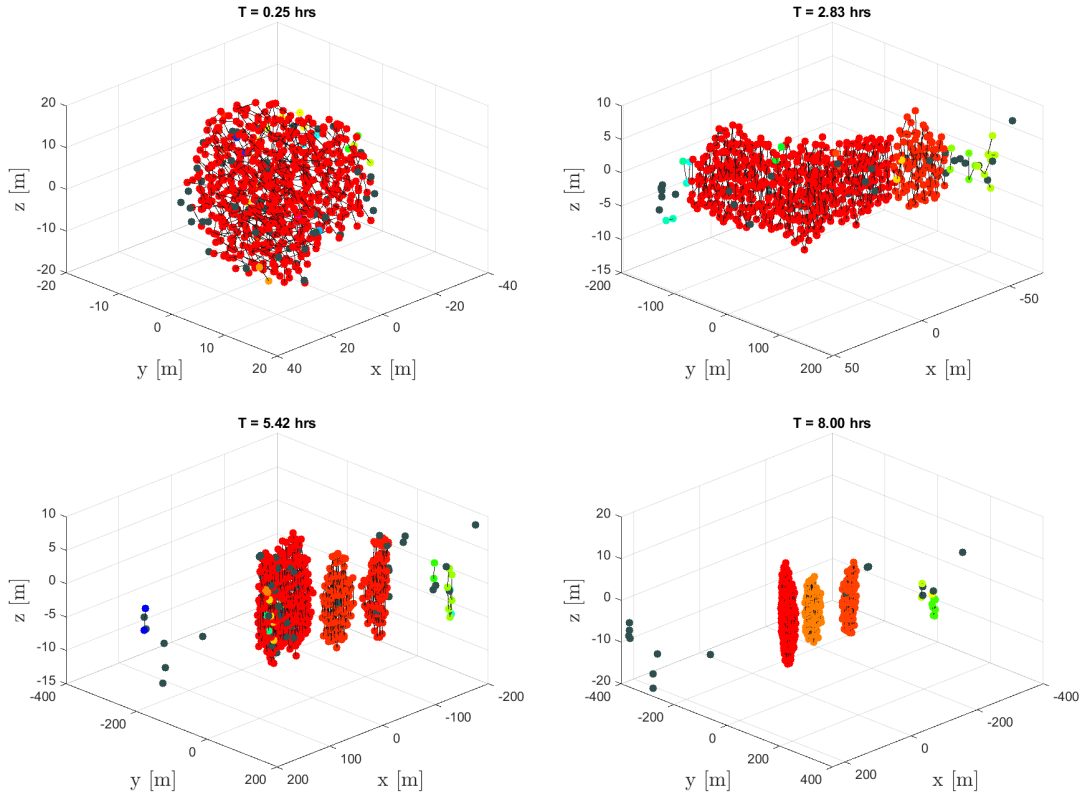

Figure B.1: Identified clusters using Algorithm 3.1 based on contact pairs for *Geographos*, for $\rho = 2000$ kg/m^3 and $P = 2.5$ hrs. Each cluster is represented by a different color, while free bodies (bodies that do not belong to any cluster), are shown in black.

.

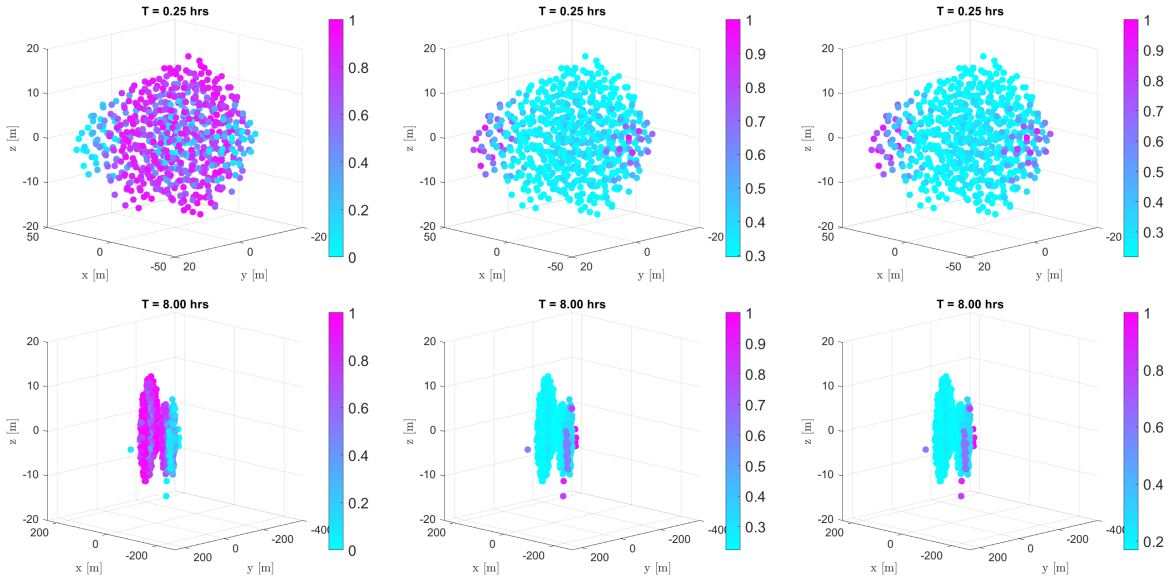

Betweenness Eigenvector Degree

Figure B.2: Energy centralities time evolution, for *Geographos* at $\rho = 2000$ kg/m^3 and $P = 2.5$ hrs. Only the initial and final time steps are shown.

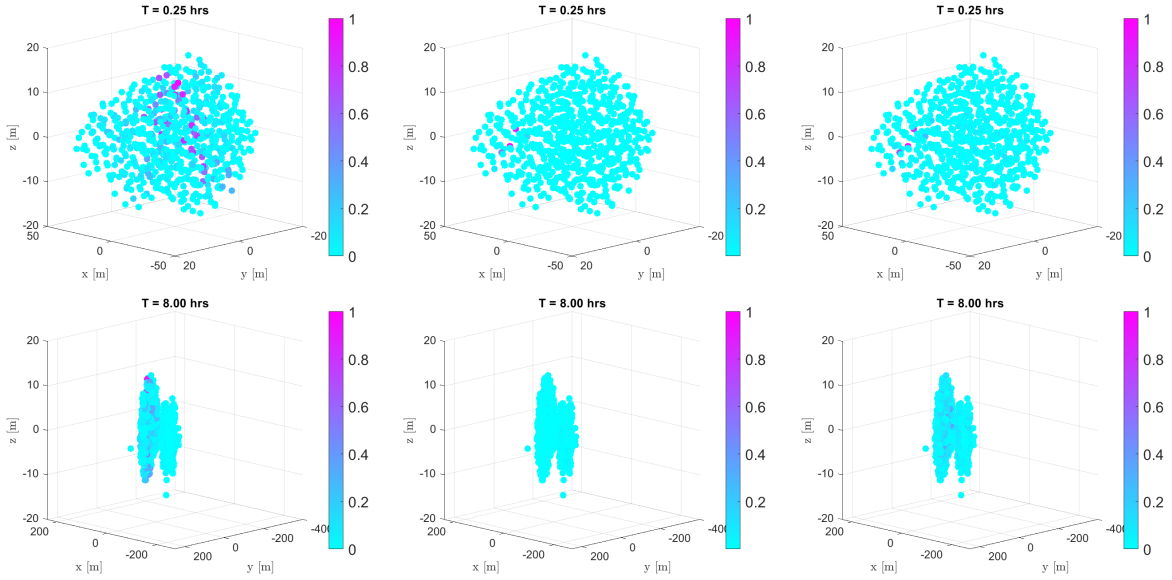

Betweenness Eigenvector Degree

Figure B.3: Contact forces centralities time evolution, for *Geographos* at $\rho = 2000$ kg/m^3 and $P = 2.5$ hrs. Only the initial and final time steps are shown.

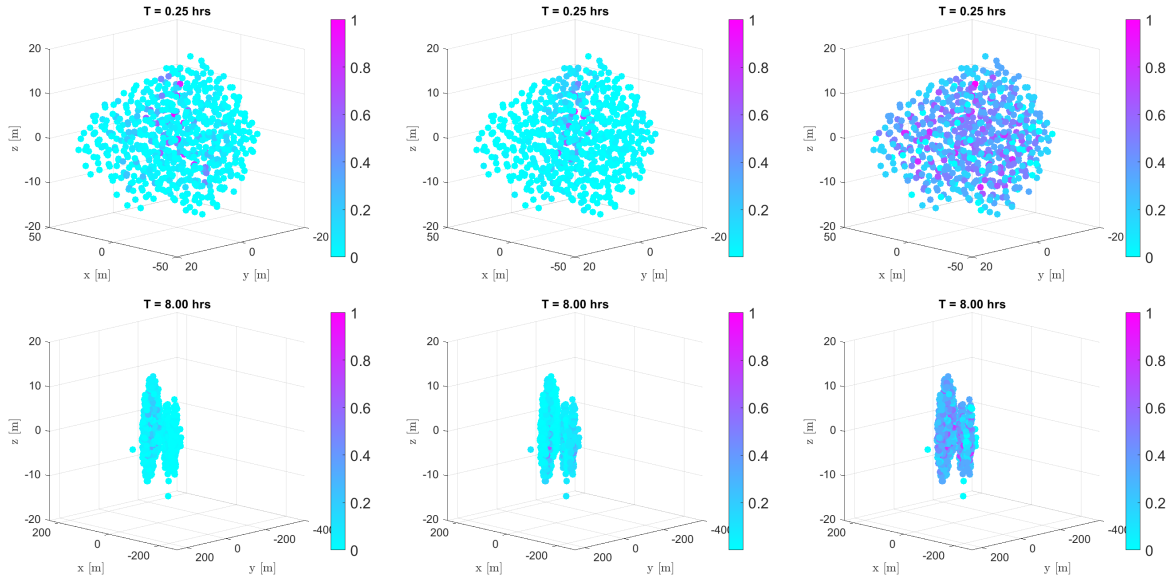

Betweenness Eigenvector Degree

Figure B.4: Contact pairs centralities time evolution, for *Geographos* at $\rho = 2000$ kg/m^3 and $P = 2.5$ hrs. Only the initial and final time steps are shown.

$\boldsymbol{\rho}$ [kg/m^3]	2000	2000	2000	2000	2000	2000
$\boldsymbol{P}$ [hrs]	21.82	5	3.2	2.5	2.1	1.9
D.R.	R.	S.	D.	D.	D.	D.

Table B.1: Dynamical regime change for *Geographos* with constant $\rho = 2000$ kg/m^3 and different P.

$\boldsymbol{\rho}$ [kg/m^3]	1200	1600	2000	2400	2800	3000
$\boldsymbol{P}$ [hrs]	2.5	2.5	2.5	2.5	2.5	2.5
D.R.	D.	D.	D.	D.	D.	R.

Table B.2: Dynamical regime change for *Geographos* with constant $P = 2.5$ hrs and different ρ.

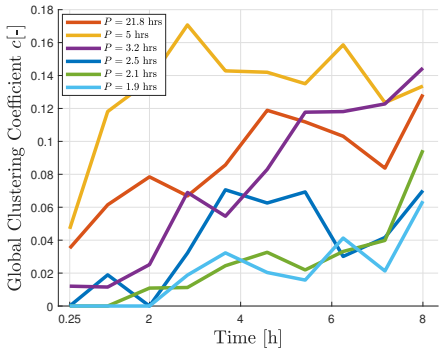

Figure B.5: Global clustering coefficient time evolution for *Geographos* at constant density $\rho = 2000$ kg/m^3.

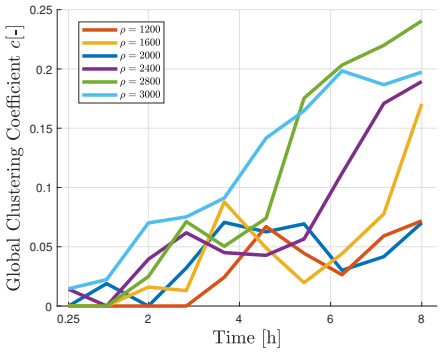

Figure B.6: Global clustering coefficient time evolution for *Geographos* at constant rotation period $P = 2.5$ hrs.

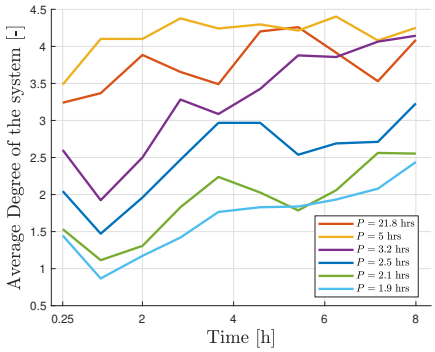

Figure B.7: Mean degree time evolution for *Geographos* at constant density $\rho = 2000$ kg/m^3.

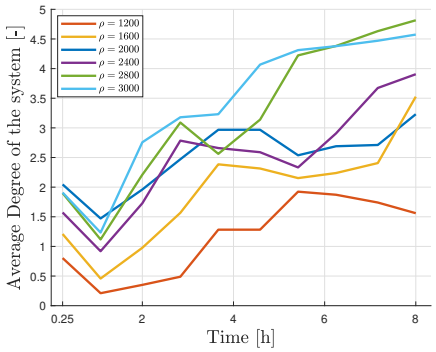

Figure B.8: Mean degree time evolution for *Geographos* at constant rotation period $P = 2.5$ hrs.

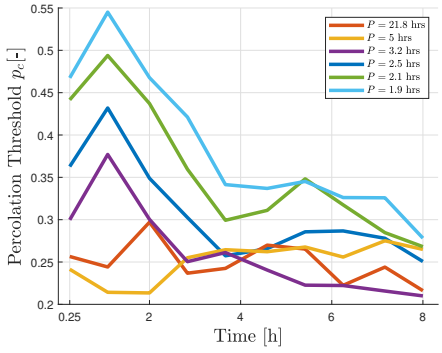

Figure B.9: Percolation threshold time evolution for *Geographos* at constant density $\rho = 2000$ kg/m^3.

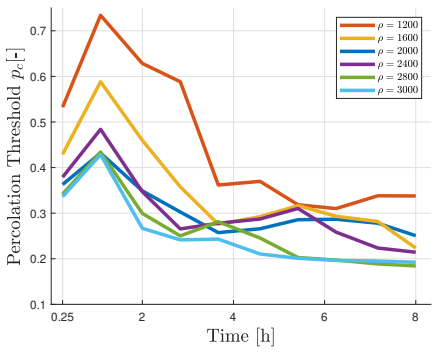

Figure B.10: Percolation threshold time evolution for *Geographos* at constant rotation period $P = 2.5$ hrs.

B.2. Bennu

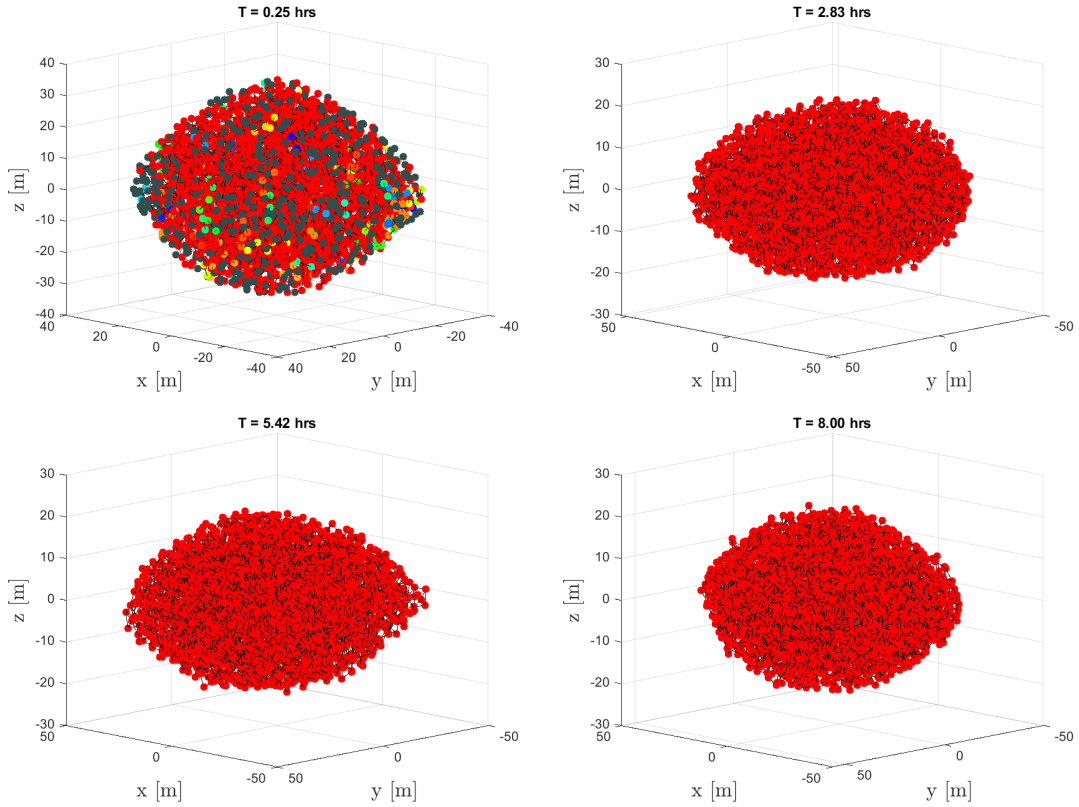

Figure B.11: Identified clusters using Algorithm 3.1 based on contact pairs for *Bennu*, for $\rho = 2000$ kg/m^3 and $P = 2.5$ hrs. Each cluster is represented by a different color, while free bodies (bodies that do not belong to any cluster), are shown in black.

.

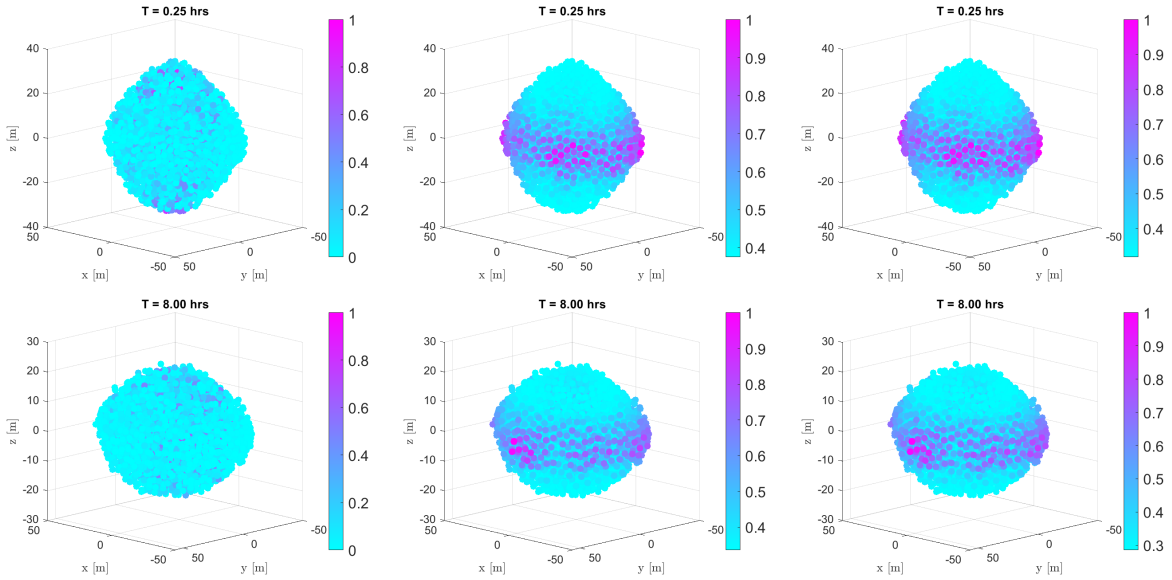

Betweenness Eigenvector Degree

Figure B.12: Energy centralities time evolution, for *Bennu* at $\rho = 2000$ kg/m^3 and $P = 2.5$ hrs. Only the initial and final time steps are shown.

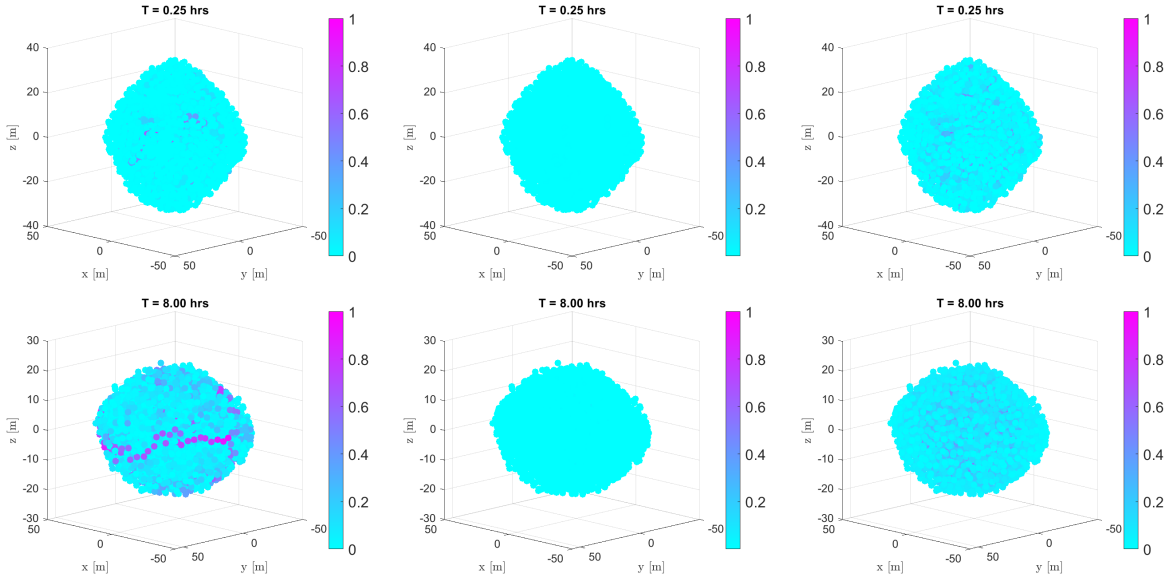

Betweenness Eigenvector Degree

Figure B.13: Contact forces centralities time evolution, for *Bennu* at $\rho = 2000$ kg/m^3 and $P = 2.5$ hrs. Only the initial and final time steps are shown.

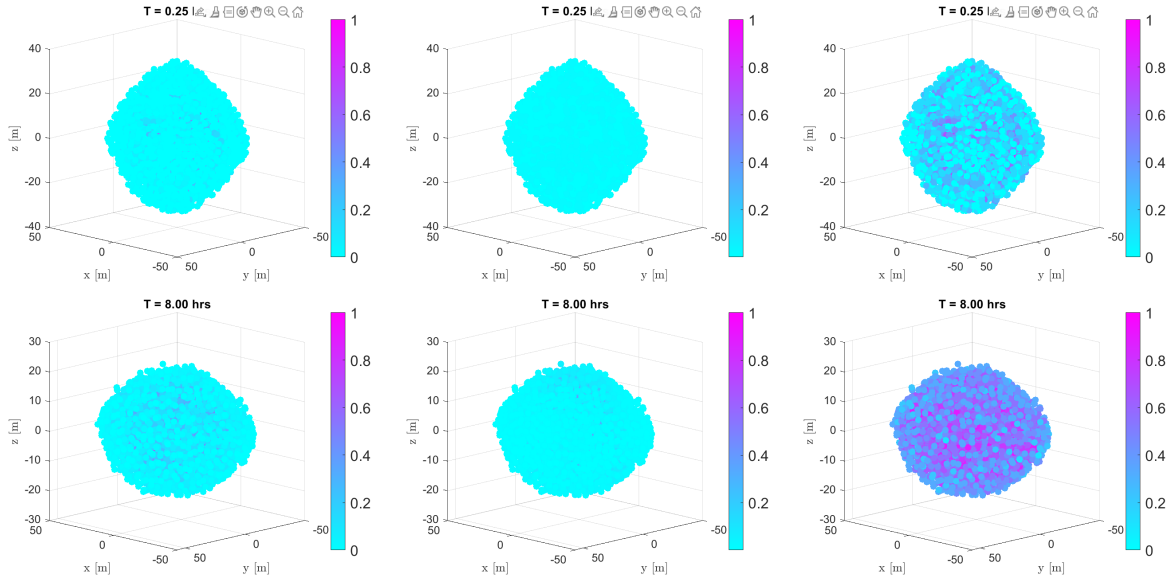

Betweenness Eigenvector Degree

Figure B.14: Contact pairs centralities time evolution, for *Bennu* at $\rho = 2000$ kg/m^3 and $P = 2.5$ hrs. Only the initial and final time steps are shown.

$\boldsymbol{\rho}$ [kg/m^3]	2000	2000	2000	2000	2000	2000
$\boldsymbol{P}$ [hrs]	21.82	5	3.2	2.5	2.1	1.9
D.R.	S.	S.	S.	R.	D.	D.

Table B.3: Dynamical regime change for *Bennu* with constant density $\rho = 2000$ kg/m^3 and different rotation period P.

$\boldsymbol{\rho}$ [kg/m^3]	1200	1600	2000	2400	2800	3000
$\boldsymbol{P}$ [hrs]	2.5	2.5	2.5	2.5	2.5	2.5
D.R.	D.	D.	R.	R.	S.	S.

Table B.4: Dynamical regime change for *Bennu* with constant rotation period $P = 2.5$ hrs and different densities ρ.

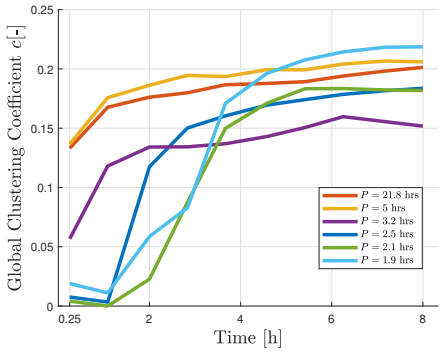

Figure B.15: Global clustering coefficient time evolution for *Bennu* at constant density $\rho = 2000$ kg/m^3.

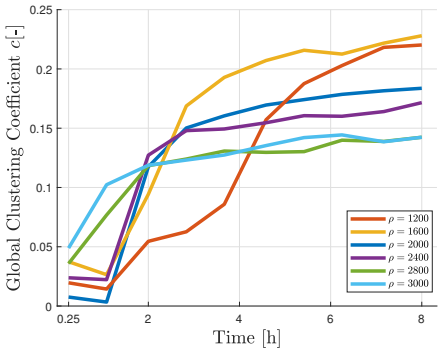

Figure B.16: Global clustering coefficient time evolution for *Bennu* at constant rotation period $P = 2.5$ hrs.

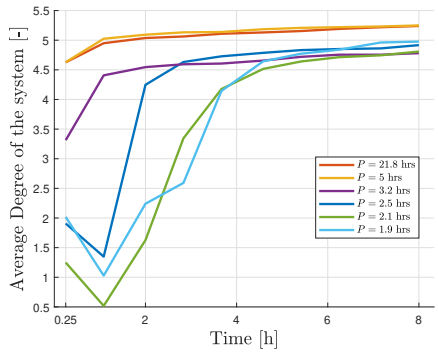

Figure B.17: Mean degree time evolution for *Bennu* at constant density $\rho = 2000$ kg/m^3.

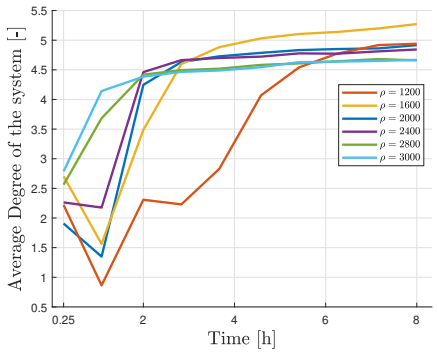

Figure B.18: Mean degree time evolution for *Bennu* at constant rotation period $P = 2.5$ hrs.

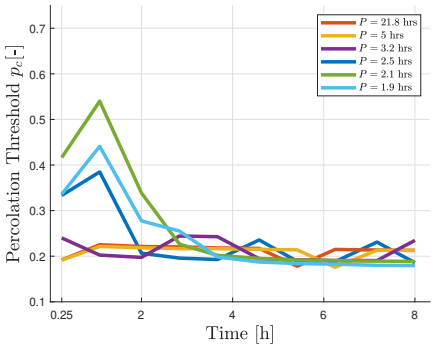

Figure B.19: Percolation threshold time evolution for *Bennu* at constant density $\rho = 2000$ kg/m^3.

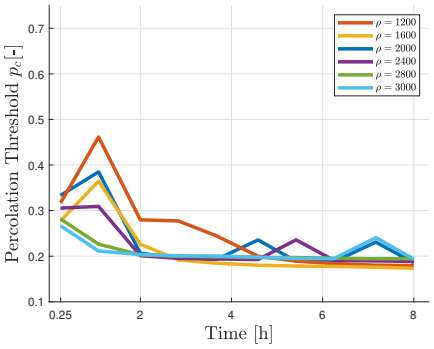

Figure B.20: Percolation threshold time evolution for *Bennu* at constant rotation period $P = 2.5$ hrs.

List of Figures

List of Tables

Acronyms

NEO - **N**ear **E**arth **O**bject
RSOs - **R**esident **S**pace **O**bjects **DEM** - **D**iscrete **E**lemet **M**odelling
SSDEM - **S**oft **S**phere **D**iscrete **E**lemet **M**odelling
SMC - **S**oft/**S**mooth Sphere Model
NSC - **N**on-smooth Sphere Model
SPH - **S**moothed **P**article **H**ydrodynamics
FEM - **F**inite **E**lement **M**ethod
E:C - **C**hrono Project **E**ngine
RTS **R**elative **T**ensile **S**trength
MC **M**ohr-**C**oulomb
DVI - **D**ifferential **V**ariational **I**nequality
CCP - **C**one **C**omplementary **P**roblem
CoM - **C**enter **o**f **M**ass
GCC - **G**iant **C**onnected **C**omponent
MCL - **M**arkov **C**hain C**L**ustering Algorithm
HARP - **H**ierarchical **A**gglomerative **R**ule-based **P**rojected clustering
GC - **G**lobal **C**lustering Coefficient

List of Symbols

Variable	Description	SI unit
$\boldsymbol{r_i}$	position	m
$\dot{\boldsymbol{r}}_{\boldsymbol{i}}$	velocity	m/s
$\boldsymbol{\varphi_i}$	orientation	rad
$\dot{\boldsymbol{\varphi}}_{\boldsymbol{i}}$	angular velocity	rad/s
$\boldsymbol{F_i}$	force	N
$\boldsymbol{M_i}$	moment	$\mathrm{N} \cdot \mathrm{m}$
m_i	mass	kg
$\hat{J}_i$	moment of inertia	$\mathrm{kg} \cdot \mathrm{m}^2$
G	universal gravitational constant	$\mathrm{m}^3/\mathrm{kg} \cdot \mathrm{s}^2$
R_i	radius	m
ξ_{ij}	deformation	m
$\boldsymbol{F_{ij}}$	contact force	N
Y	Young's Modulus	Pa
R^{eff}	velocity	m
ν	Poisson ratio	[-]
A	dissipation constant	[-]
$F^{t,n}$	tangential/normal force	N
$\boldsymbol{e^{t,n}}$	unit vector	[-]
μ	friction coefficient	[-]
U	potential energy	J
$\boldsymbol{I_i}$	inertia tensor	$\mathrm{kg} \cdot \mathrm{m}^2$
K_i, K_{rot_i}	kinetic energy (linear and rotational)	J

Variable	Description	SI unit
E_t/E	total mechanical energy (particle/system)	J
P_{crit}	critical rotation period	s
ϵ	ellipticity	[–]
ε	amended potential	J
H	angular momentum	$\mathrm{kg} \cdot \mathrm{m}^2/\mathrm{s}$
d_i	node degree	[–]
$\boldsymbol{A}$	adjacency matrix	[–]
$\boldsymbol{D}$	degree matrix	[–]
$\boldsymbol{L}$	graph Laplacian matrix	[–]
λ	eigenvalue	[–]
C_i	centrality	[–]
w_i	edge weight	Variable (e.g. N, J, m)
$\sigma(s,t)$	total number of shortest paths s and t	[–]
c	centralization index	[–]
c_i	node centrality	[–]
p_c	percolation threshold	[–]
p_{ij}	edge probability	[–]
T_g	characteristic time step	s
δ	maximum overlap	m

Acknowledgements

I would like to thank my two supervisors, Ferrari Fabio and Alessi Elisa Maria, for their guidance, technical feedback, and direction in resources and algorithms throughout the work. I would also like to thank Iosto Fodde, who provided the initial cut-out code for GRAINS and for his guidance during the creation of the rubble piles. Finally, I am deeply grateful to Cortese Federico, whose support during the development of this thesis was invaluable. His expertise provided guidance, and his technical assistance was fundamental in bringing this work to completion.